MITNE-197

A COARSE-MESH NODAL DIFFUSION METHOD BASED ON RESPONSE MATRIX CONSIDERATIONS

BY

ALLAN F. HENRY, RANDAL N. SIMS

MARCH 1977

DEPARTMENT OF NUCLEAR ENGINEERING
MASSACHUSETTS INSTITUTE OF TECHNOLOGY
CAMBRIDGE, MASSACHUSETTS 02139

ELECTRIC POWER RESEARCH INSTITUTE

MITNE-197

A COARSE-MESH NODAL DIFFUSION METHOD BASED ON RESPONSE MATRIX CONSIDERATIONS

by

Allan F. Henry, Randal N. Sims

March 1977

Department of Nuclear Engineering
Massachusetts Institute of Technology
Cambridge, Massachusetts 01293

Electric Power Research Institute

A COARSE-MESH NODAL DIFFUSION METHOD BASED ON RESPONSE MATRIX CONSIDERATIONS

by

Randal Nee Sims

Submitted to the Department of Nuclear Engineering on March 11, 1976, in partial fulfillment of the requirements for the Degree of Doctor of Science

ABSTRACT

The overall objective of this thesis is to develop an economical computational method for multidimensional transient analysis of nuclear power reactors. Specifically, the application of nodal methods based on the multigroup diffusion theory approximation to reactors composed of regular arrays of large homogeneous (or homogenized) zones was investigated.

A nodal scheme is formulated using the response matrix approach as a conceptual basis. Solutions of equivalent sets of coupled one-dimensional problems are used to treat the local multidimensional response problems. Polynomial expansions in conjunction with weighted residual procedures are employed to obtain approximate solutions of the one-dimensional problems. A linear set of nodal equations expressed in terms of nodal average fluxes and interface average partial currents is obtained.

Applications to two-dimensional few-group, static and transient problems demonstrate that the nodal scheme can be an order of magnitude more computationally efficient than conventional finite difference methods.

Thesis Supervisor: Allan F. Henry

Title: Professor of Nuclear Engineering

TABLE OF CONTENTS

Page

Page

Page

Page

LIST OF FIGURES

LIST OF TABLES

ACKNOWLEDGMENTS

The author expresses his sincerest appreciation to his thesis supervisor, Professor Allan F. Henry, for his guidance, encouragement, and support throughout the course of this thesis work. It has been a pleasure, as well as an extremely rewarding experience, to be associated with him during the author's stay at M.I.T.

The financial support of this research by the Electric Power Research Institute is gratefully acknowledged.

All computation was performed on an IBM 370/168 computer at the MIT Information Processing Center.

The author also thanks Mrs. Esther Grande for her skill, care, and patience shown in the typing of this thesis.

BIOGRAPHICAL NOTE

Randal Nee Sims was born August 13, 1950 in Dyer, Tennessee. He attended elementary and secondary school in Dyer, Tennessee, and received a high school diploma in May, 1968.

He enrolled in the University of Tennessee at Martin in June, 1969. There he began participation in the industry-university cooperative program with his work experience carried out at the DuPont Savannah River Plant and Laboratory in Aiken, South Carolina. After transfer to the University of Tennessee at Knoxville in March, 1971, he received the degree of Bachelor of Science in Engineering Physics in June, 1973.

In September, 1973, he entered the Massachusetts Institute of Technology as a graduate student in the Department of Nuclear Engineering. While at M.I.T., his association with the Savannah River Plant and Laboratory continued through participation in their summer graduate program.

Chapter 1

INTRODUCTION

1.1 Overview

There exists a strong economic incentive to perform accurate, reliable, and reasonably inexpensive multidimensional static and transient reactor calculations. The accurate prediction of multidimensional reactor behavior can lead to direct gains in terms of an increase in operating efficiency and reactor utilization or more indirect benefits such as a relaxation of safety margins or an increased confidence in their reliability.

The standard computational technique for power distribution calculations in full-size reactors is the finite difference method. However, the limited spatial accuracy of the method with the corresponding necessity for excessive spatial discretization place severe demands on computer resources. Thus, only recently, with the development of new computational procedures and a dramatic improvement in computer technology, have three-dimensional finite-difference static calculations been undertaken on a routine basis. Moreover, accurate multidimensional modeling using finite difference techniques of realistic transients for the large power reactors currently being built and designed is prohibitively expensive.

A number of recently developed higher order computational schemes have been demonstrated to be efficient alternatives to the finite difference method for multidimensional static calculations. For a comprehensive overview, we refer the reader to a number of excellent review papers on

the requirements of multidimensional static and dynamic calculations and the development of computational methods to meet those needs.[1-6] In particular, nodal techniques have reached a high degree of sophistication in application to static problems.[5] This demonstrated success with static nodal schemes has prompted us to investigate the various nodal formulations with particular emphasis on developing a spatially accurate and computationally efficient technique for transient calculations. Other researchers have pursued this same approach.[6]

The overall objective of this thesis is to develop an economical method for transient analysis of nuclear power reactors. In particular, nodal schemes for time-dependent analysis of light water reactors will be investigated. However, the basic intent is to develop a method with adequate generality to treat the principal reactor types currently under design.

1.2 Statement of the Problem

It is generally assumed that multigroup diffusion theory is an acceptably accurate neutronics model for the prediction of detailed reactor behavior.[7] Thus the basic set of time- and spatially-dependent equations for which we shall discuss approximate solutions are

$$\underline{\nabla} \cdot D_g(\underline{r},t)\,\underline{\nabla}\phi_g(\underline{r},t) - \Sigma_{rg}(\underline{r},t)\,\phi_g(\underline{r},t)$$

$$+ \sum_{g'=1}^{G} \left[\delta_{g'\neq g}\,\Sigma_{gg'}(\underline{r},t) + (1-\beta)\,\chi_g \frac{\nu}{\gamma}\,\Sigma_{fg'}(\underline{r},t) \right] \phi_{g'}(\underline{r},t)$$

$$+ \sum_{k=1}^{K} \chi_{gk} C_k(\underline{r},t) = \frac{1}{s_g}\frac{\partial}{\partial t}\phi_g(\underline{r},t); \qquad g = 1,2,\ldots G \qquad (1.1a)$$

$$\beta_k \sum_{g=1}^{G} \frac{\nu}{\gamma} \Sigma_{fg}(\underline{r}, t)\, \phi_g(\underline{r}, t) - \lambda_k C_k(\underline{r}, t) = \frac{\partial}{\partial t} C_k(\underline{r}, t); \qquad k = 1, 2, \ldots K \tag{1.1b}$$

where

$G \equiv$ total number of neutron energy groups

$K \equiv$ total number of delayed precursor families

$\phi_g \equiv$ neutron flux in group g ($cm^{-2}\ sec^{-1}$)

$C_k \equiv$ density of delayed precursor in family k (cm^{-3})

$D_g \equiv$ diffusion coefficient for group g (cm)

$\Sigma_{rg} \equiv$ macroscopic removal cross section for group g (cm^{-1})

$\Sigma_{gg'} \equiv$ macroscopic transfer cross section from group g' to group g (cm^{-1})

$$\left[\delta_{g' \neq g} \equiv \begin{cases} 0 & g' = g \\ 1 & g' \neq g \end{cases} \right]$$

$\beta \equiv$ total fractional yield of delayed precursors per fission

$\chi_g \equiv$ prompt fission spectrum for group g

$\frac{\nu}{\gamma} \Sigma_{rg} \equiv$ the number of neutrons per fission divided by a normalizing parameter which is adjusted to establish a steady-state condition for the reactor with time-independent properties times the macroscopic fission cross section for group g (cm^{-1})

$\chi_{gk} \equiv$ delayed spectrum for family k to group g

$\lambda_k \equiv$ decay constant for family k

$\beta_k \equiv$ fractional yield of delayed precursors in family k per fission

and the implicit assumption has been made that only one fissionable isotope is present. Stated nonmathematically, the particular boundary conditions imposed are that the solution of Eq. (1.1) be restrained to equal zero on the reactor boundary or be such that the reactor is effectively imbedded in a vacuum. At internal interfaces, continuity of the flux and normal component of the neutron current are required. For the reactor with time-independent properties, the static solution (or initial condition for the time-dependent Eq. (1.1)) is obtained effectively by varying the parameter γ until all time derivatives vanish for any arbitrary initial condition. The static equations are

$$\underline{\nabla} \cdot D_g(\underline{r})\, \underline{\nabla}\phi_g(\underline{r}) - \Sigma_{rg}(\underline{r})\, \phi_g(\underline{r}) + \sum_{g'=1}^{G} \left(\delta_{g' \neq g} \Sigma_{gg'}(\underline{r}) + \chi_g \frac{\nu}{\gamma} \Sigma_{fg'}(\underline{r}) \right) \phi_{g'}(\underline{r}) = 0; \qquad g = 1, 2, \ldots G. \tag{1.2}$$

The geometrical complexity of most large power reactors is so great that it is generally impractical to treat the spatial detail directly. To alleviate this difficulty, prescriptions have been developed for obtaining equivalent homogenized diffusion theory parameters which are spatially constant over relatively large reactor regions[7] (for instance, the size of a single fuel assembly in the radial plane). Thus the global reactor problem is normally partitioned into an array of subregions with constant material properties and typically uniform geometric properties. This thesis will only approach the solution of the "homogenized problem."

1.3 General Review of Solution Techniques

Among the most successful of methods for solution of static multidimensional problems, Eq. (1.2), are finite difference, finite element, synthesis, and nodal techniques. We cannot adequately detail each of these approaches here and therefore refer the reader to the comprehensive reviews previously mentioned.[3,5] We merely summarize the advantages and faults of each general class.

The finite difference method[8,9] is based on nodewise integral neutron balance with a low-order difference approximation used to represent spatial integrals of the leakage term $\underline{\nabla} \cdot D_g(\underline{r})\, \underline{\nabla}\phi_g(\underline{r})$. The resulting equations are sparsely coupled in space and energy making them relatively easy to solve. The spatial coupling is of the "nearest neighbor" type, meaning that only adjacent nodes are coupled in the representation of the spatial leakage terms. Powerful numerical solution techniques using sophisticated iterative strategies have been developed for systems of equations with this particular type of structure.[10-12] Also, it can be shown that the finite difference method converges to the exact solution of the multigroup diffusion equations in the limit of vanishing node size. However, the finite difference method applied to the "homogenized" problem has been found to require an excessive number of unknowns to achieve adequate accuracy.[3] Nevertheless, because of the inherent simplicity and reliability of the method, it is the industry standard for full-scale reactor analysis, and accordingly, the one to which we shall compare our schemes.

The finite element method[13,14] uses local polynomial expansions

for approximation of the detailed spatial variables. Variational procedures are applied to determine the unknown polynomial coefficients. The use of high-order spatial approximations allows a substantial reduction in the number of unknowns in relation to the finite difference method to achieve comparable spatial accuracy. Convergence to the exact solution of the multigroup diffusion equations in the limit of vanishing mesh size can be shown. However, the coupling of the unknowns in the finite element equations is much less sparse than that of the finite difference method, and because of this complexity, the advantage in computational efficiency of the finite element method is severely limited.[5]

The synthesis schemes[7,15] employ variational procedures using precomputed "trial functions" applicable over large regions of the reactor, such as two-dimensional planes, modulated by unknown coefficients with a reduced spatial dependence. This method can be used to treat the full spatial detail of the heterogeneous reactor with a vastly reduced number of unknowns compared with other more direct procedures. However, the solution accuracy is dependent on a proper choice by the user of the trial functions. Moreover, systematic error bounds have not been established. This lack of guaranteed reliability has severely limited the use of synthesis methods, especially in cases where safety considerations are important.

Nodal methods are derived directly from integral neutron balances and relate integral quantities, such average fluxes and neutron currents, over relatively large spatial regions. Nodal equations can be obtained directly from the transport equation and thus are not necessarily limited by the diffusion theory approximation. This class of methods

includes many variants which are described in a number of review articles.[5,7,16-19] Here we shall pursue in detail only the particular items which have immediate application to our problem.

One subset of the general class of nodal schemes uses a representation of interface currents as well as nodal fluxes allowing a system of equations to be constructed with a nearest neighbor spatial coupling formulation. Nodal balance equations (neutron conservation equations for individual subvolumes relating net nodal reaction rates and leakages in terms of average fluxes and interface currents) identical in structure to those of the finite difference method can be obtained if spatial coupling parameters specifying the relationship between fluxes of neighboring nodes and interface currents are introduced. This nodal approach offers the advantages of simply-structured equations and a substantial reduction in the number of unknowns by using average parameters over large regions. Nevertheless, its use has been severely restricted because of difficulties in predicting accurate spatial coupling parameters.

Fortunately, there seems to be a way around this difficulty. Recent work on interface current type nodal techniques using an averaged solution representation which incorporates schemes for the self-generation of spatial coupling parameters as an integral part of the overall calculational procedure or which deal directly with the interface currents has shown much promise for producing efficient methods for multidimensional static calculations.[5] In this thesis, we will pursue a nodal scheme based on the interface currents approach in which the neutron currents are directly employed.

1.4 Nodal Method Development – Motivations and Objectives

The recent success with the interface currents type of approach previously discussed prompts us to look further at this particular variant of the general class of nodal methods. In general, the prospect of a substantial reduction in the number of unknowns obtained by dealing only with avarage quantities over large nodal volumes plus the formulation of the equations with a nearest neighbor spatial coupling scheme seems quite advantageous. However, we feel that previously developed nodal techniques based on a diffusion theory approach have not fully exploited the strong conceptual basis underlying the interface currents approach in conjunction with formulations in which only integral quantities are represented.

Our specific objective is to develop a nodal method for solution of the "homogenized," time-dependent, multidimensional, multigroup diffusion theory problem. We intend to use the conceptual basis provided by the interface currents approach and maintain a formulation involving only integral quantities. We shall attempt to develop a linear method without the introduction of auxiliary parameters not directly expressible in terms of the integral quantities of interest, the nodal average fluxes and interface average currents.

1.5 Summary

This thesis will be concerned with the development of computationally efficient nodal methods for multidimensional transient analysis. In Chapter 2, the derivation of the spatially-discretized, time-dependent

nodal equations is presented. Solution techniques and results are discussed for one- and two-dimensional static problems in Chapter 3. Time-dependent solution techniques and results are presented for two-dimensional problems in Chapter 4. A summary of the investigation, a statement of general conclusions, and recommendations for future work are given in Chapter 5.

Chapter 2

DERIVATION OF THE SPATIALLY-DISCRETIZED, TIME-DEPENDENT NODAL EQUATIONS

2.1 Introduction

The derivation in the context of multigroup diffusion theory of a multidimensional, spatially-discretized set of time-dependent equations for the determination of average nodal fluxes is presented in this chapter. In this formulation, only average quantities are represented and a nearest neighbor spatial coupling scheme is preserved in the lowest order linear approximation and in implied nonlinear higher order schemes.

Since the immediate goal in considering nodal schemes is the replacement of the finite difference neutronics model in the pressurized (PWR) and boiling (BWR) light water reactor transient analysis code MEKIN,[20] basic approximations pertaining to geometrical and material representations as used in that code are employed here. The assumption is made in the MEKIN code that equivalent homogenized group parameters, spatially constant over large nodal volumes, can be used to predict adequately reactor transient behavior (see Sec. 1.2). Therefore, only Cartesian geometry and nodes having constant material properties are considered. Also, for simplicity, only two dimensions are treated. The reader should find the generalization to hexagonal geometry in two dimensions (liquid metal fast breeder reactor, LMFBR) and three-dimensional Cartesian (PWR, BWR) or hexagonal-axial (LMFBR) geometry straightforward. Other researchers are investigating the representation of mild nonuniformities in nodal properties in the context of

depletion studies for nodal schemes of the type presented here.[21]

2.2 Motivation

2.2.1 A Response Matrix Viewpoint

It is well recognized that much of the trouble encountered in determining spatial coupling parameters which predict accurate leakage rates based on the average fluxes alone of a node and its nearest neighbors is due to the fact that these parameters depend on the spatial detail of the fluxes and currents as well as on material and geometrical properties of a node and its neighbors.[5, 16] Difficulties obviously arise when an attempt is made to infer spatial coupling parameters predicting leakage rates based on nearest neighbor average fluxes without some prior knowledge of the true solution. However, until only recently, this has been the conventional nodal approach.[16]

Basically, the difficulties are due to the fact that, in attempting to use the nodal balance equation without auxiliary relations dealing either with coupling parameters or with the nodal leakages themselves, an incomplete system of equations is being used. For instance, the previously discussed interface current schemes have the nodal balance equation as only one member of a coupled set that includes relations for the interface leakages of a node expressed in terms of the leakage currents from neighboring nodes. Thus there is no reason to try to pursue the idea of a single nodal balance equation with (necessarily nonlinear) predetermined spatial coupling parameters to predict nodal leakage rates based on relations among average fluxes in nearest neighbor nodes.

A number of recently developed coarse-mesh diffusion methods employing variants of the interface currents approach in both linear and nonlinear formulations have been demonstrated to be efficient computational techniques for multidimensional static calculations.[5] (It should be noted that we neglect the success of the sophisticated high-order transport interface current approaches essentially because their sophistication vastly exceeds the difficulty of our problem.[17]) The similarity of the nodal balance equations using nonlinear spatial coupling parameters to the finite difference equations, for which well-established and powerful solution procedures exist, have prompted some researchers to pursue formulations in which the spatial coupling coefficients are generated in auxiliary calculations included as an integral part of the overall computational procedure.[22-24] Others have used linear formulations of the interface currents approach (linear in the sense that neutron currents are treated directly) in low-order transport[25] and diffusion theory[18,26-31] approximations. In these efforts it is generally true that auxiliary parameters not directly expressible in terms of the average quantities of interest (nodal fluxes and interface currents) or an explicit representation of the detailed spatial dependence of the solution have been used in order to achieve adequate spatial accuracy.

We follow the interface currents approach also. In particular, we consider the response matrix method.[18] However, we find that the approximate solution can be restrained to a representation by average quantities and a high-order spatial accuracy can be achieved without the introduction of nonlinearities or auxiliary parameters not directly expressible in terms of the average quantities of principal interest (i.e.,

nodal fluxes and interface currents).

The essential feature of the response matrix method is the determination of reaction and leakage rates and distributions due to incident current boundary conditions with continuity of interface currents applied to complete the global system of nodal equations. Application of this procedure results in a set of nodal equations with the advantageous features of local parameter determination (response parameters are only dependent on the properties of a single node) and nearest neighbor coupling.

Of course, for practical application, this system must be discretized in terms of all the transport variables – angle, energy, and space. We work in the context of multigroup diffusion theory, so only the spatial dependence of the solution is of real concern (and the time dependence for the transient problem). The treatment of the spatial dependence of the nodal fluxes and interface currents is not a trivial matter, however, especially since we desire to maintain a solution representation in terms of average quantities only. This problem is discussed in the following section.

2.2.2 Reduction of the Multidimensional Problem to an Equivalent Coupled Set of One-dimensional Problems

In order to pursue the response matrix procedure discussed in Sec. 2.2.1, conceptually we must solve, using multigroup diffusion theory, local multidimensional problems in homogeneous rectangular nodes with time- and space-dependent incident current boundary conditions. We desire to find the time-dependent nodal average fluxes and

time- and space-dependent boundary leakage currents. For solution of this problem, it is necessary to treat the spatial dependence of the nodal fluxes as well as the interface currents. However, since we want to minimize the number of unknowns by working only with average quantities, we must find approximations for the spatial dependence of the nodal fluxes and interface currents in terms of the corresponding average quantities. Alternatively, we can circumvent the problem by some transformation or reduction to an equivalent but more manageable system whose solution can be expressed in terms of average quantities. We employ both tactics.

We find that a high order of approximation can be achieved in the spatial solution of the local multidimensional response problem and the solution representation by average quantities only can be maintained, if the multidimensional problem is reduced to a set of equivalent one-dimensional problems by a straightforward spatial averaging procedure, and the spatial dependence of the unknowns in these equations are approximated in terms of average quantities associated with each coordinate direction. In particular, polynomial expansions which have coefficients that can be interpreted as the average nodal fluxes and the interface average currents associated with each coordinate direction are used for approximation of the spatially-averaged one-dimensional fluxes. A proper choice of polynomials allows a high-order approximation for the one-dimensional average fluxes to be used without introducing auxiliary parameters other than nodal average fluxes and interface average currents. Spatially-dependent terms representing transverse leakage effects

appearing in the one-dimensional equations are expanded in polynomials which have interface average currents as coefficients. A simple weighted residual procedure is used to determine the unknown time-dependent polynomial coefficients.

2.3 Derivation in Two-dimensional Cartesian Geometry with Uniform Nodal Properties and a General Energy Group Structure

2.3.1 Formulation of the Coupled Set of One-dimensional Problems

First, introduce the notational convention

$$u \equiv x, y; \qquad v \equiv y, x; \qquad v \neq u.$$

With x and y indicating the coordinate directions, u and v will be used as coordinate subscripts. The global problem is subdivided into a regular array of rectangular, nuclearly homogeneous regions. The partitioning of the spatial domain is given by a grid defined by

$$u_\ell; \qquad \ell = 1, 2, \ldots L; \qquad u = x, y$$

where the following notation has been introduced for the grid indexing

$$\ell \equiv \begin{cases} i = 1, 2, \ldots I; & u, v = x \\ j = 1, 2, \ldots J; & u, v = y. \end{cases}$$

Since we do not exclude the use of an irregular spatial domain, there are a maximum of $I \times J$ nodes. For node (ij) defined by

$$x \in [x_i, x_{i+1}]$$

$$y \in [y_j, y_{j+1}]$$

the node widths are defined as

$$h_\ell^u \equiv u_{\ell+1} - u_\ell; \qquad u = x, y$$

and the node volume as

$$V_{ij} \equiv h_i^x h_j^y.$$

Now the multidimensional problem is reduced to an equivalent set of coupled one-dimensional equations by spatially averaging over the direction transverse to each coordinate direction. For space direction u, introduce the one-dimensional average neutron flux in energy group g

$$\phi_{g,ij}^u(u,t) \equiv \frac{1}{h_\ell^v} \int_{v_\ell}^{v_{\ell+1}} dv\, \phi_g(u,v,t), \tag{2.1}$$

and the one-dimensional average delayed precursor density in delayed family k

$$C_{k,ij}^u(u,t) \equiv \frac{1}{h_\ell^v} \int_{v_\ell}^{v_{\ell+1}} dv\, C_k(u,v,t). \tag{2.2}$$

By spatially averaging Eqs. (1.1) over each coordinate direction and inserting the definitions (2.1) and (2.2), the equivalent coupled set of one-dimensional time-dependent equations is obtained for node (ij)

$$D_{g,ij}(t)\frac{\partial^2}{\partial u^2}\phi^u_{g,ij}(u,t) - \Sigma_{rg,ij}(t)\,\phi^u_{g,ij}(u,t) - L^u_{g,ij}(u,t)$$

$$+\sum_{g'=1}^{G}\left(\delta_{g'\neq g}\Sigma_{gg',ij}(t) + \chi_g(1-\beta)\frac{\nu}{\gamma}\Sigma_{fg',ij}(t)\right)\phi^u_{g',ij}(u,t)$$

$$+\sum_{k=1}^{K}\chi_{gk}\lambda_k C^u_{k,ij}(u,t) = \frac{1}{s_g}\frac{\partial}{\partial t}\phi^u_{g,ij}(u,t); \qquad \begin{matrix} g = 1,2,\ldots G \\ u = x,y \end{matrix} \qquad (2.3a)$$

and

$$\beta_k\sum_{g=1}^{G}\frac{\nu}{\gamma}\Sigma_{fg,ij}(t)\,\phi^u_{g,ij}(u,t) - \lambda_k C^u_{k,ij}(u,t) = \frac{\partial}{\partial t}C^u_{k,ij}(u,t); \qquad \begin{matrix} k = 1,2,\ldots K \\ u = x,y \end{matrix}$$

(2.3b)

where L is the transverse leakage given by

$$L^u_{g,ij}(u,t) \equiv -\frac{1}{h^v_\ell}\int_{v_\ell}^{v_{\ell+1}} dv\, D_{g,ij}(t)\frac{\partial^2}{\partial v^2}\phi_g(u,v,t)$$

$$= -\frac{D_{g,ij}(t)}{h^v_\ell}\left(\frac{\partial}{\partial v}\phi_g(u,v_{\ell+1},t) - \frac{\partial}{\partial v}\phi_g(u,v_\ell,t)\right). \qquad (2.4)$$

2.3.2 Restraints Imposed on the Solution

For node (ij), define the nodal average flux for energy group g

$$\phi_{g,ij}(t) \equiv \frac{1}{V_{ij}}\int_{x_i}^{x_{i+1}} dx \int_{y_j}^{y_{j+1}} dy\,\phi_g(x,y,t) \qquad (2.5)$$

and the nodal average delayed precursor density for delayed family k

$$C_{k,ij}(t) \equiv \frac{1}{V_{ij}}\int_{x_i}^{x_{i+1}} dx \int_{y_j}^{y_{j+1}} dy\, C_k(x,y,t). \qquad (2.6)$$

It follows from the definition of the average one-dimensional fluxes and precursors, Eqs. (2.1) and (2.2), that

$$\frac{1}{h_\ell^u}\int_{u_\ell}^{u_{\ell+1}} du\, \phi_{g,ij}^u(u,t) = \phi_{g,ij}(t); \qquad u = x, y \tag{2.7}$$

and

$$\frac{1}{h_\ell^u}\int_{u_\ell}^{u_{\ell+1}} du\, C_{k,ij}^u(u,t) = C_{k,ij}(t); \qquad u = x, y. \tag{2.8}$$

These relations, Eqs. (2.7) and (2.8), are just the formal statement of a consistency condition that must be imposed on any approximate solution technique we employ. This consistency condition states that, when averaged over the node, a one-dimensional average quantity must return the corresponding nodal average quantity.

Let us now consider the boundary conditions imposed on the one-dimensional solutions. Because the delayed precursors are required to obey no explicit boundary or interface continuity conditions, we need only consider the one-dimensional average flux. It is easily seen that the one-dimensional average flux obeys interface average incident current boundary conditions. We define the interface average incident (in) and leakage (out) partial currents by the normal diffusion theory relations[7]

$$J_{g,ij}^{in,u-}(t) \equiv \left(\frac{1}{4}\phi_{g,ij}^u(u,t) - \frac{1}{2}D_{g,ij}(t)\frac{\partial}{\partial u}\phi_{g,ij}^u(u,t)\right)_{u=u_\ell} \tag{2.9a}$$

$$J_{g,ij}^{out,u-}(t) \equiv \left(\frac{1}{4}\phi_{g,ij}^u(u,t) + \frac{1}{2}D_{g,ij}(t)\frac{\partial}{\partial u}\phi_{g,ij}^u(u,t)\right)_{u=u_\ell} \tag{2.9b}$$

$$J^{in,u+}_{g,ij}(t) \equiv \left(\frac{1}{4} \phi^{u}_{g,ij}(u,t) + \frac{1}{2} D_{g,ij}(t) \frac{\partial}{\partial u} \phi^{u}_{g,ij}(u,t) \right)_{u=u_{\ell+1}} \quad (2.9c)$$

$$J^{out,u+}_{g,ij}(t) \equiv \left(\frac{1}{4} \phi^{u}_{g,ij}(u,t) - \frac{1}{2} D_{g,ij}(t) \frac{\partial}{\partial u} \phi^{u}_{g,ij}(u,t) \right)_{u=u_{\ell+1}} . \quad (2.9d)$$

It is assumed that the J^{in}'s are the J^{out}'s of neighboring nodes and thus are known by continuity in the solution of the local response problems.

The boundary conditions implicitly incorporated in the transverse leakage terms, Eqs. (2.3) and (2.4), will not be discussed in detail at this time. As will be seen in a later discussion, the particular high-order treatment used for the spatial dependence of the transverse leakage is meaningful only in the context of the coupled global system of equations. However, just as in the treatment of the one-dimensional average flux, the interface average quantities associated with the transverse leakage are always preserved.

2.3.3 Approximate Solution

2.3.3.1 Choice of Approximating Functions

2.3.3.1a One-dimensional Average Flux

A basic approximation of the nodal method to be developed is the expansion of the one-dimensional average flux in polynomials with a weighted residual procedure used to determine the unknown coefficients. As discussed in Sec. 2.3.2, particular consistency and boundary condition restraints must be imposed on this approximate solution. Because these restraints are expressed directly in terms of the nodal average flux and interface average partial currents, we choose to incorporate

terms in the polynomial expansion for the one-dimensional average flux which satisfy these restraints and thus involve coefficients which can be directly interpreted in terms of those quantities. We also desire to find the interface average leakage partial currents. The leakage partial currents are directly expressible in terms of the one-dimensional average flux. Therefore, we also incorporate terms in the polynomial expansions having coefficients which can be interpreted as the interface average leakage partial currents. The polynomial expansion for the one-dimensional average flux in space direction u and energy group g which incorporates these features is

$$\begin{aligned}\phi^{u}_{g,ij}(u,t) \approx{}& \phi_{g,ij}(t)\,\rho^{\phi,u}_{g,ij}(u,t) \\ &+ J^{in,u-}_{g,ij}(t)\,\rho^{in,u-}_{g,ij}(u,t) + J^{out,u-}_{g,ij}(t)\,\rho^{out,u-}_{g,ij}(u,t) \\ &+ J^{in,u+}_{g,ij}(t)\,\rho^{in,u+}_{g,ij}(u,t) + J^{out,u+}_{g,ij}(t)\,\rho^{out,u+}_{g,ij}(u,t)\end{aligned} \tag{2.10}$$

where the ρ's are quartic polynomials dependent only on the geometrical and time-dependent material properties of a single node and chosen such that the conditions implied by the coefficients in Eq. (2.10) hold. For instance, the enforcement of the integral requirement on the average flux gives

$$\frac{1}{h^u}\int du\,\rho^{\phi}(u) = 1$$

$$\int du\,\rho^{in,u-}(u) = \int du\,\rho^{out,u-}(u) = \int du\,\rho^{in,u+}(u) = \int du\,\rho^{out,u+} = 0$$

where the limits of integration are over the node extent. The particular form of ρ^{ϕ} obeying these constraints is

$$\rho^{\phi,u}(u) = 30\left(\frac{u - u_{\ell}}{h^{u}_{\ell}}\right)^{2} - 60\left(\frac{u - u_{\ell}}{h^{u}_{\ell}}\right)^{3} + 30\left(\frac{u - u_{\ell}}{h^{u}_{\ell}}\right)^{4}.$$

Note that because the boundary currents are explicitly treated, the form of ρ^{ϕ} is also chosen such that derivatives at the nodal boundaries vanish. The complete set of conditions used to determine the expansion functions as well as their general mathematical form are given in Appendix 1. The spatial expansion for the one-dimensional average flux is complete in the quartic sense (4^{th}-degree, 5^{th}-order) in that any function not exceeding 4^{th} degree in spatial dependence may be exactly represented by this polynomial.

2.3.3.1b One-dimensional Average Delayed Precursors

The choice of approximation for the one-dimensional average delayed precursors is restrained only by the consistency condition because no explicit interface continuity or boundary conditions are imposed on the precursor shape. Furthermore, since no spatial derivatives of the delayed precursors are involved, there is no reason to form explicit polynomial expansions to obtain a high-order representation of the one-dimensional average delayed precursors. We may merely choose an implicit spatial shape representation based on the choice of polynomials used for approximation of the average one-dimensional flux. The imposition of the consistency condition follows quite readily if a complete

set of weight functions is used in the weighted residual procedure (or if the unit weight function is included in the weight function space) applied to each coordinate direction. This condition occurs because application of the unit weight function in any coordinate direction returns the nodal balance equation which involves only the nodal average delayed precursors. Other weighted integrals of the one-dimensional average delayed precursors involving higher order moments are treated directly as time-dependent unknowns in the implicit representation of the precursor shape.

An explicit approximation for the spatial shape of the one-dimensional average delayed precursors has been implemented as an alternative to the implicit shape representation in an attempt to reduce the number of precursor-associated unknowns. This approximation is to assume that the spatial dependence of the one-dimensional average delayed precursors is a constant with a magnitude equal to that of the nodal average delayed precursors. For delayed family k and space direction u, the approximation is given by

$$C^{u}_{k,ij}(u,t) = C_{k,ij}(t). \tag{2.11}$$

For each delayed family, the reduction in unknowns is equal to the total number of nonunit weight functions employed in the weighted residual procedure. Intermediate levels of approximation between those of the constant and implicit shape representations have not been tried.

2.3.3.1c Transverse Leakage

For energy group g and space direction u, the approximation which we use for the transverse leakage, Eqs. (2.3) and (2.4), expressed in

terms of interface average partial currents is

$$L^{u}_{g,ij}(u,t) \approx J^{out,v-}_{g,ij}(t)\left(1 + f^{out,v-}_{g,ij}(u,t)\right) - J^{in,v-}_{g,ij}(t)\left(1 + f^{in,v-}_{g,ij}(u,t)\right)$$
$$+ J^{out,v+}_{g,ij}(t)\left(1 + f^{out,v+}_{g,ij}(u,t)\right) - J^{in,v+}_{g,ij}(t)\left(1 + f^{in,v+}_{g,ij}(u,t)\right). \quad (2.12)$$

The general form is one in which the magnitude is given in terms of the interface average partial currents in a transverse direction and the shape by expansion functions consisting of a flat function with a time-dependent shape correction term.

Two approximations have been used. The simplest is a low-order approximation in which the shape correction terms, f's, are set equal to zero. We shall refer to this as the "flat" or "constant" transverse leakage approximation.

The other approximation we have used is one in which the f's are represented in terms of nonlinear quantities derived from information from neighboring nodes. For instance,

$$f^{out,y-}_{g,ij}(x,t) \equiv \left[\frac{J^{out,y-}_{g,i-1j}(t) - J^{out,y-}_{g,ij}(t)}{J^{out,y-}_{g,ij}(t)}\right] \rho^{out,y-}_{g,\binom{ij}{i-1j}}(x)$$
$$+ \left[\frac{J^{out,y-}_{g,i+1j}(t) - J^{out,y-}_{g,ij}(t)}{J^{out,y-}_{g,ij}(t)}\right] \rho^{out,y-}_{g,\binom{ij}{i+1j}}(x)$$

where the ρ's are expansion functions chosen such that the interpretation of interface average partial currents is preserved when the expression

is averaged over each node.

Although there is a great deal of flexibility incorporated in the notational convention presented here, the expansion functions, ρ's, however, are much simpler than the notation implies. The expansion functions used are members of the complete set of quadratic polynomials defined over the interval $[x_{i-1}, x_{i+1}]$ or $[y_{j-1}, y_{j+1}]$ possessing the integral property discussed above. We shall refer to this as the "quadratic" transverse approximation. Conditions used to determine the polynomial expansion functions as well as the general mathematical form and graphical form for a particular case of the polynomials are given in Appendix 2.

The approximation for the transverse leakage, Eq. (2.12), is applied only over the extent of a single node even though information from surrounding nodes is used to construct the approximation. Also note that, although the shape correction factors, f's, are inherently nonlinear, the transverse leakage approximation itself is a linear function of average partial currents. Furthermore, because of the particular choice of expansion functions, ρ's, the transverse leakage approximation we employ can be written in a formulation involving net transverse leakages of nearest neighbor nodes as the quadratic polynomial coefficients. This form is the one suggested by Finnemann[21] and used in his Nodal Expansion Method.[31] In application to the global problem, terms requiring data derived from spatial positions outside the reactor boundary are set equal to zero.

2.3.3.2 The Weighted Residual Procedure

Upon insertion of the polynomial approximations for the one-dimensional average flux, Eq. (2.10), and the transverse leakage, Eq. (2.12), into the one-dimensional equations, Eqs. (2.3), there remain five coefficients to be determined for each energy group. These unknowns are the nodal average flux and the two interface average leakage partial currents associated with each coordinate direction. The interface average incident partial currents are assumed to be known from applying the continuity of average partial current condition to interface average leakage partial currents of adjacent nodes. Alternatively, if we consider the solution in each coordinate direction individually, it is reasonable to regard the average one-dimensional flux, Eq. (2.1), as the principal unknown in the one-dimensional diffusion equations. Thus, three weight functions, which in order to maintain integral consistency must give the unit function in some linear combination, are to be applied in each energy group and coordinate direction to determine the unknown flux and leakage current polynomial coefficients. We have chosen a very simple weighted residual procedure, weighting and integrating with quadratic moments[32] (essentially 1, u, and u^2). The actual weight functions used are the equivalent set consisting of unity and the two symmetric functions of the Lagrange quadratics.[14] The choice of a symmetric set was made in order to minimize the coefficient storage and generation requirements. These weight functions are explicitly defined and graphically represented in Appendix 3.

The inclusion of the unit weight function (or equivalently, the use of

a complete set of weight functions) along with the incorporation of the integral consistency conditions in the approximations of the one-dimensional average flux and transverse leakage return the nodal balance equation repeated for each coordinate direction. The higher order moments completely determine the average leakage response.

If the implicit shape representation of the one-dimensional average delayed precursors is used, then the same quadratic moments weighting is applied in each delayed family and each coordinate direction of the one-dimensional delayed precursor equations, Eq. (2.3b). As expected, the nodal average equation is returned for each direction by application of the unit weight function and integral consistency condition. Weighted integrals resulting from the application of higher order moments are treated directly as time-dependent unknowns. A total of $5G + 5K$ equations result for each node for the G nodal average fluxes, 4G interface average leakage partial currents, K nodal average precursors, and 4K precursor-associated weighted integrals.

In the constant shape approximation for the one-dimensional average delayed precursors, only the nodal average delayed precursor equations are used. In this case, there is a total of $5G + K$ resulting equations.

The final form of the nodal equations obtained from this procedure is summarized in the following section.

2.3.3.3 Final Form

The time-dependent nodal balance equations for node (ij) are

$$\sum_{\substack{u=x,y \\ v\neq u}} \frac{h_{\ell}^{v}}{V_{ij}} \left(J_{g,ij}^{in,u-}(t) - J_{g,ij}^{out,u-}(t) + J_{g,ij}^{in,u+}(t) - J_{g,ij}^{out,u+}(t) \right) - \Sigma_{rg,ij}(t)\, \phi_{g,ij}(t)$$

$$+ \sum_{g'=1}^{G} \left(\delta_{g'\neq g} \Sigma_{gg',ij}(t) + (1-\beta)\, \chi_g \frac{\nu}{\gamma} \Sigma_{fg',ij}(t) \right) \phi_{g',ij}(t)$$

$$+ \sum_{k=1}^{K} \chi_{gk} \lambda_k C_{k,ij}(t) = \frac{1}{s_g} \frac{d}{dt} \phi_{g,ij}(t); \qquad g = 1, 2, \ldots G \qquad (2.13a)$$

and

$$\beta_k \sum_{g=1}^{G} \frac{\nu}{\gamma} \Sigma_{fg,ij}(t)\, \phi_{g,ij}(t) - \lambda_k C_{k,ij}(t) = \frac{d}{dt} C_{k,ij}(t); \qquad k = 1, 2, \ldots K. \qquad (2.13b)$$

Denoting the symmetric Lagrange weight function in space direction u and node (ij) as

$$w_{n,ij}^{u-}(u); \qquad n = 0, 1$$

and the weighted integral of the function F(u)

$$\int_{u_{\ell}}^{u_{\ell+1}} w_n^u(u)\, F(u)$$

as $\langle w_n^u | F \rangle$, the interface average leakage response equations can be written as

$$\sum_{\alpha=\begin{cases}\text{in,u-}\\ \text{out,u-}\\ \text{in,u+}\\ \text{out,u+}\end{cases}} \left\{\left[D_{g,ij}(t)\langle w^u_{n,ij}\left|\frac{d^2}{du^2}\rho^\alpha_{g,ij}(t)\right\rangle - \Sigma_{rg,ij}(t)\langle w^u_{n,ij}\left|\rho^\alpha_{g,ij}(t)\right\rangle\right] J^\alpha_{g,ij}(t)\right.$$

$$+ \sum_{g'=1}^{G}\left[\delta_{g'\neq g}\Sigma_{gg',ij}(t) + (1-\beta)\,\chi_g\frac{\nu}{\gamma}\Sigma_{fg',ij}(t)\right]\langle w^u_{n,ij}\left|\rho^\alpha_{g',ij}(t)\right\rangle J^\alpha_{g',ij}(t)\Bigg\}$$

$$+ \left\{\left[D_{g,ij}(t)\langle w^u_{n,ij}\left|\frac{d^2}{du^2}\rho^\phi_{g,ij}(t)\right\rangle - \Sigma_{rg,ij}(t)\langle w^u_{n,ij}\left|\rho^\phi_{g,ij}(t)\right\rangle\right]\phi_{g,ij}(t)\right.$$

$$+ \sum_{g'=1}^{G}\left[\delta_{g'\neq g}\Sigma_{gg',ij}(t) + (1-\beta)\,\chi_g\frac{\nu}{\gamma}\Sigma_{fg',ij}(t)\right]\langle w^u_{n,ij}\left|\rho^\phi_{g',ij}(t)\right\rangle\phi_{g',ij}(t)\Bigg\}$$

$$+ \sum_{\alpha'=\begin{cases}\text{in,v-}\\ \text{out,v-}\\ \text{in,v+}\\ \text{out,v+}\end{cases}} \theta\left[\langle w^u_{n,ij}\left|1\right\rangle + \langle w^u_{n,ij}\left|f^{\alpha'}_{g,ij}(t)\right\rangle\right] J^{\alpha'}_{g,ij}(t)$$

$$\alpha' = \begin{cases}\text{in,v-}\\ \text{out,v-}\\ \text{in,v+}\\ \text{out,v+}\end{cases},\quad \theta = \begin{cases}+1, \alpha'=\text{in}\\ -1, \alpha'=\text{out}\end{cases}$$

$$+ \sum_{k=1}^{K}\chi_{gk}\lambda_k\tilde{C}^{u,\,n}_{k,\,ij}(t) = \sum_{\alpha=\begin{cases}\text{in,u-}\\ \text{out,u-}\\ \text{in,u+}\\ \text{out,u+}\end{cases}} \left\{\frac{1}{s_g}\frac{d}{dt}\left[\langle w^u_{n,ij}\,\rho^\alpha_{g,ij}(t)\rangle\, J^\alpha_{g,ij}(t)\right]\right\}$$

$$+ \frac{1}{s_g}\frac{d}{dt}\left[\langle w^u_{n,ij}\left|\rho^\phi_{g,ij}(t)\right\rangle\phi_{g,ij}(t)\right]; \qquad \begin{array}{l} u = x, y \\ v \neq u \\ n = 0, 1 \\ g = 1, 2, \ldots G \end{array} \qquad (2.14a)$$

and, in addition, for the implicit delayed precursor shape representation

$$\beta_k \sum_{g=1}^{G} \frac{\nu}{\gamma} \Sigma_{fg,ij}(t) \left\{ \langle w^u_{n,ij} | \rho^{\phi}_{g,ij}(t) \rangle \phi_{g,ij}(t) + \sum_{\alpha = \begin{cases} in,u- \\ out,u- \\ in,u+ \\ out,u+ \end{cases}} \langle w^u_{n,ij} | \rho^{\alpha}_{g,ij}(t) \rangle J^{\alpha}_{g,ij}(t) \right\}$$

$$- \lambda_k \tilde{C}^{u,n}_{k,ij}(t) = \frac{d}{dt} \tilde{C}^{u,n}_{k,ij}(t); \qquad \begin{matrix} u = x,y \\ n = 0,1 \\ k = 1,2,\ldots K \end{matrix} \qquad (2.14b)$$

where

$$\tilde{C}^{u,n}_{k,ij}(t) \equiv \langle w^u_{n,ij} | C^u_{k,ij}(t) \rangle .$$

All weighted integrals are evaluated in Appendix 4.

We now present the interface average leakage current response equations in matrix form. The discretized spatial components are partitioned in a matrix format. A discrete energy group structure is retained. The reader should draw correspondence with Eq. (2.14) in order to determine individual matrix elements. In matrix form, Eq. (2.14) becomes

$$\left\{ \left[R^{out}_{g,ij}(t) \right] + \left[L^{out,flat}_{g,ij} \right] + \left[L^{out,shape}_{g,ij}(t) \right] \right\} \left[J^{out}_{g,ij}(t) \right]$$

$$+ \left\{ \left[R^{in}_{g,ij}(t) \right] + \left[L^{in,flat}_{g,ij} \right] + \left[L^{in,shape}_{g,ij}(t) \right] \right\} \left[J^{in}_{g,ij}(t) \right] + \left[R^{\phi}_{g,ij}(t) \right] \phi_{g,ij}(t)$$

$$+ \sum_{g'=1}^{G} \left\{ \left(\left[T^{out}_{gg',ij}(t) \right] + \frac{\chi_g}{\gamma} (1-\beta) \left[P^{out}_{g',ij}(t) \right] \right) \left[J^{out}_{g',ij}(t) \right] \right.$$

$$\left. + \left(\left[T^{in}_{gg',ij}(t) \right] + \frac{\chi_g}{\gamma} (1-\beta) \left[P^{in}_{g',ij}(t) \right] \right) \left[J^{in}_{g',ij}(t) \right] + \right.$$

$$+\left(\left[T^{\phi}_{gg',ij}(t)\right]+\frac{\chi_g}{\gamma}\ (1-\beta)\left[P^{\phi}_{g',ij}(t)\right]\right)\phi_{g',ij}(t)\Bigg\}$$

$$+\sum_{k=1}^{K}\chi_{gk}\lambda_k\left[\tilde{C}_{k,ij}(t)\right]=\frac{d}{dt}\left\{\left[S^{out}_{g,ij}(t)\right]\left[J^{out}_{g,ij}(t)\right]+\left[S^{in}_{g,ij}(t)\right]\left[J^{in}_{g,ij}(t)\right]\right.$$

$$\left.+\left[S^{\phi}_{g,ij}(t)\right]\phi_{g,ij}(t)\right\};$$

$$g=1,2,\ldots G$$

(2.15a)

where for each energy group the overall interpretation of the notation is

$[R] \equiv$ diffusion and removal

$[L] \equiv$ transverse leakage (split into flat component and shape correction component

$[T] \equiv$ group transfer $\qquad [S] \equiv$ inverse speed

$[P] \equiv$ fission production

$\left[J\binom{out}{in}\right] \equiv$ 4-element column vector of interface average $\binom{\text{leakage}}{\text{incident}}$ partial currents

and all matrix operators are (4 × 4) except the ones operating on the nodal average flux which are (4 × 1). Special attention should be given to the delayed precursor term. For the implicit precursor shape representation $[\tilde{C}_k]$ is a 4-element column vector of unknown delayed precursor weighted integrals for delayed family k. For the constant shape approximation, $[C_k]$ becomes

$$[\langle w|1\rangle]\, C_{k,ij}(t),$$

a 4-element column vector whose elements are integrals of the weight

functions multiplied by the nodal average delayed precursor density in delayed family k.

In addition, for the implicit delayed precursor shape representation, the following matrix equations are included:

$$\beta_k \sum_{g=1}^{G} \frac{1}{\gamma} \left\{ \left[P^{out}_{g,ij}(t) \right] \left[J^{out}_{g,ij}(t) \right] + \left[P^{in}_{g,ij}(t) \right] \left[J^{in}_{g,ij}(t) \right] + \left[P^{\phi}_{g,ij}(t) \right] \phi_{g,ij}(t) \right\}$$

$$- \lambda_k \left[\tilde{C}_{k,ij}(t) \right] = \frac{d}{dt} \left[\tilde{C}_{k,ij}(t) \right]; \qquad k = 1,2,\ldots K. \tag{2.15b}$$

Equations (2.13) and (2.15) form the basis of the nodal scheme we propose. The assumption of continuity of interface average partial currents along with the application of the reactor boundary conditions (for instance, with vacuum boundaries, J^{in} on the surface of the reactor are set equal to zero) complete the global system of time-dependent nodal equations.

2.4 Relationship to Other Work

The mechanics of the derivation presented here are similar to the procedures employed by other researchers in derivation of their coarse-mesh finite difference and nodal methods.[5,23,24,29-31] The idea of treating equivalent sets of one-dimensional problems in order to solve the multidimensional problem has been quite successfully exploited by Wagner and Finnemann in their nodal codes.[22-24,29-31] Finnemann has employed various polynomial approximations with weighted residual procedures for solution of the one-dimensional equations; however, unlike the method we propose, he introduces auxiliary spatial coupling parameters in his high-order approximations in order to achieve adequate

spatial accuracy. The very useful procedure of expanding the transverse leakage in a polynomial based on information from surrounding nodes was originally suggested by Finnemann.[21] The final form he employs for computation is based on an interface current approach as is our method, but the motivation seems to have been the adaptation of the solution strategy used in Wagner's nodal collision probability code.[25]

The relationship of the response matrix method to conventional nodal schemes has been recognized by other researchers.[18,19] Weiss has done much work recently on the reduction of the response relations to conventional nodal coupling formulations.[18]

2.5 Summary

In this chapter, a set of time-dependent nodal equations based on multigroup diffusion theory were derived from a response matrix approach for a global problem consisting of a regular array of two-dimensional rectangular homogeneous zones. The equations are written only in terms of nodal average fluxes and interface average partial currents. The spatial coupling scheme is of the nearest neighbor type, but nonlinear terms have been introduced in the highest order of approximation in order to achieve this particular formulation.

Chapter 3

STATIC APPLICATIONS

3.1 Introduction

In Chapter 2, a set of time-dependent, spatially-discretized nodal equations was derived for solution of the multigroup diffusion equations for a two-dimensional reactor consisting of rectangular, homogeneous (or homogenized) zones. In this chapter, the set of time-dependent equations is reduced to the conventional static eigenvalue problem. Numerical solution techniques are discussed and results are presented for a number of one- and two-dimensional problems. The method has been applied only to thermal reactor problems using a two-group formulation. However, the proposed scheme is capable of treating a general energy group structure. Also, as in the derivation of Chapter 2, only two-dimensional problems in rectangular geometry are considered.

3.2 Reduction of the Spatially-Discretized Time-Dependent Nodal Equations to the Static Case

In order to formulate the static problem, all time derivatives in the nodal balance equations, Eq. (2.13), and leakage response equations, Eq. (2.15), are set equal to zero. The resulting expressions for the delayed precursors obtained from Eqs. (2.13b) and (2.15b) are used to eliminate the delayed precursors from the flux and current equations, Eqs. (2.13a) and (2.15a). This procedure gives the spatially-discretized, static system of equations analogous to the spatially-dependent formulation of Eq. (1.2).

The system of static nodal equations is composed of the nodal balance equations

$$\sum_{\substack{u=x,y \\ v\neq u}} \frac{h_{\ell}^{v}}{V_{ij}} \left[J_{g,ij}^{in,-} - J_{g,ij}^{out,u-} + J_{g,ij}^{in,u+} - J_{g,ij}^{out,u+} \right] - \Sigma_{rg,ij}\phi_{g,ij}$$

$$+ \sum_{g'=1}^{G} \left[\delta_{g'\neq g}\Sigma_{gg',ij} + \chi_g \frac{\nu}{\gamma} \Sigma_{fg',ij} \right] \phi_{g,ij} = 0 \qquad (3.1a)$$

and the leakage response equations

$$\left(\left[R_{g,ij}^{out} \right] + \left[L_{g,ij}^{out,flat} \right] + \left[L_{g,ij}^{out,shape} \right] \right) \left[J_{g,ij}^{out} \right]$$

$$+ \left(\left[R_{g,ij}^{in} \right] + \left[L_{g,ij}^{in,flat} \right] + \left[L_{g,ij}^{in,shape} \right] \right) \left[J_{g,ij}^{in} \right] + \left[R_{g,ij}^{\phi} \right] \phi_{g,ij}$$

$$+ \sum_{g'=1}^{G} \left\{ \left(\left[T_{gg',ij}^{out} \right] + \frac{\chi_g}{\gamma} \left[P_{g',ij}^{out} \right] \right) \left[J_{g',ij}^{out} \right] \right.$$

$$+ \left(\left[T_{gg',ij}^{in} \right] + \frac{\chi_g}{\gamma} \left[P_{g',ij}^{in} \right] \right) \left[J_{g',ij}^{in} \right]$$

$$\left. + \left(\left[T_{gg',ij}^{\phi} \right] + \frac{\chi_g}{\gamma} \left[P_{g',ij}^{\phi} \right] \right) \phi_{g',ij} \right\} = 0 \qquad (3.1b)$$

for

$$g = 1, 2, \ldots G$$

$$\left.\begin{matrix} i = 1, 2, \ldots I \\ j = 1, 2, \ldots J \end{matrix}\right\} \quad (ij) \in \mathcal{R}.$$

The notation $(ij) \in \mathcal{R}$ indicates that the coordinate indices are over only sets (ij) which indicate nodes within the spatial domain of the reactor. This type of notation is used because we allow an irregular spatial

domain. The total number of nodes will be denoted as $L_{\mathcal{R}}$. The nodal equations are not complete without the nodal interface continuity condition, which stated nonmathematically, is that a J_g^{in} on a nodal interface is equal to the J_g^{out} on that interface of the adjacent node which shares the interface. Finally, the static nodal equations are completed by the specification of the reactor boundary conditions in terms of interface average partial currents. A general boundary condition can be written in terms of albedo conditions[33] such that for a node face comprising a segment of the reactor boundary

$$J_g^{in} = \sum_{g=1}^{G} \alpha_{gg'} J_{g'}^{out} \qquad (3.2)$$

where the albedos (α's) may depend on the location of the particular boundary segment. For instance, the zero entering partial current condition is given by

$$\alpha_{gg'} = 0; \qquad \text{for all } gg'$$

and the reflective symmetry condition is given by

$$\alpha_{gg'} = \delta_{g'=g}.$$

With the application of partial current continuity and the reactor boundary conditions, the total number of unknowns for "N" dimensions in Cartesian geometry is $(1 + 2N) \times G \times L_{\mathcal{R}}$. The factor $(1 + 2N)$ is derived from the fact that there is one nodal average flux per group per node and two interface average leakage partial currents per coordinate direction per group per node. Thus for two-dimensional rectangular geometry, $(N = 2)$, there are 5 unknowns per group per node.

The solution of the system of nodal equations for the largest eigenvalue γ (the "k-effective" of the reactor) and the corresponding fundamental flux-current mode is addressed in the next section.

3.3 Numerical Solution of the Static Eigenvalue Problem

3.3.1 General Formulation

We write the static nodal equations, Eqs. (3.1), in the matrix form

$$[A][\psi] = \frac{1}{\gamma}[\chi][B]^T[\psi] \tag{3.2}$$

where the major block partitioning of these matrices is by the energy group structure, and the group submatrices contain the spatial detail within each energy group. The submatrix form of Eq. (3.2) is

$$\begin{bmatrix} A_{11} & A_{12} & \cdots & A_{1G} \\ A_{21} & A_{22} & & \\ \vdots & & \ddots & \\ A_{G1} & & & A_{GG} \end{bmatrix} \begin{bmatrix} \psi_1 \\ \psi_2 \\ \vdots \\ \psi_G \end{bmatrix} = \begin{bmatrix} \chi_1 I \\ \chi_2 I \\ \vdots \\ \chi_G I \end{bmatrix} \begin{bmatrix} B_1 & B_2 & \cdots & B_G \end{bmatrix} \begin{bmatrix} \psi_1 \\ \psi_2 \\ \vdots \\ \psi_G \end{bmatrix}. \tag{3.3}$$

These submatrices are defined as

$[\psi_g] \equiv$ column vector of nodal average fluxes and interface average partial currents in group g

$$[A_{gg'}] \equiv \begin{cases} \text{for } g' = g, \text{ the spatial diffusion-removal operator for group } g \\ \text{for } g' \neq g, \text{ the spatial group transfer (scattering) operator for group } g' \text{ to group } g \end{cases}$$

$[\chi_g I] \equiv$ the group g fission spectrum times the identity matrix

$[B_g] \equiv$ the spatial fission production operator for group g.

We rewrite Eq. (3.2) as

$$\gamma[\psi] = [Q][\psi] \tag{3.4}$$

where

$$[Q] \equiv [A]^{-1}[\chi][B]^T. \tag{3.5}$$

The discrete static eigenvalue problem is then to determine the largest (in modulus) eigenvalue of the operator [Q] and its corresponding eigenvector $[\psi]$. The numerical solution of this eigenvalue problem is discussed in the following section.

3.3.2 Fission Source Iterations

We shall assume that the eigenvalues of [Q], Eqs. (3.4) and (3.5), are such that there is a simple, real eigenvalue, largest in modulus. With these assumptions, we apply the power method[11,34] to Eq. (3.4) in order to obtain approximations to the fundamental eigenvalue and eigenvector of [Q]. The power method, which essentially consists of repeated operation by [Q], is guaranteed to converge to the fundamental mode under the specified assumptions. The power iterations are referred to as "fission source" iterations, or alternatively, in multidimensional geometries when additional lower levels of iteration are employed, as "outer iterations."

Also, we use Chebyshev polynomials to accelerate the convergence of the outer iterations.[8,34] The acceleration strategy we employ uses

the additional assumptions that the eigenvalue spectrum of [Q] is real and nonnegative and that the corresponding eigenvectors form a basis for the associated vector space.

No attempt has been made to prove the validity of these assumptions theoretically. However, the proper predicted numerical behavior has been observed with the application of the Chebyshev-accelerated power iterations to our nodal equations.

It can be seen from Eqs. (3.4) and (3.5) that, for application of the power method, the inverse of the diffusion-removal-transfer operator, [A], on the fission source $[\chi][B]^T[\psi]$ must be found. For problems with no upscattering, the inversion can be effectively performed by a single sweep down through the energy group structure because of the lower diagonal structure of the blocks comprising [A] for this particular case. We shall treat only problems with no upscattering in this work and, therefore, shall use the procedure noted here.

To carry out this procedure, within each energy group it is necessary to solve a spatial problem of the form

$$[A_{gg}][\psi_g] = [S_g] \tag{3.6}$$

where

$$[S_g] \equiv \sum_{g'=1}^{g-1} [A_{gg'}][\psi_{g'}] + \chi_g \sum_{g'=1}^{G} [B_{g'}][\psi_{g'}]. \tag{3.7}$$

The total group source, $[S_g]$, is known. Thus a one-group fixed source problem must be solved within each group. The solution of this within-group spatial problem is discussed in the following section.

3.3.3 Within-Group Spatial Solutions

3.3.3.1 Flux Condensation

We partition the within-group spatial problem, Eq. (3.6), by fluxes and currents to give

$$\begin{bmatrix} A_{gg}^{JJ} & A_{gg}^{J\phi} \\ A_{gg}^{\phi J} & A_{gg}^{\phi\phi} \end{bmatrix} \begin{bmatrix} J_g \\ \phi_g \end{bmatrix} = \begin{bmatrix} S_g^J \\ S_g^\phi \end{bmatrix} \tag{3.8}$$

where

$[J_g] \equiv$ column vector of interface average currents in group g

$[\phi_g] \equiv$ column vector of nodal average fluxes in group g.

The submatrix equation

$$\left[A_{gg}^{\phi J}\right][J_g] + \left[A_{gg}^{\phi\phi}\right][\phi_g] = \left[S_g^\phi\right] \tag{3.9}$$

are the nodal balance equations, Eqs. (3.1a), for group g, and the submatrix equation

$$\left[A_{gg}^{JJ}\right][J_g] + \left[A_{gg}^{J\phi}\right][\phi_g] = \left[S_g^J\right] \tag{3.10}$$

are the leakage response equations, Eqs. (3.1b), for group g where $\left[S_g^\phi\right]$ and $\left[S_g^J\right]$ are the total group sources due to fission and scattering. As can be seen from the nodewise form of the balance equation, Eq. (3.1a), the structure of $\left[A_{gg}^{\phi\phi}\right]$ of Eq. (3.9) is scalar diagonal where the diagonal elements are total removal terms. Thus, $\left[A_{gg}^{\phi\phi}\right]$ is easily inverted and $[\phi_g]$ can be eliminated from the leakage current response equations, Eq. (3.10), giving a system in terms of currents only. Also, only

currents on the faces of a single node are coupled in each scalar balance or leakage current equation. Thus, the elimination of the nodal flux from the leakage current equations does not modify the spatial coupling scheme of the leakage current equations. This condensation procedure in terms of the submatrix equations is given by the flux solution

$$[\phi_g] = \left[A_{gg}^{\phi\phi}\right]^{-1} \left(-\left[A_{gg}^{\phi J}\right][J_g] + \left[S_g^{\phi}\right]\right) \tag{3.11}$$

and the condensed leakage current equations

$$\left[\tilde{A}_{gg}^{JJ}\right][J_g] = \left[\tilde{S}_g^{J}\right] \tag{3.12}$$

where

$$\left[\tilde{A}_{gg}^{JJ}\right] = \left[A_{gg}^{JJ}\right] - \left[A_{gg}^{J\phi}\right]\left[A_{gg}^{\phi\phi}\right]^{-1}\left[A_{gg}^{\phi J}\right] \tag{3.13}$$

and

$$\left[\tilde{S}_g^{J}\right] = \left[S_g^{J}\right] - \left[A_{gg}^{J\phi}\right]\left[A_{gg}^{\phi\phi}\right]^{-1}\left[S_g^{\phi}\right] \tag{3.14}$$

Equation (3.12) is to be solved within each energy group for the current vector $[J_g]$ given the known source vector $\left[\tilde{S}_g^{J}\right]$. Because of the simple structure of the diffusion-removal leakage current operator, $\left[\tilde{A}_{gg}^{JJ}\right]$ of Eq. (3.12), this problem can be solved efficiently in one dimension by direct means. The complications introduced in the two-dimensional case make it necessary to apply iterative solution techniques to this problem. The solution procedures for one and two dimensions are discussed in Sec. 3.3.3.2 and Sec. 3.3.3.3, respectively.

3.3.3.2 Solution in One Dimension

In order to formulate the one-dimensional nodal equations, we delete all currents associated, for instance, with the y direction in the nodal equations, Eq. (3.1). It should be noted that this procedure completely eliminates the transverse leakage terms from the leakage response equations, Eq. (3.1b). All matrix operators and solution vectors appearing in the leakage current equations are reduced from an order of four to an order of two. Also, appropriate modifications must be made to the nodal geometrical factors in order to achieve a consistent set of one-dimensional equations.

We partition the currents for group g by node with the vector defined by

$$[J_{g,i}] \equiv \begin{bmatrix} J^{out,x-}_{g,i} \\ J^{out,x+}_{g,i} \end{bmatrix}; \qquad i = 1,2,\ldots I. \tag{3.15}$$

With a consecutive numbering of the nodes, we form the group g current vector by using the nodal vectors of Eq. (3.15). The current vector for group g is given by

$$[J_g] \equiv \begin{bmatrix} J_{g,1} \\ J_{g,2} \\ \vdots \\ J_{g,I} \end{bmatrix}. \tag{3.16}$$

For this ordering of unknowns, the matrix $\left[\tilde{A}^{JJ}_{gg}\right]$ of Eq. (3.12) is

block tridiagonal where the submatrices are scalar (2 × 2). The (i-1), (i), and (i+1) rows have a nonzero block structure shown below:

$$
\begin{array}{lccccc}
 & (i-2) & (i-1) & (i) & (i+1) & (i+2) \\
(i-1) & \begin{bmatrix} 0 & x \\ 0 & x \end{bmatrix} & \begin{bmatrix} x & x \\ x & x \end{bmatrix} & \begin{bmatrix} x & 0 \\ x & 0 \end{bmatrix} & & \\
(i) & & \begin{bmatrix} 0 & x \\ 0 & x \end{bmatrix} & \begin{bmatrix} x & x \\ x & x \end{bmatrix} & \begin{bmatrix} x & 0 \\ x & 0 \end{bmatrix} & \\
(i+1) & & & \begin{bmatrix} 0 & x \\ 0 & x \end{bmatrix} & \begin{bmatrix} x & x \\ x & x \end{bmatrix} & \begin{bmatrix} x & 0 \\ x & 0 \end{bmatrix}
\end{array}
$$

Furthermore, as can be seen from the diagram above, the nonzero scalar elements form a striped structure which is pentadiagonal (5-stripe). The block tridiagonal system or the scalar pentadiagonal system can be solved by means of generalized factorization techniques.[10,11] We apply a factorization scheme to the block tridiagonal form with special considerations given to the zero elements of the submatrices.

3.3.3.3 Solution in Two Dimensions

3.3.3.3.1 Inner Iterations

We find that the extension of the nodal equations to more than one dimension results in a spatial coupling scheme for the within-group spatial equations such that the determination of a matrix structure for $\left[\tilde{A}^{JJ}_{gg}\right]$ of Eq. (3.12) which lends itself to efficient use of direct inversion procedures does not seem feasible. Thus we resort to iterative techniques for the solution of the within-group spatial problem. These

iterations are referred to as "inner" iterations. In particular, we use Chebyshev polynomial semi-iterative schemes[10, 12, 35] applied to block partitionings of the matrix equations. By application to block partitionings, we imply that groups of unknowns are solved for simultaneously by direct means.[10]

We consider two block partitionings of the matrix structure. The first scheme is referred to as the "Row-Column" (RC) structure. This block structure permits the simultaneous solution for currents directed along rows and columns and the solution procedure is essentially the extension of the one-dimensional method to a set of directionally-coupled equations with a dominant one-dimensional character. The second scheme is referred to as the "Response Matrix" (RM) structure. All leakage currents of a single node are solved for simultaneously which results in a formulation similar to that of the conventional response matrix procedure.[18]

In the application of the Chebyshev polynomial iterative methods to both block structures, iteration parameters that optimize the convergence rates can be determined if the spectral radius of the associated Jacobi iteration matrix, denoted here as r_J, is known.[10, 12, 35] This parameter is predetermined using power iterative techniques applied to the Jacobi matrix, or corresponding Gauss-Seidel matrix, before the start of the outer iterations.[10, 34] In addition, assumptions made in the application of these iteration procedures are that the eigenvalues of the Jacobi matrix are real and distributed on the interval $[-r_J, r_J]$, and that the corresponding eigenvectors include a basis for the associated

vector space.[10, 12, 35]

A fixed number of inner iterations are done per outer iteration. This number is determined such that the spectral norm of the continued product of iteration matrices is less than some desired error reduction factor. The spectral norm expressions are in terms of the spectral radius of the Jacobi matrix and make the assumption that this matrix is Hermitian.[10] The error reduction criterion is chosen such that a proper balance is obtained between the number of outer iterations (insufficient convergence of the inners slows outer iteration convergence[8]) and number of inner iterations per outer iteration in order to minimize overall computational time.

3.3.3.3.2 The "Row-Column" Block Iterative Method

We form the solution vector by partitioning the leakage currents of each node as

$$\left[J^{x}_{g,ij}\right] \equiv \begin{bmatrix} J^{out,x-}_{g,ij} \\ \\ J^{out,x+}_{g,ij} \end{bmatrix} \tag{3.17a}$$

$$\left[J^{y}_{g,ij}\right] \equiv \begin{bmatrix} J^{out,y-}_{g,ij} \\ \\ J^{out,y+}_{g,ij} \end{bmatrix}; \qquad \left.\begin{matrix} i = 1,2,\ldots I \\ j = 1,2,\ldots J \end{matrix}\right\} \qquad (ij) \in \mathcal{R}$$

and using these nodal partitions to form the row- and column-associated vectors

$$\left[J^{r}_{g,j}\right] \equiv \begin{bmatrix} J^{x}_{g,1j} \\ J^{x}_{g,2j} \\ \cdot \\ \cdot \\ \cdot \\ J^{x}_{g,Ij} \end{bmatrix}; \qquad j = 1,2,\ldots J \tag{3.18a}$$

$$\left[J^{c}_{g,i}\right] \equiv \begin{bmatrix} J^{y}_{g,i1} \\ J^{y}_{g,i2} \\ \cdot \\ \cdot \\ \cdot \\ J^{y}_{g,iJ} \end{bmatrix}; \qquad i = 1,2,\ldots I. \tag{3.18b}$$

From the row- and column-associated vectors of Eq. (3.18), we now form vectors of all row-directed and column-directed unknowns which are given by

$$\left[J^{r}_{g}\right] \equiv \begin{bmatrix} J^{r}_{g,1} \\ J^{r}_{g,2} \\ \cdot \\ \cdot \\ \cdot \\ J^{r}_{g,J} \end{bmatrix} \tag{3.19a}$$

$$\left[J^{c}_{g}\right] \equiv \begin{bmatrix} J^{c}_{g,1} \\ J^{c}_{g,2} \\ \cdot \\ \cdot \\ \cdot \\ J^{c}_{g,I} \end{bmatrix}. \tag{3.19b}$$

With this notation, the block partitioning of Eq. (3.12) which we employ is

$$\begin{bmatrix} \tilde{A}^{rr}_{gg} & \tilde{A}^{rc}_{gg} \\ \tilde{A}^{cr}_{gg} & \tilde{A}^{cc}_{gg} \end{bmatrix} \begin{bmatrix} J^{r}_{g} \\ J^{c}_{g} \end{bmatrix} = \begin{bmatrix} \tilde{S}^{r}_{g} \\ \tilde{S}^{c}_{g} \end{bmatrix}. \tag{3.20}$$

If the explicit form of the leakage response equations, Eq. (2.14a), is examined, it is found that rows and columns of currents are coupled only by the transverse leakage terms (regardless of whether the treatment of shape correction factors is linear or nonlinear). Thus the diagonal blocks of Eq. (3.20) can be formulated as one-dimensional diffusion-removal spatial operators with the off-diagonal blocks containing only transverse leakage factors. The diagonal blocks have a block diagonal submatrix structure with each submatrix being the one-dimensional diffusion-removal operator (see Sec. 3.3.3.2) for a particular row or column. Thus, the diagonal blocks of Eq. (3.20) can be directly inverted by applying a factorization technique to the diagonal submatrices. This procedure results in the simultaneous solution of all currents in one direction with an iteration between directions. The cyclic Chebyshev semi-iterative method[10,12,35] (CCSI) is used to accelerate the iteration between directions. It should be noted that the CCSI method is only applicable to the particular block (2 × 2) structure as in Eq. (3.20).

3.3.3.3.3 The "Response Matrix" Block Iterative Method

We now return to the nodewise formulation of the leakage response equations, Eq. (3.1b), with the total group source and flux condensation notation introduced. The leakage response equation for group g and node (ij) is

$$-\left(\left[\tilde{R}^{out}_{g,ij}\right]+\left[\tilde{L}^{out,\,flat}_{g,ij}\right]+\left[L^{out,\,shape}_{g,ij}\right]\right)\left[J^{out}_{g,ij}\right]$$

$$-\left(\left[\tilde{R}^{in}_{g,ij}\right]+\left[\tilde{L}^{in,\,flat}_{g,ij}\right]+\left[L^{in,\,shape}_{g,ij}\right]\right)\left[J^{in}_{g,ij}\right]=\left[\tilde{S}^{J}_{g,ij}\right]. \qquad (3.21)$$

Let us now consider certain aspects of the transverse leakage shape correction terms. First, note that the flux condensation has been formulated such that the transverse leakage shape correction matrices, $[L^{shape}]$, are not modified by the condensation procedure. Thus, the constant transverse leakage approximation can be obtained by setting the $[L^{shape}]$'s equal to the null matrix. It should also be recalled that these matrices are nonlinear. This is because information from surrounding nodes regarding the spatial shape of the current is incorporated into the $[L^{shape}]$. However, the product of these matrices with the nodal leakage and incident current vectors, as in Eq. (3.21), gives a linear expression for the transverse leakage shape correction. This

expression involves currents of neighboring nodes on interfaces not common to the node for which the leakage response equations apply. Thus, the spatial coupling scheme is somewhat more extensive in the linear formulation of the transverse leakage shape correction. In order to minimize the extent of the spatial coupling of the currents, we could use information from the preceding outer iteration to generate $[L^{shape}]$'s which would then be held constant for solution of the inner iteration problem. The alternative is to use the linear expression for the transverse leakage shape correction and directly treat the increased spatial coupling in the iteration scheme. We convert Eq. (3.21) into the final form we desire for computation and then discuss these options further.

We rewrite Eq. (3.21) as

$$-\left(\left[\tilde{R}^{out}_{g,ij}\right] + \left[\tilde{L}^{out,\,flat}_{g,ij}\right] + \theta\left[L^{out,\,shape}_{g,ij}\right]\right)\left[J^{out}_{g,ij}\right]$$

$$= \left(\left[\tilde{R}^{in}_{g,ij}\right] + \left[\tilde{L}^{in,\,flat}_{g,ij}\right] + \theta\left[L^{in,\,shape}_{g,ij}\right]\right)\left[J^{in}_{g,ij}\right] + \left[\tilde{S}^{J}_{g,ij}\right]$$

$$+ (1-\theta)\left(\left[L^{in,\,shape}_{g,ij}\right]\left[J^{in}_{g,ij}\right] - \left[L^{out,\,shape}_{g,ij}\right]\left[J^{out}_{g,ij}\right]\right) \qquad (3.22)$$

where θ is a parameter restricted to the interval $[0, 1]$. Inverting the left-hand side of Eq. (3.22) and considering the entire nodal system, we form the within-group set of leakage response equations

$$\left[J^{out}_{g,ij}\right] = \left[\tilde{H}^{J}_{g,ij}\right]\left[J^{in}_{g,ij}\right] + \left[\tilde{H}^{S}_{g,ij}\right]\left\{\left[\tilde{S}^{J}_{g,ij}\right] + (1-\theta)\left(\left[L^{in,\,shape}_{g,ij}\right]\left[J^{in}_{g,ij}\right] + \left[L^{out,\,shape}_{g,ij}\right]\left[J^{out}_{g,ij}\right]\right)\right\};$$

$$\left.\begin{matrix} i = 1,2,\ldots I \\ j = 1,3,\ldots J \end{matrix}\right\} \quad (ij) \in \mathcal{R} \qquad (3.23)$$

where

$$\left[\tilde{H}^{S}_{g,ij}\right] \equiv -\left(\left[\tilde{R}^{out}_{g,ij}\right] + \left[\tilde{L}^{out,\,flat}_{g,ij}\right] + \theta\left[L^{out,\,shape}_{g,ij}\right]\right)^{-1} \qquad (3.24)$$

$$\left[\tilde{H}^{J}_{g,ij}\right] \equiv \left[\tilde{H}^{S}_{g,ij}\right]\left(\left[\tilde{R}^{in}_{g,ij}\right] + \left[\tilde{L}^{in,\,flat}_{g,ij}\right] + \theta\left[L^{in,\,shape}_{g,ij}\right]\right) \qquad (3.25)$$

along with the conditions of interface current continuity and appropriate boundary restraints. We now discuss our use of the parameter θ in relation to the adoption of linear or nonlinear solution schemes.

For the nonlinear form of the transverse leakage shape correction, in which the matrices $[L^{shape}]$ are nonlinear and are evaluated using data from a preceding outer iteration, we choose θ equal to one. Equation (3.23) then has the standard form of a one-group response matrix equation for a fixed source problem with a single current mode per interface.[18] The current response operator $[\tilde{H}^{J}]$ gives the average leakage response to average incident currents and the source response operator $[\tilde{H}^{S}]$ gives the average leakage response to averaged components of

a distributed volume source. In this procedure the response matrices, $[\tilde{H}^J]$ and $[\tilde{H}^S]$, are improved each outer iteration in order to incorporporate effects of the current spatial shape.

If the $[L^{shape}]$ are set equal to the null matrix in order to obtain the constant transverse leakage approximation, the spatial coupling pattern of the response equations, Eq. (3.23), is seen to be the same as when θ is equal to one and the nonlinear $[L^{shape}]$ are used. If we consider an unknown block to be the leakage currents of a single node, the five-point coupling pattern shown below results.

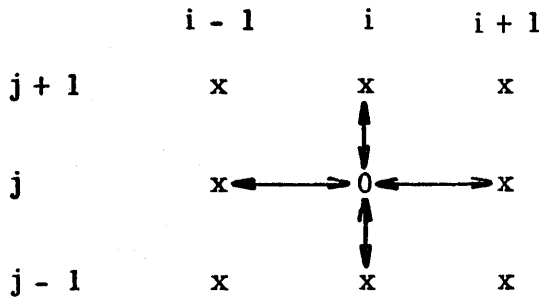

We now take advantage of this coupling pattern to form a block iterative method in which half of the spatial unknowns are treated simultaneously at each step of the iteration procedure.

Consider a mesh numbering scheme in which we classify nodes into two types, 1 and 2, as shown below:

	i - 1	i	i + 1
j + 1	(1)	(2)	(1)
j	(2)	(1)	(2)
j - 1	(1)	(2)	(1)

where the pattern is assumed to repeat throughout the mesh structure.

We use the fact that in the five-point scheme, nodes of type 1 are connected only to nodes of type 2 and vice versa. We form the vectors

$$\left[J_g^n\right] \equiv \begin{bmatrix} \cdot \\ \cdot \\ \cdot \\ J^{out}_{g,ij} \\ \cdot \\ \cdot \\ \cdot \end{bmatrix}; \qquad \begin{array}{l} (ij) \in \mathcal{R} \\ (ij) = \text{type } n \\ n = 1, 2 \end{array} \tag{3.26}$$

and from these type 1 and type 2 vectors, we construct the solution vector

$$[J_g] \equiv \begin{bmatrix} J_g^1 \\ \\ J_g^2 \end{bmatrix}. \tag{3.27}$$

The block form of Eq. (3.12) becomes

$$\begin{bmatrix} \tilde{A}^{11}_{gg} & \tilde{A}^{12}_{gg} \\ \\ \tilde{A}^{21}_{gg} & \tilde{A}^{22}_{gg} \end{bmatrix} \begin{bmatrix} J_g^1 \\ \\ J_g^2 \end{bmatrix} = \begin{bmatrix} \tilde{\tilde{S}}^1_g \\ \\ \tilde{\tilde{S}}^2_g \end{bmatrix} \tag{3.28}$$

where we have assumed that the response formulation of Eq. (3.23) has been used to construct the submatrices $\left[\tilde{A}^{nn'}\right]$ and that the operations by the source response matrices, Eq. (3.24), have been performed as shown in Eq. (3.23) in order to form the $[\tilde{\tilde{S}}]$ of Eq. (3.28).

By inspection of Eq. (3.23), we find that the diagonal blocks of Eq. (3.28) are identity matrices. All response elements, Eq. (3.25), are incorporated in the off-diagonal blocks of Eq. (3.28). Thus all nodes of type n can be solved simultaneously by matrix multiplications of response operators into leakage current vectors of type n' nodes. The

spatial iteration is between type 1 and type 2 nodes. The cyclic Chebyshev semi-iterative (CCSI) method[10, 12, 35] can be used to accelerate this block iterative scheme.

We now consider the linear form of the transverse leakage shape correction in which the linear expression resulting from the $[L^{shape}][J]$ product is used. Because the spatial coupling of the currents is more extensive than that of just the faces of a single node, the response matrices of Eq. (3.24) and Eq. (3.25) cannot be generated directly. Therefore we set θ equal to zero. The form of Eq. (3.23) with θ equal to zero suggests that we will use the transverse leakage shape correction terms as a source in order to calculate the leakage from a single node. This is exactly the case as will be shown in the description of the iteration procedure we consider for solution of these equations. Note that once again the interpretation of the $[\tilde{H}]$'s as response matrices is valid. However, these response matrices are based on the assumption of a constant spatial shape for the transverse leakage.

The spatial coupling pattern for the linear formulation of the quadratic transverse leakage approximation with a block structure consisting of leakage currents from a single node is

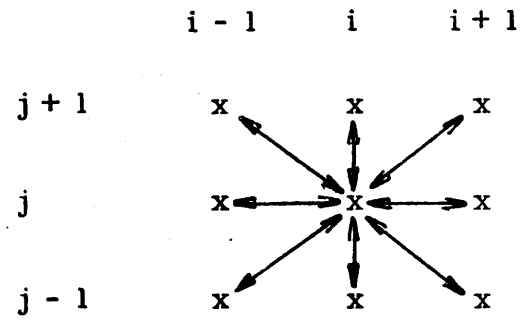

which is a "nine-point" scheme. We find that it is not practical to use the block partitioning of Eq. (3.28) in this case because the submatrix form of the diagonal blocks is too complicated (type-n nodes are coupled to other type-n nodes) to be effectively handled by direct inversion. Moreover, we find no multinode block partitionings which appear to be computationally efficient. Thus we resort to block iterative schemes in which the basic block consisting of the leakage currents of a single node is the largest partition treated directly.

In Varga's terms,[10] the nine-point coupling scheme is not two-cyclic. Thus successive overrelaxation (SOR) parameters based on factors which we can estimate numerically (for instance, the spectral radius of the Jacobi matrix) and which optimize the rate of convergence are not known. Therefore we must resort to the Chebyshev semi-iterative (CSI) method[10,12,35] which does not require the two-cyclic condition for its application. However, the CSI method has an asymptotic rate of convergence half that of the SOR or CCSI methods when applicable to the same matrix structure,* and, in addition, requires extra storage.

The basic iteration scheme is essentially one in which all nodes are advanced using Eq. (3.23) with unknowns that appear on the right-hand side evaluated using data from the preceding inner iteration. The CSI method accelerates this basic iteration scheme. This same technique could be employed with the previously discussed five-point scheme. However, since we would be dealing with the direct solution of much

---

*The SOR and CCSI methods have the same asymptotic rate of convergence. However, the CCSI method has a greater average rate of convergence. Thus we choose the CCSI method when applicable.

smaller unknown partitions as well as with a more slowly convergent iterative scheme, that application would be counterproductive.

We choose the linear formulation of the quadratic transverse leakage shape corrections for computation. As we have seen, the iterative technique applicable for solution of this formulation of the equations is not as powerful as that available for solution of the nonlinear formulation. However, in the nonlinear formulation the response matrices must be frequently updated (for instance, every outer iteration in the scheme we proposed). The calculational expense of forming the response matrices can be quite high and we desire to minimize the frequency with which they are recalculated. Also, inclusion of effects of the spatial shape of the current in the response matrices destroys all symmetry properties and consequently increases core storage requirements considerably.

In both the constant and quadratic transverse leakage schemes, boundary conditions are handled by adding nodes at the reactor boundary with response matrices that are albedos for the appropriate symmetry or vacuum conditions. This is done because the incorporation of boundary conditions into the actual nodal response matrices adds asymmetries that complicate the response matrix calculations and increase the storage requirements for the response elements.

For the linear schemes we have selected, the response matrices are dependent only on groupwise material properties and the geometrical configuration of a single node. These matrices are precalulated before the start of the outer iterations. The necessary matrix inversions are performed by considering successive subdivisions of the matrices into (2×2) systems and employing analytic expressions for a block (2×2) matrix inverse. Advantage is taken of symmetry in the response elements in order to reduce storage requirements.

3.3.3.3.4 Comparison of the Numerical and Computational Aspects of the Proposed Block Iterative Schemes

For notational convenience, we shall denote the row-column block iterative methods using the constant and quadratic transverse leakage approximations as the RC-C and RC-Q methods, respectively. Likewise, the response matrix block iterative methods with the two transverse leakage approximations are denoted as RM-C and RM-Q.

We first discuss the physical aspects of the RC partitioning as compared to the RM partitioning which affect convergence behavior. Then, we briefly discuss general numerical considerations of size of block structure and acceleration techniques. Finally, we review some operational details concerning implementation of these methods on a computer.

In LWR's with assembly-size nodes where the neutron mean-free path is quite short compared to the node size, we expect reflection to dominate the leakage current response system. Thus a direct treatment of the coupled reflective components on nodal interfaces is preferred. The RC partitioning treats all the components of reflection and transmission from a node face to the opposing face simultaneously. Side transmission is handled iteratively. In the RM partitioning, transmission is treated directly; however, the coupling of the reflective components on nodal interfaces is dealt with iteratively. Therefore we expect the RC block partitioning to converge more rapidly than the RM block partitioning in our applications to thermal systems.

It has been found that in general the convergence rates of iterative schemes increase with use of larger block partitionings in which greater

portions of the problem are solved simultaneously. The RC-C, RC-Q, and RM-C methods solve for half of the spatial unknowns simultaneously. The RM-Q method solves simultaneously only for the unknowns of a single node. Also, the RM-Q method employs the CSI acceleration scheme which, for the same block structure, is more slowly convergent than the CCSI or SOR acceleration techniques. Thus, from numerical considerations alone we would expect the RM-Q method to be more slowly convergent than the other methods.

Because of the physical arguments stated above along with the numerical points just discussed, we expect the schemes to be ordered with respect to increasing rate of convergence as the RM-Q method, the RM-C method, and the RC methods. We see no apparent reasons why the convergence behavior of the RC-C method should differ considerably from that of the RC-Q method. This general behavior has been verified from observations of the numerically estimated spectral radius of the inner iteration matrix.

The details of implementation of the RC and RM schemes are quite different. The RC method requires inversion of block (2×2) tridiagonal or scalar pentadiagonal systems of equations. The matrices can be prefactorized before the outer iterations begin and a forward elimination-backward substitution procedure used to determine the unknown solution vector. This type of procedure must be done for each row and column of the spatial problem during one inner iteration.

The RM method requires the generation of within-group nodal response matrices. These can be precalculated and stored before the

outer iterations start. The calculation of these matrices can prove to be rather expensive since matrix inversion is involved. Symmetry properties of the response elements can be used to reduce significantly the storage requirements. Compared to the RC method, the operations necessary to do an inner iteration are much less complicated. For each node, only simple matrix multiplications are necessary to advance the solution.

In conclusion, we expect that the convergence rates for the RC methods per iteration are greater than those of the RM methods, but the RM methods have a higher computational efficiency per iteration. The balance between convergence and efficiency has not been quantified and will be investigated numerically in a later section.

3.3.3.4 Extension to Three Dimensions

The block partitioning of the three-dimensional problem into the row-column (RC) type format is straightforward. Rather than just treating the coupled set of x- and y-directed one-dimensional problems in the plane, we now solve a coupled set of x-, y-, and z-directed one-dimensional problems. The matrix structure shown in Eq. (3.20) becomes block (3 × 3) where the block partitioning is once again by coordinate direction. Unfortunately, the block (3 × 3) matrix does not have the proper numerical properties in order to apply the CCSI or SOR (with rigorously determined optimum over-relaxation parameters) acceleration schemes (in Varga's[10] terms, the block partitioned matrix is not two-cyclic). However, the CSI shceme could be employed. Another problem

with the extension to three dimensions of the RC methods is that the requirement of sweeps of the mesh in all coordinate directions could present a severe data-handling problem.

The extension of the RM methods to three dimensions is readily done. The only apparent problems are the additional cost of generating response matrices (6×6 matrices must be manipulated) and the development of efficient data management strategies.

3.3.4 Computer Codes – Applications and Comparisons

Computer codes were written to solve the one- and two-dimensional nodal equations. Numerical methods as discussed in previous sections of this chapter were implemented.

For two dimensions, separate codes employing the RC-C, Q methods and the RM-C, Q methods have been written. Both codes are written in the IBM FORTRAN IV language except for some core storage allocation routines. The RC code is in double precision, the RM code in single precision. The RC code was compiled under the IBM Level-H compiler, the RM code under the Level-G compiler. Both compilations used full optimization procedures. All computation was done on an IBM 370/168 computer.

The RC code handles only one or two energy groups and uses regular geometry with uniform mesh spacing. The RM code uses a general multigroup structure limited to no upscattering and treats irregular geometry with a nonuniform mesh. The limitations of the RC code imply no general restrictions on the method, however.

It was found that the required error reduction for the inner iterations which minimized overall computation time was significantly greater for the RM method than for the RC method. An error reduction factor of 0.1 was chosen for the RC method, while the RM method required a value of 0.01. Possible reasons for this difference in required inner iteration error reduction are the violation of assumptions made for the matrix properties (specifically, the eigenvalue spectrum) in use of the acceleration procedures because of matrix asymmetries, or increased detrimental effects on outer iteration convergence of error modes introduced by lack of inner iteration convergence of the RM method as compared to that of the RC method. This matter has not yet been resolved.

Only the RM code has been documented and retained.[45] This is because, as will be seen later, only the RM method was extended to time-dependent analysis.

3.4 Results

3.4.1 Foreword

The static nodal method is applied to a number of one- and two-dimensional problems in this section. Complete test problem descriptions are given in Appendix 5.

Nodal solutions are compared with reference solutions which have been demonstrated to be essentially spatially converged. For a summary comparison of power distributions, we use the maximum error in region power and the power-weighted average of the region power errors. These errors are defined as the maximum error

$$\epsilon_{max} \equiv \underset{\text{all } r}{\text{maximum}} (\epsilon_r)$$

and the average error

$$\epsilon_{avg} \equiv \frac{\Sigma\ P_r \epsilon_r}{\Sigma\ P_r}$$

where P_r is the total power in region r and ϵ_r, the region power error for region r, is given by

$$\epsilon_r \equiv \frac{|P_r - P_r^{reference}|}{P_r^{reference}} \times 100.$$

Regionwise power distributions are given in Appendix 6.

3.4.2 One Dimension

3.4.2.1 Kang's One-Dimensional LWR Problem

This problem, which was originally solved by Kang and Hansen,[13] is a one-dimensional, two-region reactor with half-core symmetry. It consists of a homogeneous fuel region and a water reflector which are treated in two-energy groups. Material properties are typical of a LWR.

Results obtained with the nodal method for uniform mesh refinement are given in Table 3.1. Finite difference results for the corresponding mesh sizes are presented for comparison. The eigenvalue, thermal flux at the midline between the core center and core-reflector interface, and integral of the thermal flux over half of the reactor are given. The thermal flux has been normalized to unity at the core center. Calculations were done using half-core symmetry. Zero flux external boundary conditions were applied. A convergence criterion of 10^{-6} was imposed on the nodal average flux. The reference solution, which is a cubic Hermite finite element solution using a one-centimeter mesh spacing, as well as the finite difference results, are taken from Kang and Hansen.[13]

The nodal results display a rapid convergence to the reference solution with decreasing mesh size. Also, results for very large mesh spacings are accurate, which is our primary goal in this development. In terms of the prediction of the integral quantities of eigenvalue and integrated flux, the nodal method is clearly superior to the finite difference method in accuracy achieved for a given mesh size as well as number of unknowns required to achieve equivalent accuracy. For instance, the 20 cm nodal solution with 9 unknowns per group compared with the

Table 3.1 Results for Kang's One-dimensional LWR Problem

Mesh Spacing (cm)	Unknowns per Group	Eigenvalue (γ^{-1})	Pointwise Thermal Flux	Integrated Thermal Flux (% error)	Number of Fission Source Iterations
20	9 [3]	0.979983 [0.976582]	0.76340 [0.808877]	37.912 (1.5%) [49.416 (28.4%)]	20
10	18 [6]	0.979584 [0.976467]	0.79101 [0.812895]	38.449 (0.1%) [45.121 (17.3%)]	18
5	36 [12]	0.979528 [0.978038]	0.79132 [0.802046]	38.476 (0.01%) [36.772 (4.4%)]	18
2.5	72 [24]	0.979526 [0.979055]	0.79133 [0.794731]	38.478 (0.005%) [39.953 (3.8%)]	18
Reference		0.979526	0.79133	38.480	

[finite difference]

2.5 cm finite difference solution using 24 unknowns per group gives equivalent accuracy in eigenvalue and significantly better results for the integrated thermal flux.

The nodal thermal flux solutions obtained with the larger mesh sizes oscillate about the reference solution in the fuel and reflector regions near the core-reflector interface. This behavior accounts for the inferior pointwise flux result compared with the finite difference method with a 20 cm mesh. These oscillations are rapidly damped, however, with mesh spacing refinement. This behavior is graphically illustrated in Figs. A6.1a, A6.1b, and A6.1c of Appendix 6 in which the pointwise thermal flux of the 20, 10, and 5 cm nodal solutions are compared with the 2.5 cm nodal solution.

In summary, we find for this problem that the nodal method gives accurate predictions of integral properties with very large mesh sizes. However, irregularities in the pointwise solution may occur for these large mesh sizes in regions in which the spatial shape of the solution is rapidly varying, such as at the core-reflector interface for this problem. This behavior is not of great concern because we are principally interested in prediction of integral properties such as average region power distributions.

3.4.2.2 A One-Dimensional Version of the IAEA PWR Problem

This problem is a one-dimensional slice through the core of the IAEA two-dimensional benchmark problem.[5] The problem is a two-group model of an idealized PWR with multizone fuel loading. Local perturbations are severe because of the insertion of control rods and

the influence of the water reflector. The difficulty of this problem is indicated by the fact that a finite difference solution using a one-centimeter mesh spacing (170 unknowns per group in half-core symmetry) reported by Shober[36] was found to be in error with $\epsilon_{avg} = 0.8\%$ and $\epsilon_{max} = 1.5\%$ in comparison with his analytic solution.

Results obtained with the nodal method are summarized in Table 3.2 for a sequence of decreasing uniform mesh sizes. Regionwise power distributions are shown in Fig. A6.2a of Appendix 6. Calculations were done using half-core symmetry. Zero flux external boundary conditions were applied. A convergence criterion of 10^{-6} was imposed on the nodal average flux. The reference solution is Shober's analytic solution.

As in Kang's test problem, the assembly-size mesh (20 cm) nodal results are very accurate. A 10 cm mesh nodal solution with 51 unknowns per group is significantly more accurate in power distribution than the reported 1 cm mesh finite difference solution with 170 unknowns per group. Also, once again the nodal solution is seen to converge rapidly to the reference solution with decreasing mesh size. It is not known if the irregular spatial convergence behavior exhibited by the 2.5 cm solution is characteristic of oscillatory convergence behavior at small mesh sizes for the nodal method or is involved with some problem of numerical convergence or precision with these calculations or the reference calculation.

We find that the same type of oscillatory behavior in the shape of the thermal flux near the core-reflector interface occurs as reported for Kang's test problem. It is reasonable to expect that a more accurate

Table 3.2 Summary of Results for the One-dimensional Version of the IAEA PWR Problem: Uniform Mesh Refinement

Mesh Spacing	Number of Unknowns per Group	Eigenvalue	ϵ_{avg} (%)	ϵ_{max} (%)	Number of Fission Source Iterations
20	27	1.004208	1.7	3.0	56
10	51	1.004489	0.2	0.3	56
5	102	1.004514	.002	.003	56
2.5	204	1.004513	.003	.006	56
Reference		1.004513			

Table 3.3 Summary of Results for the One-dimensional Version of the IAEA PWR Problem: Improved Reflector Treatment

Mesh Layout	Number of Unknowns per Group	Eigenvalue	ϵ_{avg} (%)	ϵ_{max} (%)	Number of Fission Source Iterations
uniform 20 cm	27	1.004208	1.7	3.0	56
20 cm within core, reflector replaced by albedo	24	1.004425	0.5	1.5	56
20 cm within core, 10 cm in reflector and adjacent fuel assembly	33	1.004552	0.3	0.8	52
Reference		1.004513			

treatment of the reflector region would substantially increase the overall solution accuracy. We approach the problem in two ways. One approach is to replace the reflector by an analytic albedo condition.[33] The other approach is to decrease the mesh size in the reflector and adjacent fuel assembly. Results of calculations using a 20 cm mesh within the core with albedo or 10 cm mesh at the core-reflector interface are shown in Table 3.3. Regionwise power distributions are shown in Fig. A6.2b of Appendix 6. Calculational details are the same as used in the previously discussed solutions.

These results for the improved reflector treatment show a significant gain in solution accuracy over that of the uniform 20 cm solution. The mesh subdivision near the core-reflector interface shows greater improvement than just the replacement of the reflector with an albedo condition. In either case, the power distribution results are as accurate as the fine-mesh finite difference solution and require the use of much fewer unknowns (24 or 33 compared with 170 per group).

In summary, we find the nodal method to give good accuracy with an assembly-size mesh for this difficult problem. The method is shown to be superior to the finite difference method in terms of number of unknowns required for equivalent accuracy. It is also found that significant improvements can be made in the nodal solutions by improving the treatment of the reflector region.

3.4.2.3 Summary of One-Dimensional Results

The proposed nodal method has been shown to be accurate with the use of very large mesh spacings for one-dimensional LWR problems.

The method was found to be superior to the finite difference scheme both in terms of accuracy for the same mesh size and in terms of number of unknowns required to achieve equivalent accuracy.

Problems were encountered in the accurate prediction of pointwise quantities with the use of large mesh sizes because of difficulties in treating the region near the core-reflector interface. However, our primary objective is the determination of region averaged power distributions for which the method has been demonstrated to do well in one dimension with large mesh spacings. Also, it should be noted that with the averaging procedures applied in the derivation of the multidimensional method, that the regeneration of pointwise quantities has been somewhat obscured.

In conclusion, we found sufficient encouragement in these results for us to pursue the application of the two-dimensional method. It should be noted that even though the one-dimensional results are promising, the two-dimensional method includes an approximation for the spatial shape of a transverse leakage term not included in the one-dimensional scheme, and thus we cannot be assured of equally accurate results in two dimensions without further numerical experimentation.

3.4.3 Two Dimensions

3.4.3.1 Comparison of Iterative Schemes for the Inner Iterations

It should be recalled that in two dimensions a within-group spatial problem must be solved in each energy group during each outer iteration by iterative techniques. We proposed two iterative schemes in Sec. 3.3.3

known as the RC (row-column) and RM (response matrix) methods. These methods are implemented with both the constant and quadratic transverse leakage approximations (RC-C,Q and RM-C,Q). We now continue our discussion of Sec. 3.3.3.3.4 concerning the comparison of numerical and computational aspects of the proposed schemes by considering their application to a particular problem.

The problem we have chosen is the IAEA two-dimensional PWR benchmark.[5] Results given are for an assembly-size node (20 cm). Numerical performance of the solution techniques is summarized in Table 3.4. Solution accuracy will be discussed in a following section. We present the estimated spectral radius of the unaccelerated group iteration matrix, the number of inners required for adequate inner iteration error reduction, the number of outers, and associated solution times. It should be recalled that the RC and RM codes differ in their implementation on the computer, with the RC code in double precision and the RM code in single precision, but with the RC code having the advantage in compiler optimization. With these factors in mind, we compare the overall problem performance as to efficiency per iteration.

As was anticipated in our previous discussion, for this thermal system, the RC method outperforms the RM method with respect to expected rate of convergence when the iteration matrices are unaccelerated. We believe this behavior to be related to the fact that in thermal systems with large node size, reflection is the dominating influence in the numerical solution. The RC method treats coupled reflective components directly while the RM method uses an iterative treatment. Thus we expect

Table 3.4 Comparison of Iterative Solution Methods Applied to the IAEA Two-Dimensional PWR Benchmark Problem

Method	Energy Group	Spectral Radius of the Unaccelerated Iteration Matrix	Number of Inners per Outer	Number of Outers	Total Solution Time (sec)	Time for Outer Iterations (sec)	Time per Outer (sec)	Time per Inner (sec)
RC-C	1	.3663	2	32	3.6	2.75	.09	.02
	2	.2531	2					
RC-Q	1	.3434	2	35	4.1	3.19	.09	.02
	2	.2238	2					
RM-C	1	.5891	5	33	5.5	3.94	.12	.01
	2	.7443	6					
RM-Q	1	.6683	6	32	11.5	9.85	.31	.02
	2	.8571	10					

the RM method to be more slowly convergent than the RC method for this particular application. This slower rate of convergence is indicated by the larger estimated values of the spectral radii of the unaccelerated iteration matrices of the RM method compared with the RC method.

The spectral radii of the RC-C and the RC-Q methods are little different. This is to be expected since the basic iteration scheme is the same for these methods with only minor differences in the coupling between the principal block structure of rows and columns of currents introduced in order to treat the transverse leakage shape correction.

The RM-Q method uses a much smaller block partitioning of unknowns than the RM-C method, and, unlike the RM-C method, does not use the most recently calculated values of unknowns during a mesh sweep. Thus we would expect the unaccelerated RM-Q method to be more slowly convergent than the unaccelerated RM-C method. The larger spectral radii of the RM-Q method compared with those of the RM-C method reflect this slower rate of convergence.

It is interesting to note the reversal in group behavior with respect to the spectral radii of the unaccelerated iteration matrices between the RC and RM methods. In the RC method, which treats reflection implicitly, the increased transmission properties of the fast group over that of the thermal group dominate in solution difficulty. This effect is indicated by a larger value of the spectral radius for the fast group. In the RM method, which treats reflection iteratively, the difficulty of treating the thermal group reflective components dominates. The larger value of the thermal group spectral radius indicates this difficulty.

We now discuss the application of acceleration schemes to the basic iteration matrices and the efficiency of the various iterative techniques per inner iteration. First we compare the number of inner iterations required per outer iteration for the accelerated schemes. This factor in combination with the computational efficiency per inner iteration are the principal factors causing variations of the total computation time among the different solution methods.

The number of inners used per outer involves a combination of factors. These numbers reflect effects of the spectral radius of the unaccelerated iteration matrix, the choice of acceleration schemes, and the error reduction required per outer iteration. The RC methods and the RM-C method use the CCSI (cyclic Chebyshev semi-iterative) acceleration scheme. The more slowly convergent CSI (Chebyshev semi-iterative) method is used to accelerate the basic RM-Q iteration. In order to provide a proper balance between the number of inners and outers which minimizes overall computational time, it has been found that greater inner iteration error reduction factors are required for the RM methods than the RC methods. Thus for the same spectral radius of the unaccelerated iteration matrix, the methods should be ordered according to the number of inners per outer as the RC methods, the RM-C method, and the RM-Q method. Moreover, we observed the spectral radius of the unaccelerated iteration matrix to increase with this same ordering, which implies an increased difference in the number of inners required among the methods.

We now turn to a discussion of computational efficiency. It should

be noted that we neglect any overhead associated with the outer iterations in the calculation of computing times per inner iteration shown in Table 3.4. We first discuss the efficiency of the various methods per inner iteration, and then make general comments on the overall solution efficiency.

The RC methods have essentially the same computational time per inner iteration. The majority of the work in an inner is devoted to the direct solution of one-dimensional problems along columns and rows. The transverse leakage terms appear as sources in these one-dimensional problems and the shape correction modifications do not significantly affect the time required to form these sources.

The RM methods differ somewhat. The RM-Q method requires that the group source be modified to account for transverse leakage shape corrections before a mesh sweep. Then the mesh sweep involves only simple matrix multiplications. The source modification is expensive in relation to a single mesh sweep, however. The RM-C method uses the same operational procedure for a mesh sweep but does not require the source modification. The computational time per inner iteration for the RM-C method is seen to be half of that of the RM-Q method for this problem. The RC methods and the RM-Q method have essentially the same time requirement per inner iteration.

The overall solution times for the RC methods and the RM-C method are quite close. The total number of outer iterations vary somewhat, but from the time per outer iteration we see that the RM-C method is only about 30% slower than the RC methods. Because of increased error

reduction requirements and a more difficult inner iteration problem, the RM-C method must do nearly three times as many inners per outer as the RC methods. However, the RM-C method has a computational speed per inner twice that of the RC methods which offsets somewhat the greater number of inners required per outer.

The overall solution time for the RM-Q method is not competitive with the other schemes. It presents the most difficult inner iteration problem and uses the slower of the acceleration schemes. Moreover, it has the same efficiency per inner as the RC methods. Thus the total solution time is quite long compared with the other schemes.

We have found the trends described above to be generally true for all LWR problems investigated. The RC methods have consistently proven to be the more efficient schemes for two-dimensional static LWR calculations. Thus we report all static test problem results from calculations made with the RC methods except for those involving irregular cores or nonuniform mesh spacing which only the RM code is programmed to handle.

As we previously discussed, difficulties may be encountered in the extension of the RC methods to three dimensions, however. Extension of the RM methods are straightforward. Moreover, the RM-C method is competitive in two-dimensional static calculations compared with the RC methods. Thus it is reasonable to pursue RM-C type methods if iterative solution schemes are required in the extension to two-dimensional time-dependent problems.

3.4.3.2 The IAEA Two-Dimensional PWR Benchmark Problem

This problem is a two-group treatment of a highly idealized PWR with multizone fuel loading. Local perturbations are severe because of the insertion of control rods and the influence of the water reflector.

Coarse-mesh schemes have experienced difficulties in treating this problem. Finite difference solutions have been found to be in error with mesh spacings as small as one centimeter. This difficulty is illustrated by the results, summarized here in Table 3.5, obtained by Kristiansen[37] with a mesh-centered finite difference code (the same difference scheme as employed in MEKIN) for a sequence of decreasing mesh spacings. The reference is an extrapolated sequence of interface-centered finite difference calculations.

Results for uniform mesh refinement obtained using the nodal method with both the constant and quadratic transverse leakage approximations are shown in Table 3.6. The problem was treated in quarter-core symmetry and with a rectangular core configuration. Vacuum boundary conditions were applied on the external surface of the reactor. A convergence criterion of 10^{-5} was imposed on the nodal average flux. The reference solution is Kristiansen's extrapolated sequence of finite-difference calculations. Regionwise power distributions obtained with the nodal method are also given in Figs. A6.3a,b of Appendix 6.

These results show high accuracy with very large mesh spacings and a rapid convergence to the reference solution with mesh spacing refinement. It is seen that an assembly-size mesh (20 cm) is adequate for this problem, giving eigenvalue errors of less than .1% and maximum

Table 3.5 Summary of Finite Difference Results for the IAEA Two-dimensional PWR Benchmark Problem

Mesh Layout nodes per assembly, mesh spacing (cm)	Number of Unknowns per Group	Eigenvalue	ϵ_{avg} (%)	ϵ_{max} (%)
(2 × 2), 10	289	1.02965	8.1	23.3
(4 × 4), 5	1156	1.02924	4.9	13.9
(8 × 8), 2.5	4624	1.02943	1.8	5.2
(16 × 16), 1.25	18496	1.02955	0.5	1.5
Reference		1.02959		

Table 3.6 Summary of Results for the IAEA Two-dimensional PWR Benchmark Problem (Regular Core)

Mesh Layout nodes per assembly, mesh spacing (cm)	Unknowns per Group	Transverse Leakage Approximation	Eigenvalue	ϵ_{avg} (%)	ϵ_{max} (%)	Inners per Outer group 1/ group 2	Outers	Problem Solution Time (sec)
(1X1), 20	405	constant	1.02996	0.6	2.3	2/2	32	3.6
		quadratic	1.02951	0.8	1.9	2/2	35	4.1
(2X2), 10	1445	constant	1.02974	0.3	1.2	3/3	36	15.8
		quadratic	1.02963	0.1	0.5	3/3	36	17.0
(4X4), 5	5780	constant	1.02964	0.1	0.6	5/5	38	85.0
		quadratic	1.02962	0.1	0.5	5/5	38	89.0
Reference			1.02959					

Code: RC-C,Q

assembly power errors of less than 3% for both transverse leakage approximations.

Overall, the results of the quadratic transverse leakage approximation are somewhat better than the results of the constant leakage approximation. Eigenvalue predictions of the quadratic approximation are significantly better than those of the constant approximation. Maximum assembly power errors occur at rodded positions for the constant approximation and at the core-reflector interface for the quadratic approximation. The constant approximation is more slowly convergent with decreasing mesh size than the quadratic approximation. Note that the quadratic approximation is essentially converged at a 10 cm mesh spacing.

From comparison of Tables 3.5 and 3.6, we find that a 20 cm nodal solution with the quadratic transverse leakage approximation is essentially as accurate as a 1.25 cm finite difference solution. This finite difference method employs approximately 45 times more unknowns than the nodal solution. If we assume a maximum error of approximately 5% in the region power distribution to be an acceptable limit, we find that the finite difference method requires a 2.5 cm mesh spacing. For this situation, the finite difference solution employs approximately 11 times more unknowns than the nodal solution with an assembly-size mesh spacing which in addition gives significantly more accurate results. Finite difference results obtained with the VENTURE code indicate a running time of several minutes for this problem[9,38] as compared with approximately 4 seconds for our nodal code. Our execution times and solution accuracy for this benchmark problem appear to be

comparable with those obtained by other researchers with their nodal methods.[5, 22, 29-31, 36]

Much work has been done recently by Kalambokas and Henry[33] on the replacement of reflectors by albedo boundary conditions. This effort is directed toward minimization of the computational requirements for solving LWR problems by eliminating the excessive number of unknowns needed by the finite difference method to represent accurately the reflector region. We find that an explicit representation of the reflector region can be maintained and total problem unknowns kept to a minimum by using coarse mesh nodal solutions with irregular cores. As was shown in the results presented above, an assembly-size mesh with an explicit treatment of the reflector gives accurate results. We have solved the IAEA problem using a 20 cm mesh with all of the reflector eliminated except for one assembly width surrounding the core. This reflector region is sufficiently thick such that results should be essentially the same as for the rectangular problem. A 15% reduction in the number of unknowns is achieved as compared with the other coarse-mesh nodal solutions. Results, which are given in Table 3.7 and Fig. A6.3c, are essentially the same as those obtained with the rectangular core. Note that in comparing solution efficiency, that the RM code has been used for these calculations. The faster RC code was used to generate the rectangular core results of Table 3.6. However, comparison may be made with Table 3.4 which gives 20 cm IAEA rectangular core results for the RM code. All other calculational details are the same as in the previously reported solutions. This indicates that it is probably not necessary to attempt to eliminate the reflector region by use of albedo condi-

Table 3.7 Summary of Results for the IAEA Two-dimensional PWR Benchmark Problem (Irregular Core)

Mesh Layout – irregular core, (1 × 1) per assembly

Transverse Leakage Approximation	Unknowns per Group	Eigenvalue	ϵ_{avg} (%)	ϵ_{max} (%)	Inners per Outer group 1/ group 2	Outers	Problem Solution Time (sec)
Constant	345	1.02993	0.7	2.1	5/6		4.8
Quadratic	345	1.02950	0.7	1.9	6/9		10.4
Reference		1.02959					

Code: RM-C, Q

tions in nodal schemes of this type.

In summary, for this difficult benchmark problem we find the nodal method to give accurate results with either transverse leakage approximation when used with an assembly-size mesh. The reduction in the number of unknowns allowed with such large node sizes permits a significant gain in computational speed compared with the finite difference method in order to achieve an equivalent acceptable level of accuracy.

3.4.3.3 The LRA Two-dimensional BWR Benchmark Problem

The LRA BWR test problem is a two- or three-dimensional, two-group kinetics benchmark problem. In this section, we treat the two-dimensional reactor in steady state. This problem has been shown to be rather difficult. For example, a one centimeter finite difference solution was reported to have a maximum error in region power distribution of about one percent.[31] Also, Shober[36] has found that using the MEKIN finite difference code, a 2.5 cm solution is necessary to obtain a maximum error in region power of less than five percent. The solution time he reports is 333 seconds (adjusted for quarter core calculation).

We summarize the results in Table 3.8 obtained with the nodal method in both the constant and quadratic transverse leakage approximations with a uniform 15 cm mesh spacing. Power distributions are shown in Fig. A6.4 of Appendix 6. The problem was treated in quarter core symmetry. Vacuum boundary conditions were applied at the external surface of the reactor. A convergence criterion of 10^{-5} was imposed on the nodal average flux. The reference solution is a fine-mesh nodal

Table 3.8 Summary of Results for the LRA Two-dimensional Static BWR Benchmark Problem

Mesh Layout – uniform 15 cm mesh spacing

Transverse Leakage Approximation	Unknowns per Group	Eigenvalue	ϵ_{avg} (%)	ϵ_{max} (%)	Inners per Outer group 1/ group 2	Outers	Problem Solution Time (sec)
constant	605	.996788	1.1	2.6	2/2	55	8.5
quadratic	605	.996245	0.5	2.0	2/2	55	8.5
Reference		.996361					

Code: RC-C,Q

calculation (4 × 4 nodes per assembly) by Shober.[36]

These results are not significantly different from those obtained in solutions of the IAEA problem. Both transverse leakage approximations give accurate results for an assembly-size mesh with the quadratic approximation being slightly superior for the mesh size shown.

In comparison with the MEKIN results, the nodal method required 605 unknowns per group and 8.5 seconds of computation time, as compared with 4356 unknowns per group and 333 seconds of computation time, to achieve equivalent solution accuracy. As in the IAEA problem comparison, we see that the nodal method can achieve equivalent accuracy with approximately an order of magnitude fewer unknowns than the finite difference method for these difficult benchmark problems. Gains in computational efficiency reflect this difference in number of unknowns as well as the benefit of less difficult iterative problems because of the large mesh sizes.

3.4.3.4 The Biblis Two-dimensional PWR Problem

The Biblis reactor is a two-group PWR problem with a "checkerboard" core loading pattern.[39] Two cases are considered based on the insertion or withdrawal of control rods in the outer region of the core.

A summary of the results obtained with the nodal method in the constant and quadratic leakage approximations for a sequence of decreasing mesh spacings is presented in Table 3.9 for the rods withdrawn case and in Table 3.10 for the rods inserted case. The problems were treated in quarter-core symmetry. Vacuum boundary conditions

Table 3.9 Summary of Results for the Biblis Two-dimensional PWR Problem (Rods Withdrawn)

Reactor Configuration – rods withdrawn

Mesh Layout nodes per assembly, mesh spacing (cm)	Unknowns per Group	Transverse Leakage Approximation	Eigenvalue	ϵ_{avg} (%)	ϵ_{max} (%)	Inners per Outer group 1/ group 2	Outers	Problem Solution Time (sec)
(1×1), ~23	405	constant	1.02573	2.3	8.1	2/2	39	3.7
		quadratic	1.02520	0.3	1.0	2/2	36	3.9
(2×2), ~11.5	1445	constant	1.02537	0.8	2.5	3/2	39	15.3
		quadratic	1.02511	0.1	0.3	3/2	38	15.6
(4×4), ~5.75	5780	constant	1.02519	0.4	0.9	5/2	42	74.8
		quadratic	1.02511	0.2	0.5	5/2	42	80.2
Reference			1.02509					

Code: RC-C,Q

Table 3.10 Summary of Results for the Biblis Two-dimensional PWR Problem (Rods Inserted)

Reactor Configuration – rods inserted

Mesh Layout nodes per assembly, mesh spacing (cm)	Unknowns per Group	Transverse Leakage Approximation	Eigenvalue	ϵ_{avg} (%)	ϵ_{max} (%)	Inners per Outer group 1/ group 2	Outers	Problem Solution Time (sec)
(1×1), ~23	405	constant	1.02020	3.1	10.2	2/2	48	4.9
		quadratic	1.01968	0.3	1.4	2/2	45	4.8
(2×2), ~11.5	1445	constant	1.01981	0.9	3.0	3/2	45	17.2
		quadratic	1.01955	0.3	0.5	3/2	44	18.0
(4×4), ~5.75	5780	constant	1.01962	0.3	1.0	5/2	48	83.2
		quadratic	1.01954	0.1	0.4	5/2	47	87.5
Reference			1.01956					

Code: RC-C,Q

were applied at the external surface of the reactor. A convergence criterion of 10^{-5} was imposed on the average nodal flux. Our standard for comparison is a (4 × 4) node per assembly nodal solution by Werner[39] which has been shown to be essentially converged in space.

These results show a behavior as indicated in previous problems for the quadratic transverse leakage approximation. Very accurate solutions are obtained with large node sizes and the solution rapidly converges to the reference case with decreasing mesh size. However, the constant transverse leakage approximation shows unacceptable errors (~10% in assembly powers) for the assembly-size mesh spacing. Halving the mesh size (to 11.5 cm) gives much improved results for the constant approximation. It is seen that the quadratic transverse leakage approximation is essentially converged at the 11.5 cm mesh spacing. An examination of the (2 × 2) and (4 × 4) node per assembly quadratic transverse leakage approximation solutions reveals good agreement with Werner's solution.

Thus, we now find that the constant transverse leakage approximation does not always give acceptable accuracy when used with an assembly-size mesh in LWR calculations. The quadratic approximation, however, produces very good results in cases where the constant approximation fails.

3.4.3.5 Summary of Two-dimensional Results

The proposed nodal method has been shown to be accurate when used with assembly-size nodes in two-dimensional LWR static benchmark calculations. The quadratic transverse leakage approximation has

consistently produced accurate results for these large node sizes. However, the constant approximation was found to give unacceptable answers for an assembly-size mesh in a PWR with a "checkerboard" loading pattern. Thus, some care should be exercised in the application of this approximation.

Various solution methods for the inner iteration problem were investigated in the course of the overall study. The RC (row-column) methods were found to be more efficient than the RM (response matrix) methods for two-dimensional applications in LWR's. The RM-C (constant transverse leakage approximation) method does appear to be competitive with the RC methods but the RM-Q (quadratic transverse leakage approximation) method was found to be significantly slower than the other schemes. Since difficulties may be encountered in the extension of the RC methods to three dimensions, further work should be devoted to improvement of other solution techniques.

The nodal solutions were compared with finite difference methods in terms of number of unknowns needed for equivalent accuracy and were found to require significantly fewer unknowns. The combination of a reduced number of unknowns and relatively easy inner iteration problems because of the use of large mesh sizes give nodal schemes of the type proposed here a much improved computational efficiency compared with the conventional finite difference techniques. Gains in computational efficiency of an order of magnitude can be realized.

3.5 Summary

In this chapter, the set of multigroup, spatially-discretized, time-

dependent nodal equations were reduced to the static formulation. The solution of the static eigenvalue problem was discussed. The method was applied to a number of one- and two-dimensional LWR problems.

Two iterative schemes were developed for solution of the within-group spatial problems in two-dimensional calculations. These schemes were compared for a particular problem and the more efficient applied to the two-dimensional test problems. The extension of this scheme to three dimensions may not be practical, however, and further investigations in this area are indicated.

Results of the one- and two-dimensional test problems clearly show that the nodal method can be used with an assembly-size mesh to obtain accurate solutions for LWR calculations. Two-dimensional calculations using the quadratic leakage approximation consistently gave maximum errors in region powers of less than three percent for difficult benchmark problems when applied with an assembly-size mesh. Results for the constant transverse leakage approximation were nearly as accurate as those of the quadratic transverse leakage approximation except for a "checkerboard" PWR core for which unacceptable errors occurred for a calculation using an assembly-size mesh.

In comparison with the finite difference method, the nodal method was found to require significantly fewer unknowns for an equivalent accuracy. It appears that gains in computational efficiency compared with the finite difference method of an order of magnitude or more can be achieved.

Chapter 4

TRANSIENT APPLICATIONS

4.1 Introduction

Let us briefly review the development up until this point: In Chapter 2, a set of time-dependent nodal equations was derived for solution of the multigroup diffusion equation for a two-dimensional reactor consisting of rectangular, homogeneous (or homogenized) zones. In Chapter 3, this set of time-dependent equations was reduced to the conventional static-eigenvalue problem. Solution procedures were developed and a number of one- and two-dimensional LWR test problems were considered. High accuracy with large mesh spacings was consistently obtained in these applications. The significant gain in computational efficiency compared with the standard finite difference method demonstrated in these test results warranted this extension to time-dependent analysis.

In this chapter, the set of two-dimensional, spatially-discretized nodal equations with continuous time dependence are written in terms of discrete time intervals by the introduction of finite difference approximations for the time behavior. Since it is not the intent of this thesis to develop improved time integration schemes, only relatively simple, conventional approximations are applied for time discretization. A numerical solution technique is developed for the discrete time-dependent system in two dimensions. The formulation of solution procedures is restricted to those immediately applicable to three-dimensional, few-

group calculations as performed in the MEKIN code. Two thermal reactor test problems are investigated and results are compared with those obtained with the finite difference method as well as other coarse-mesh schemes.

4.2 Discretization in Time

We desire to approximate the solution of the time-dependent, spatially-discretized nodal equations, Eq. (2.13) and (2.15), at the times

$$t = t_o, t_1, t_2, \ldots, t_n, \ldots,$$

separated by the time intervals

$$\Delta_n \equiv t_{n+1} - t_n.$$

In order to formulate the discrete time-dependent system, we apply a simple, single-level, backwards difference scheme[40] to the nodal balance equations, Eq. (2.13), and leakage response equations, Eq. (2.15), over the time interval Δ_n. Thus the spatial operators are treated in a fully-implicit manner (evaluated at $t = t_{n+1}$).

We make one exception to this fully-implicit differencing, however. Recall the discussion in Chapter 3 regarding the treatment of transverse leakage shape corrections. There it was noted that the spatial coupling scheme of the nodal equations can be reduced to a nearest-neighbor formulation if nonlinear transverse leakage shape correction matrices are used in the solution procedure. However, if a linear formulation is desired, the resulting spatial coupling scheme is no longer of the nearest-

neighbor type. This prohibits the use of some of the more rapidly convergent solution techniques which are applicable for the nearest-neighbor formulation. Disadvantages are associated with the nonlinear formulation also because of requirements of frequent updating of matrices and increased coefficient storage. In order to avoid these difficulties for the time-dependent problem, we choose a fully explicit representation (evaluated at $t = t_n$) for the transverse leakage shape correction terms. Thus, the transverse leakage shape correction is evaluated from known data and does not complicate the principal part of the spatial operator which is handled implicitly.

After time differencing the nodal equation, the expression for the delayed precursors obtained from Eqs. (2.13b) and (2.15b) is used to eliminate delayed precursor unknowns evaluated at t_{n+1} from the flux and current equations, Eqs. (2.13a) and (2.15a). This procedure gives a set of equations for fluxes and currents at t_{n+1} in terms of fluxes, currents, and precursors at t_n which consists of the nodal balance equations,

$$
\begin{aligned}
&- \sum_{\substack{u=x,y \\ v\neq u}} \frac{h_\ell^v}{V_{ij}} \left(J_{g,ij}^{in,u-}(t_{n+1}) - J_{g,ij}^{out,u-}(t_{n+1}) + J_{g,ij}^{in,u+}(t_{n+1}) - J_{g,ij}^{out,u+}(t_{n+1}) \right) \\
&\quad + \left(\frac{1}{\Delta_n s_g} + \Sigma_{rg,ij}(t_{n+1}) \right) \phi_{g,ij}(t_{n+1}) \\
&\quad - \sum_{g'=1}^{G} \left(\delta_{g'\neq g} \Sigma_{gg',ij}(t_{n+1}) + \chi_g \left(1-\tilde{\beta}_g^n \right) \frac{\nu}{\gamma} \Sigma_{fg',ij}(t_{n+1}) \right) \phi_{g',ij} \\
&= \frac{1}{\Delta_n s_g} \phi_{g,ij}(t_n) + \sum_{k=1}^{K} \chi_{gk} \tilde{\lambda}_k^n C_{k,ij}(t_n)
\end{aligned}
\qquad (4.1a)
$$

and the leakage current response equations,

$$\left(\frac{1}{\Delta_n}\left[S^{out}_{g,ij}(t_{n+1})\right] - \left[R^{out}_{g,ij}(t_{n+1})\right] - \left[L^{out,flat}_{g,ij}(t_{n+1})\right]\right)\left[J^{out}_{g,ij}(t_{n+1})\right]$$

$$+ \left(\frac{1}{\Delta_n}\left[S^{in}_{g,ij}(t_{n+1})\right] - \left[R^{in}_{g,ij}(t_{n+1})\right] - \left[L^{in,flat}_{g,ij}(t_{n+1})\right]\right)\left[J^{in}_{g,ij}(t_{n+1})\right]$$

$$+ \left(\frac{1}{\Delta_n}\left[S^{\phi}_{g,ij}(t_{n+1})\right] - \left[R^{\phi}_{g,ij}(t_{n+1})\right]\right)\phi^{n+1}_{g,ij}$$

$$- \sum_{g'=1}^{G}\left\{\left(\left[T^{out}_{gg',ij}(t_{n+1})\right] + \chi_g\left(1-\tilde{\beta}^n_g\right)\frac{1}{\gamma}\left[P^{out}_{g',ij}(t_{n+1})\right]\right)\left[J^{out}_{g',ij}(t_{n+1})\right]\right.$$

$$+ \left(\left[T^{in}_{gg',ij}(t_{n+1})\right] + \chi_g\left(1-\tilde{\beta}^n_g\right)\frac{1}{\gamma}\left[P^{in}_{g',ij}(t_{n+1})\right]\right)\left[J^{in}_{g',ij}(t_{n+1})\right]$$

$$\left. + \left(\left[T^{\phi}_{gg',ij}(t_{n+1})\right] + \chi_g\left(1-\tilde{\beta}^n_g\right)\frac{1}{\gamma}\left[P^{\phi}_{g',ij}(t_{n+1})\right]\right)\phi_{g',ij}(t_{n+1})\right\}$$

$$= \frac{1}{\Delta_n}\left(\left[S^{out}_{g,ij}(t_n)\right]\left[J^{out}_{g,ij}(t_n)\right] + \left[S^{in}_{g,ij}(t_n)\right]\left[J^{in}_{g,ij}(t_n)\right] + \left[S^{\phi}_{g,ij}(t_n)\right]\phi_{g,ij}(t_n)\right)$$

$$+ \sum_{k=1}^{K}\chi_{gk}\tilde{\lambda}^n_k[\tilde{C}_{k,ij}(t_n)]$$

$$+ \left(\left[L^{out,shape}_{g,ij}(t_n)\right]\left[J^{out}_{g,ij}(t_n)\right] + \left[L^{in,shape}_{g,ij}\right]\left[J^{in}_{g,ij}(t_n)\right]\right)$$

$$\left.\begin{array}{l} g = 1,2,\ldots,G \\ i = 1,2,\ldots I \\ j = 1,2,\ldots J \end{array}\right\} \quad (ij) \in \mathcal{R} \qquad (4.1b)$$

where

$$\tilde{\beta}^n_g \equiv \begin{cases} \beta\left(1 - \sum_{k=1}^{K}\dfrac{\dfrac{\chi_{ig}}{\chi_g}\dfrac{\beta_k}{\beta}\Delta_n\lambda_k}{(1+\Delta_n\lambda_k)}\right); & \chi_g \neq 0 \\ 0; & \chi_g = 0 \end{cases}$$

and

$$\tilde{\lambda}_k^n \equiv \frac{\lambda_k}{(1 + \Delta_n \lambda_k)}.$$

After determination of the fluxes and currents at t_{n+1}, the nodal average precursors are advanced by

$$C_{k,ij}(t_{n+1}) = \frac{\tilde{\lambda}_k^n}{\lambda_k} C_{k,ij}(t_n) + \tilde{\beta}_k^n \sum_{g=1}^{G} \frac{\nu}{\gamma} \Sigma_{fg,ij}(t_{n+1})\, \phi_{g,ij}(t_{n+1})$$

$$\left.\begin{array}{l} k = 1, 2, \ldots K \\ i = 1, 2, \ldots, I \\ j = 1, 2, \ldots, J \end{array}\right\} \quad (ij) \in \mathcal{R}$$

(4.2a)

where

$$\tilde{\beta}_k^n \equiv \frac{\Delta_n \beta_k}{(1 + \Delta_n \lambda_k)}.$$

Additional precursor unknowns associated with the implicit precursor shape approximation are advanced by

$$[\tilde{C}_{k,ij}(t_{n+1})] = \frac{\tilde{\lambda}_k^n}{\lambda_k} [\tilde{C}_{k,ij}(t_{n+1})] + \tilde{\beta}_k^n \sum_{g=1}^{G} \frac{1}{\gamma} \left(\left[P_{g,ij}^{out}(t_{n+1}) \right] \left[J_{g,ij}^{out}(t_{n+1}) \right] + \left[P_{g,ij}^{in}(t_{n+1}) \right] \left[J_{g,ij}^{in}(t_{n+1}) \right] + \left[P_{g,ij}^{\phi}(t_{n+1}) \right] \phi_{g,ij}(t_{n+1}) \right)$$

(4.2b)

The inclusion of the interface current continuity condition and the reactor boundary conditions along with the specification of the initial conditions (t = 0) complete the system of discrete time-dependent equations.

The notation used here is the same as that originally introduced in

Chapter 2. It should be recalled that the $[J_{g,ij}]$'s are four element column vectors of incident or leakage interface average partial currents in group g on the faces of node (ij). The $[\tilde{C}_k]$'s are four element column vectors of weighted integrals of the precursor density in delayed family k when the implicit precursor shape approximation is used. These vectors reduce to coefficients multiplying the average precursor density when the constant shape approximation is used for the precursor shape.

Note that, as previously discussed, the transverse leakage shape correction terms have been treated explicitly in the leakage response equations, Eq. (4.1b). However, the constant portion of the transverse leakage approximation, which includes integral properties conserving net leakage, is treated implicitly as is the remainder of the spatial operator.

We consider the solution of the discrete time-dependent nodal equations, Eqs. (4.1) and (4.2), in the following section.

4.3 Solution of the Discrete Time-Dependent Equations

4.3.1 Problem Formulation

In advancing the time-dependent solution over the interval (t_n, t_{n+1}), the quantities at t_n are known and the right-hand sides of the nodal balance equations, Eq. (4.1a), and the leakage response equations, Eq. (4.1b), can be evaluated. Unknown currents and fluxes are to be determined for t_{n+1}. This problem can be written as

$$[A(t_{n+1})][\psi(t_{n+1})] = [S(t_n)] \tag{4.3}$$

where [A] is the multigroup spatial operator appearing on the left-hand sides of Eqs. (4.1), $[\psi]$ is the unknown vector of fluxes and currents at t_{n+1}, and [S] is a known source evaluated from data at the beginning of the time interval. The solution of this multigroup, two-dimensional fixed source problem requires the use of iterative techniques. We discuss the choice of iterative schemes in Sec. 4.3.2 and consider the numerical implementation of the solution procedure in Sec. 4.3.3.

4.3.2 Solution Method

Recall that our immediate goal in examining nodal schemes is to develop a potential replacement for the finite difference method used to solve three-dimensional, two-group diffusion problems in the program MEKIN. Thus in development of the solution technique for the time-dependent nodal equations we only consider one or two groups and restrict ourselves to the use of two-dimensional solution methods which have straightforward extensions to three dimensions. With this in mind, we consider the solution of Eq. (4.3).

The operator [A] of Eq. (4.3) contains group transfer terms both from fissioning and scattering. Thus, the group structure is fully coupled. In the general case, solution methods which treat the group structure iteratively must be employed. Also, an additional level of iteration is required for the spatial problem in each group. However, because we are imposing a limitation of two energy groups, we consider methods which treat the group structure simultaneously and thus eliminate a level of iteration. We now discuss the iterative solution of the spatial problem.

Because of the simultaneous treatment of the group structure, we consider the unknowns in all groups associated with a particular spatial variable to be a single block unknown. With this viewpoint, we see that Eq. (4.3) has exactly the same block structure as that of the scalar structure of the within-group spatial problem, Eq. (3.6), solved in each group during a fission-source iteration in the static eigenvalue problem. If we manipulate the groupwise block structure of Eq. (4.3) as we did the scalar structure of the within-group problem, we may use exactly the same solution procedures as developed in Chapter 3 for the inner iterations. This is the technique we employ.

As in Sec. 3.3.3.1, the nodal balance equations, Eq. (4.1a), are used to eliminate the nodal average flux from the leakage response equations, Eq. (4.1b). This procedure gives a spatial problem in terms of interface average partial currents only. We employ the RM (response matrix) method of Sec. 3.3.3.3, for which the extension to three dimensions is conceptually straightforward, to solve these equations.

Because we have used an explicit time differencing of the transverse leakage shape correction terms, only the constant portion of the transverse leakage approximation is incorporated into the spatial operator [A]. Thus, with the basic block unknown defined to be leakage currents from a node in all groups, the RM-C (constant transverse leakage) solution method is applied. Recall that this method partitions the nodes into two blocks which essentially can be thought of as the "red" and "black" squares of a "checkerboard." In the nearest-neighbor coupling scheme which occurs with use of the constant transverse leakage approximation,

nodes of a particular type ("color") are not connected to nodes of the same type. Thus if "response matrices" which give leakage currents due to incident currents are formed prior to the start of the spatial iterations, all leakage currents of a particular node type can be improved simultaneously by multiplication of the response matrices with latest values of the leakage currents of the other node type. The spatial iteration is between node types. The CCSI[10, 12, 35] (Chebyshev semi-iterative) method is used to accelerate this basic iteration.

The formulation of the response matrices is not a trivial matter, however. With simultaneous treatment of the groups in two dimensions the response matrices are of order 4G. Moreover, costly matrix inversions are required to construct the response matrices. Fortunately, symmetry conditions can be used to reduce storage requirements significantly. However, the response matrices depend on nodal geometrical and material properties, and consequently, must be modified to reflect time-dependent changes in material parameters. Frequent regeneration of these matrices can become excessively expensive. We have not investigated alternative schemes for updating the response matrices which may be less costly, such as correlation of response elements with material states.

4.3.3 Numerical Considerations

In this section we consider actual numerical implementation of the RM-C iterative method described in the preceding section. The determination of acceleration parameters is first discussed, followed by the description of a procedure for predicting improved guesses with which

to begin the iterations. Finally, we describe briefly the computer code used for time-dependent calculations.

The acceleration parameters of the CCSI method are determined from the bounds of the eigenvalue spectrum of the associated Jacobi iteration matrix.[10, 12, 35] The properties of the iteration matrix vary significantly with timestep size and material properties for a fixed geometrical configuration. For effective use of the acceleration procedure we must estimate accurately bounds for the eigenvalue spectrum of the Jacobi matrix. We divide a transient problem into a number of time domains in which the timestep size is constant. Eigenvalue estimates are made before each time domain based on material properties at the beginning of the domain. The RM-C iteration matrix is nonsymmetric and thus complex eigenvalues may occur.[11] We have attempted to treat this condition in the choice of acceleration parameters.[35] The procedure used to estimate bounds for the eigenvalue spectrum of the nonsymmetric iteration matrix is one suggested by Wachpress.[11] It should be noted that we do not examine the convergence rate obtained during the iterations of each timestep of a time domain in order to determine if the acceleration parameters being used are adequate or need to be reestimated because of changes in the properties of the iteration matrix caused by changes in material properties.

A fixed convergence criterion is imposed on the iterations of each timestep. The convergence test is essentially the same as that employed in TWIGL code.[41-43] Effectively, a norm of the relative error in the pointwise solution is tested. A minimum number of iterations (typically

5 to 10) are required before convergence is allowed.

In order to minimize the number of iterations per timestep, it is important to have a good initial guess with which to begin the iterative procedure. We use an extrapolation procedure applied to the solution of the preceding timestep to obtain an improved starting guess. The time dependence of the solution vector is assumed to be exponential and the thermal group behavior is used to determine extrapolation factors. For example, in order to obtain an initial guess for a group g spatial variable in node (ij), denoted here as $\tilde{\psi}_{g,ij}$, to begin the iterations for timestep n, we use

$$\tilde{\psi}_{g,ij}(t_{n+1}) = \exp\left(\Omega_{ij}^{\psi,n}\Delta_n\right)\psi_{g,ij}(t_n); \qquad g = 1,\ldots G$$

where

$$\Omega_{ij}^{\psi,n} = \frac{1}{\Delta_{n-1}} \ln\left(\frac{\psi_{2,ij}(t_n)}{\psi_{2,ij}(t_{n-1})}\right).$$

Because flux condensation is applied to reduce the spatial problem to one in terms of currents only, it is necessary only to extrapolate the currents. Nodal fluxes are regenerated after convergence of the spatial iteration.

The RM-C method and the associated numerical procedures described above have been incorporated into a computer code for one- or two-group, two-dimensional, time-dependent calculations. The code is basically an extension of the RM-C,Q static code and uses the output of this code as its initial condition. The code is written in the IBM FORTRAN IV

language except for a few core storage routines. It was compiled using the IBM Level-G compiler with full optimization. All calculations were performed on an IBM 370/168 computer. This code has been documented and retained for future reference.[45]

4.4 Results

4.4.1 The TWIGL Two-dimensional Seed-Blanket Reactor Problem

This test problem is a two-dimensional unreflected seed-blanket reactor 160 cm square with eighth-core symmetry. The problem is treated in two energy groups and one delayed family. A complete problem description is given in Appendix 5. Transient solutions for step and ramp perturbations of the corner seed assemblies were originally done by Hageman and Yasinsky[41] using the finite difference code TWIGL.[42,43] We shall present results of nodal calculations for both perturbations.

Reference results for comparison with our nodal calculations are not available. This is because our use of vacuum boundary conditions for this unreflected core prohibits us from making direct comparisons with other results obtained using zero flux boundary conditions, such as TWIGL[41] or Shober's nodal scheme.[36] Nevertheless, we shall establish our own reference solution in the course of examining aspects of spatial, temporal, and numerical convergence of our method.

We treat this problem in quarter-core symmetry. For the 80 cm square quarter core, we use two mesh layouts which are denoted as the "coarse" mesh and the "very coarse" mesh. These mesh structures are defined as follows:

linear ramp perturbation is introduced in 0.2 seconds, after which time the reactor properties are fixed. The duration of the calculations are taken to be 0.5 sec.

The time-dependent nodal code was used to solve these problems with both transverse leakage approximations (constant and quadratic) and both precursor shape approximations (constant and implicit). Also, both mesh layouts were considered. Before we discuss overall solution accuracy, we consider the numerical and temporal convergence behavior of the nodal method. The step perturbation case was used for these investigations. Note that for all calculations, the initial total power is normalized to unity.

First we discuss the degree of convergence required for the spatial iterations of a timestep. The constant transverse leakage approximation and the implicit precursor shape approximation were used for these calculations. However, these approximations do not affect the form of the spatial operator which is to be inverted iteratively at each timestep. The timestep size was 10 ms for these calculations. (TWIGL results indicate that a temporal accuracy of approximately 1% may be achieved with a 10 ms timestep for a fully-implicit solution of the finite difference equations with an 8 cm mesh.) Also, exponential extrapolation was applied in these calculations. Total power versus time is shown in Table 4.2 for both mesh layouts with convergence criteria of 10^{-3}, 10^{-4}, and 10^{-5} imposed on the spatial iterations. Computing times are also reported.

It is seen that with use of a 10^{-3} convergence criterion oscillations

Region (u = x, y)	Mesh Division: Coarse Mesh	Mesh Division: Very Coarse Mesh
0 cm ≤ u ≤ 24 cm	12 cm	24 cm
24 cm ≤ u ≤ 56 cm	16 cm	32 cm
56 cm ≤ u ≤ 80 cm	12 cm	24 cm

We now consider solution of the static reactor. A summary of static results is presented in Table 4.1 for the two mesh structures with both the constant and quadratic transverse leakage approximations. Results for the region power distributions are shown in Fig. A6.5a of Appendix 6. Once again, we use the power-weighted average error and maximum error in region powers for a summary comparison of power distributions. The reference solution is a nodal calculation with the quadratic transverse leakage approximation for a uniform 4 cm mesh. This solution has been shown to be essentially spatially converged by comparison with a sequence of calculations with successive mesh refinements.

We find that results even for the very coarse mesh are accurate. As in previous static problems, the quadratic transverse leakage approximation gives better results than the constant approximation for both mesh layouts. The results for the coarse mesh calculations appear to be nearly spatially converged.

We now consider transient calculations for both the step and ramp perturbations. These perturbations are introduced by a change in the thermal absorption cross section of the corner seed assembly. The total perturbation, which is the same in both cases, corresponds to a reactivity insertion which is positive but below prompt critical. The

Table 4.2 Total Power versus Time for the TWIGL Two-dimensional Seed-Blanket Reactor (Step Perturbation): Investigation of the Spatial Iteration Convergence Criterion

Part a) Very Coarse Mesh (10 ms timestep)

	Convergence Criteria		
Time (sec)	10^{-3}	10^{-4}	10^{-5}
(.05)	2.047	2.015	2.012
.1	2.091	2.057	2.054
.2	2.057	2.071	2.071
.3	2.094	2.088	2.088
.4	2.106	2.106	2.106
.5	2.124	2.123	2.123
Computing Time (sec)	5.8	9.3	14.2

Part b) Coarse Mesh (10 ms timestep)

Time (sec)	10^{-3}	10^{-4}	10^{-5}
(.05)	2.066	2.027	2.023
.1	2.114	2.071	2.066
.2	2.072	2.085	2.085
.3	2.097	2.100	2.102
.4	2.130	2.121	2.120
.5	2.134	2.138	2.138
Computing Time (sec)	24.3	43.4	85.2

Table 4.1 Summary of Static Results for the TWIGL Two-dimensional Seed-Blanket Reactor Problem

Mesh Layout	Number of Unknowns per Group	Transverse Leakage Approximation	Eigenvalue	ϵ_{avg} (%)	ϵ_{max} (%)	Inners per Outer group 1/ group 2	Outers	Solution Time (sec)
very coarse	45	constant	.91664	0.8	1.6	5/5	16	0.6
		quadratic	.91573	0.5	1.4	6/5	16	0.8
coarse	180	constant	.91531	0.2	0.6	5/5	17	1.6
		quadratic	.91533	0.2	0.4	8/6	16	2.9
Reference			.91541					

Code: RM [illegible],Q

occur in the total power at the beginning of the calculation when the solution is most rapidly varying. These oscillations are damped and a smooth power behavior is obtained with use of a 10^{-4} convergence criterion. Use of a 10^{-5} convergence criterion changes the results only slightly. However, the running time increases substantially. Choice of mesh size does not appear to be a factor.

The oscillations encountered in these calculations with loose convergence criteria can be attributed to the use of the exponential extrapolation procedure. This effect is shown in the total power versus time results given in Table 4.3 in which these same calculations are compared with 10^{-3} and 10^{-4} convergence criteria but with and without exponential extrapolation. Computing times are also shown.

We find that the calculations with the 10^{-3} convergence criterion and without extrapolation do not display the oscillatory behavior in the initial phases of the transient as do those with extrapolation. However, the total power at the end of the calculations is in error by more than 1% compared with the numerically converged results. The use of a 10^{-4} convergence criterion without extrapolation gives accurate results but the running times are significantly longer. Once again, the effect of mesh layout is not important.

Although not shown, similar results are found in the ramp perturbation case in which oscillations, as described above for the step perturbation, appear at the termination of the ramp with a loose convergence criterion and the use of extrapolation. Here it is also found that from a viewpoint of combined accuracy and computational efficiency, the use

Table 4.3 Total Power versus Time for the TWIGL Two-dimensional Seed-Blanket Reactor Problem (Step Perturbation): Investigation of the Effects of Exponential Extrapolation

Part a) Very coarse Mesh (10 ms timestep)

	Convergence Criteria			
	with Extrapolation		without Extrapolation	
Time (sec)	10^{-3}	10^{-4}	10^{-3}	10^{-4}
(.05)	2.047	2.015	1.975	2.008
.1	2.091	2.057	2.014	2.049
.2	2.057	2.071	2.041	2.067
.3	2.094	2.088	2.063	2.084
.4	2.106	2.106	2.082	2.102
.5	2.124	2.123	2.100	2.119
Computing Time (sec)	5.8	9.3	4.9	12.7

Part b) Coarse Mesh

	Convergence Criteria			
	with Extrapolation		without Extrapolation	
Time (sec)	10^{-3}	10^{-4}	10^{-3}	10^{-4}
(.05)	2.066	2.027	1.979	2.018
.1	2.114	2.071	2.018	2.061
.2	2.072	2.085	2.042	2.080
.3	2.097	2.100	2.063	2.097
.4	2.130	2.121	2.083	2.115
.5	2.134	2.138	2.101	2.132
Computing Time (sec)	24.3	43.4	21.7	64.4

of extrapolation with a tighter convergence criterion is preferred. Therefore, we conclude that a convergence criterion of 10^{-4} and the use of extrapolation should give better than 1% accuracy in total power with the minimum computing time.

We show results for iteration count versus timestep for both the step and ramp perturbations in Fig. A6.5e-h. A 10^{-4} convergence criterion has been used. Both coarse mesh and very coarse mesh results are presented. The exponential extrapolation is found to be very effective in decreasing the iteration count except in the case when abrupt changes in reactor properties occur. For example, the termination of the ramp insertion causes a temporary, but significant, increase in the iteration count per timestep.

We now turn to a discussion of temporal convergence. For these considerations, we present calculations with both the constant and quadratic transverse leakage approximations. Only the implicit precursor shape approximation was used. (Additional calculations indicate that the choice of precursor shape approximations has no effect on these results.) We note that the behavior of the quadratic transverse leakage approximation is of particular interest since, unlike the fully-implicit time-differencing of the constant approximation, a portion of the spatial operator (the transverse leakage shape correction) is treated explicitly.

Results of total power versus time for the step perturbation with timesteps of 10 ms, 5 ms, and 1 ms are shown in Tables 4.4 and 4.5 for the constant and quadratic transverse leakage approximations, respectively. Both coarse mesh and very coarse mesh results are

Table 4.4 Total Power versus Time for the TWIGL Two-dimensional Seed-Blanket Reactor Problem (Step Perturbation): Investigation of Temporal Convergence for the Constant Transverse Leakage Approximation

Part a) Very Coarse Mesh

	Timestep Size		
Time (sec)	10 ms	5 ms	1 ms
(.05)	2.015	2.030	2.038
.1	2.057	2.057	2.054
.2	2.071	2.072	2.071
.3	2.088	2.089	2.089
.4	2.106	2.106	2.106
.5	2.123	2.124	2.124
Computing Time (sec)	9.3	10.2	26.0

Part b) Coarse Mesh

Time (sec)	10 ms	5 ms	1 ms
(.05)	2.027	2.044	2.054
.1	2.071	2.072	2.067
.2	2.085	2.084	2.084
.3	2.100	2.102	2.102
.4	2.121	2.120	2.120
.5	2.138	2.138	2.138
Computing Time (sec)	43.4	46.6	96.8

Table 4.5 Total Power versus Time for the TWIGL Two-dimensional Seed-Blanket Reactor Problem (Step Perturbation): Investigation of Temporal Convergence for the Quadratic Transverse Leakage Approximation

Part a) Very Coarse Mesh

	Timestep Size		
Time (sec)	10 ms	5 ms	1 ms
(.05)	2.065	2.064	2.063
.1	2.084	2.082	2.079
.2	2.096	2.097	2.096
.3	2.116	2.115	2.114
.4	2.134	2.133	2.132
.5	2.152	2.151	2.151
Computing Time (sec)	9.9	11.3	27.4

Part b) Coarse Mesh

Time (sec)	10 ms	5 ms
(.05)	2.044	2.055
.1	2.080	2.080
.2	2.093	2.093
.3	2.110	2.111
.4	2.130	2.129
.5	2.147	2.147
Computing Time (sec)	43.3	47.0

presented. Extrapolation was used and a convergence criterion of 10^{-4} was imposed on the spatial iterations. Running times are also shown.

It is seen that, except for minor differences in the prompt jump region, the solutions are essentially converged in time with the 10 ms timestep size. There are no significant differences regarding effects of mesh layout or of order of the transverse leakage approximation. We have performed similar calculations for the ramp perturbation with a maximum timestep size of 5 ms and have found these solutions also to be essentially converged in time.

We see that with refinement of the mesh the total power at the end of the calculation changes by approximately 0.7% with the constant transverse leakage approximation and approximately 0.2% with the quadratic transverse leakage approximation. Also, recall that the static solutions for both transverse leakage approximations with the coarse mesh were practically converged in space. These results indicate that these calculations with the coarse mesh and with either transverse leakage approximation are quite accurate. The solution with the quadratic transverse leakage approximation and with a 5 ms timestep size appears to be the most accurate calculation. We believe it to be essentially converged in time and space. Except in the prompt jump region, the same calculation with a 10 ms timestep size shows no real differences. Similar results have been obtained for the ramp perturbation.

Thus in further comparisons, the coarse mesh solutions for the step and ramp perturbations obtained by using the quadratic transverse leakage approximation and the implicit precursor shape approximation

will be used as reference cases. Plots of total reactor power versus time are shown in Fig. A6.5c for the step perturbation (10 ms timestep size) and in Fig. A6.5d for the ramp perturbation (5 ms timestep size) for these calculations.

As an aside, it is interesting to note the computing times obtained with decreasing timestep size shown in Tables 4.4 and 4.5. We find that it is nearly as efficient to solve this problem with a 5 ms timestep as with a 10 ms timestep. This reflects the decrease in difficulty of the spatial iterations with decreasing timestep size. With further decreases in timestep size, the effect of increased total number of timesteps dominates and significantly increases the solution time. Since, in the general case, temporal accuracy is increased by decreasing the timestep size, it may not be beneficial from the viewpoint of combined overall solution accuracy and computational efficiency for implicit time-differencing schemes of this type to use the maximum timestep size for which adequate temporal accuracy can be achieved.[41,42]

We now present results for the various combinations of transverse leakage approximations and precursor shape approximations. Results for both mesh layouts are given. Total reactor power versus time is presented in Table 4.6 for the step perturbation and Table 4.7 for the ramp perturbation. Timestep sizes of 10 ms and 5 ms have been used for the step and ramp solutions, respectively. A 10^{-4} convergence criterion was imposed on the spatial iterations. Extrapolation was used for the step perturbation calculations. However, extrapolation was not used for the ramp perturbation calculations. These results are summarized in Table 4.8. Errors in total reactor power at the

Table 4.6 Total Power versus Time for the TWIGL Two-dimensional Seed-Blanket Reactor Problem (Step Perturbation): Comparison of Transverse Leakage and Precursor Shape Approximation

Part a) Very Coarse Mesh

	Approximation			
	(transverse leakage):	constant	quadratic	quadratic
	(precursor shape):			
Time (sec)	constant	implicit	constant	implicit
.1	2.078	2.057	2.105	2.084
.2	2.092	2.071	2.119	2.096
.3	2.110	2.088	2.139	2.116
.4	2.129	2.106	2.157	2.134
.5	2.146	2.123	2.176	2.152
Solution time (sec)	9.4	9.3	9.3	9.9

Part b) Coarse Mesh

	Approximation			
	(transverse leakage):	constant	quadratic	quadratic
	(precursor shape):			
Time (sec)	constant	implicit	constant	implicit
.1	2.077	2.071	2.086	2.080
.2	2.091	2.085	2.099	2.093
.3	2.107	2.100	2.116	2.110
.4	2.127	2.121	2.137	2.130
.5	2.144	2.138	2.153	2.147
Solution time (sec)	42.6	43.4	42.9	43.3

Table 4.7 Total Power versus Time for the TWIGL Two-dimensional Seed-Blanket Reactor Problem (Ramp Perturbation): Comparison of Transverse Leakage and Precursor Shape Approximations

Part a) Very Coarse Mesh

	Approximation (transverse leakage): constant	constant	quadratic	quadratic
	(precursor shape):			
Time (sec)	constant	implicit	constant	implicit
(0.05)	1.132	1.122	1.136	1.127
0.1	1.316	1.304	1.325	1.315
(0.15)	1.577	1.562	1.593	1.581
0.2	1.969	1.950	2.003	1.988
(0.25)	2.072	2.052	2.094	2.079
0.3	2.082	2.062	2.104	2.089
0.4	2.100	2.079	2.122	2.106
0.5	2.118	2.096	2.140	2.124
Computing Time (sec)	23.7	24.0 (8.3)*	26.8	26.8

*Extrapolation applied

Table 4.7 (continued)

Part b) Coarse Mesh

Time (sec)	Approximation (transverse leakage): constant / (precursor shape): constant	Approximation (transverse leakage): constant / (precursor shape): implicit	Approximation (transverse leakage): quadratic / (precursor shape): constant	Approximation (transverse leakage): quadratic / (precursor shape): implicit
(0.05)	1.125	1.121	1.127	1.125
0.1	1.309	1.304	1.312	1.311
(0.15)	1.570	1.563	1.576	1.574
0.2	1.964	1.955	1.976	1.974
(0.25)	2.067	2.058	2.076	2.075
0.3	2.078	2.068	2.087	2.085
0.4	2.095	2.085	2.104	2.103
0.5	2.113	2.103	2.122	2.120
Computing Time (sec)	120.0	114.9 (29.2)*	123.6	135.6

*Extrapolation applied

Table 4.8 Summary of Results for the TWIGL Two-dimensional Seed-Blanket Reactor Problems

Approximation Transverse Leakage/ Precursor Shape	Mesh Layout	Error in Total Power at Time = 0.5 sec (%)		ϵ_{avg} at Time = 0.5 (%) (normalized power distribution)	ϵ_{max} at Time = 0.5 (%) (normalized power distribution)
		Step	Ramp		
constant/constant	very coarse	-0.05	-0.1	0.7	1.9
	coarse	-0.1	-0.3	0.2	0.9
constant/implicit	very coarse	-1.1	-1.1	0.5	1.9
	coarse	-0.4	-0.8	0.2	0.9
quadratic/constant	very coarse	1.4	0.9	0.2	0.7
	coarse	0.3	0.1	0.03	0.1
quadratic/implicit	very coarse	0.2	0.2	0.3	0.9
	coarse	—	—	—	—

end of the calculations as well as average and maximum errors in the asymptotic power distribution are reported. (Note that both perturbations reach an asymptotic state at the end of calculation and thus normalized power distribution results are the same for both cases.) The reference in each case is the coarse mesh calculation with the quadratic transverse leakage approximation and the implicit precursor shape approximation. Power distributions are shown in Fig. A6.5b.

We find all of the results to be very accurate. For all calculations, the maximum error in total power at the end of the calculation is less than 1.5% and the maximum error in the asymptotic power distribution is less than 2%. In general, the total power is overestimated with the use of the constant precursor shape approximation and underestimated with the use of the constant transverse leakage approximation. The choice of precursor shape approximations has little effect on the errors in the asymptotic power distribution. As was observed in static calculations, the quadratic transverse leakage approximation gives somewhat improved power distribution results as compared with the constant approximation.

Note also that computational times for a particular mesh size do not vary widely among the various approximations. Since the delayed precursors can be advanced simply and separately from the fluxes and currents (see Eqs. 4.1, 4.2), savings incurred with the use of the constant precursor shape approximation are principally in storage requirements and not in computation time. The treatment of the transverse leakage does not dramatically affect solution times because the shape correction terms appearing in the quadratic transverse leakage approx-

imation have been treated explicitly in the time-differencing scheme. Only a modification of the source term for the spatial iterations is required at the beginning of each timestep to account for these corrections. Results of computing times for the ramp perturbation show that factors of 3 can be gained in computational efficiency with the use of the extrapolation procedure.

TWIGL solution times are available for these problems for full-core calculations using an 8 cm finite-difference mesh.[41] We compare with TWIGL results given for the fully-implicit solution technique , which is the scheme we employ. The TWIGL times are for a CDC 6600 computer which is comparable in speed to the IBM 370/168 computer used for our nodal calculations. Dividing the TWIGL times by 4 to adjust for quarter-core symmetry, we obtain running times of 86.5 sec for the step perturbation with a 10 ms timestep size and 137.5 sec for the ramp perturbation with a 5 ms timestep size with a problem duration of 0.5 sec in both cases. These times are for a 10^{-4} convergence criterion which is the same as that used for our calculations. For quarter-core symmetry and an 8 cm finite-difference mesh, 100 flux unknowns are required per group. This gives computing times per group flux unknown of approximately 0.9 sec and 1.4 sec for the step and ramp cases. Considering both mesh layouts and using results without extrapolation (which TWIGL does not use), we obtain maximum running times for our nodal code of approximately 0.4 sec and 0.8 sec per group flux-current unknown for the step and ramp perturbations. Thus we see that the computing speeds per unknown of the codes are roughly comparable for the

mesh spacings considered. However, we would expect the coarse mesh nodal solution to be much more accurate than the 8 cm finite difference solution. As we have seen in static applications, for some problems an order of magnitude fewer unknowns may be required with the nodal method as compared with the finite difference method in order to obtain equivalent accuracy. Therefore, even if we only maintain a rough equality in computational speed per unknown with implicit schemes such as TWIGL, we can make dramatic improvements in efficiency merely by using a reduced number of unknowns. The results of this problem demonstrate this to be the case since we have shown that, even with the very coarse mesh layout, high accuracy can be achieved.

4.4.2 The LRA Two-dimensional BWR Benchmark Problem

This problem is a two-dimensional, quarter-core, BWR kinetics problem treated in two energy groups and two delayed precursor families. A superprompt critical transient results from the simulated ejection of a control rod from the reactor at low power. The transient is induced by a linear variation of the thermal absorption cross section of the ejected rod position over the interval 0.0 to 2.0 seconds and is followed to 3.0 seconds. Thermal feedback is modeled using adiabatic heatup with space-dependent Doppler feedback. The feedback model is given by the following relations:

$$\text{adiabatic heatup} - \alpha_T[\Sigma_{f1}(\underline{r}, t)\,\phi_1(\underline{r}, t) + \Sigma_{f2}(\underline{r}, t)\,\phi(\underline{r}, t)] = \frac{\partial}{\partial t} T(\underline{r}, t)$$

$$\text{Doppler feedback} - \Sigma_{a1}(\underline{r}, t) = \Sigma_{a1}(\underline{r}, t=0)\left\{1 + \alpha_\Sigma[\sqrt{T(\underline{r}, t)} - \sqrt{T_o}\,]\right\}$$

A uniform initial temperature distribution (T_o) is assumed. All problem parameters are given in Appendix 5.

This test problem has been found to be very difficult. Small mesh sizes are necessary for finite difference calculations in order to achieve adequate spatial accuracy for the initial conditions. Also, the reactor power varies over many orders of magnitude during the transient.

For the nodal calculations, we specify two mesh layouts. One mesh layout, which we shall refer to as the "coarse" mesh, is an assembly-size mesh (15 cm × 15 cm). The other mesh layout, which we shall refer to as the "very coarse" mesh, is defined as follows for the 165 cm square quarter core:

region (u = x, y)	mesh division
0 cm ≤ u ≤ 15 cm	15 cm
15 cm ≤ u ≤ 105 cm	30 cm
105 cm ≤ u ≤ 135 cm	15 cm
135 cm ≤ u ≤ 165 cm	30 cm

The nodal array is (11 × 11) for the coarse mesh and (7 × 7) for the very coarse mesh. For our nodal method, there are 605 and 245 flux-current unknowns per group for the coarse mesh and very coarse mesh, respectively.

Let us first consider the static solution. We have already solved this problem in Chapter 3 with the coarse mesh. It was found that the coarse mesh solution with the quadratic transverse leakage approximation was in error by 0.01% in eigenvalue and had average and maximum

region power errors of 0.5% and 2.0%. (The reference solution is a nodal calculation with 16 nodes per assembly by Shober.[36]) A summary of results is presented in Table 4.9 for the very coarse mesh with the quadratic transverse leakage approximation. Also, results are presented with this same calculation for the final state of the reactor without thermal feedback. A reference solution is not available for this case. Power distributions obtained from these calculations are shown in Fig. A6.6a,b of Appendix 6. Both calculations used vacuum external boundary conditions and a 10^{-5} convergence criterion on the nodal average flux.

We find that an accurate solution for the initial state is obtained with the very coarse mesh. The eigenvalue is in error by 0.04% and the maximum error in region power is approximately 4%.

In Table 4.10, we compare static eigenvalues for the initial state and final state without feedback predicted by our method with coarse mesh nodal calculations of Werner,[39] Finnemann,[44] and Shober.[36] In this tabulation we also include coarse mesh results for our method. Relatively good agreement among all the calculations is observed in terms of the predicted reactivity worth of the perturbation without feedback which is approximated here as $\frac{\Delta k}{k}$.

Let us now turn to a discussion of the transient calculation. In order to minimize computational expense, we have performed the time-dependent calculation only with the very coarse mesh layout with the quadratic transverse leakage approximation. Before summarizing our results, we consider a few computational details.

Table 4.9 Summary of Static Results for the LRA Two-dimensional BWR Benchmark Problem: Very Coarse Mesh

State	Eigenvalue	ϵ_{avg} (%)	ϵ_{max} (%)	Inners per Outer group 1/group 2	Outers	Solution Time (%)
Initial	0.99595*	1.5	4.1	5/9	43	8.6
Final (without feedback)	1.01476	—	—	5/9	53	9.1

*Reference – 0.99636

Code: RM-Q

Table 4.10 Static Eigenvalues for the Initial State and Final State (without Feedback) of the LRA Two-dimensional BWR Kinetics Benchmark Problem

State	Eigenvalue (method): Werner (mesh layout): Coarse	Finnemann Coarse	Shober Coarse	Sims Coarse	Sims Very Coarse
Initial*	.99629	.99630	.99693	.99625	.99595
Final (without feedback)	1.01537	1.01531	1.01693	1.01521	1.01476
$\frac{(\gamma_{final}-\gamma_{initial})}{\gamma_{final}}$ $(\times 10^2)$	1.88	1.87	1.97	1.87	1.85

*Reference – .99636

Recall that, in the iterative method we employ to solve the spatial problem at a timestep, group-coupled response matrices are required (see Sec. 4.3.2). These response matrices must be modified on a node-wise basis in order to account for the spatially-dependent thermal feedback of this problem. The only approach we have considered for the formulation of the response matrices is to generate them from the basic data. Schemes such as correlation of the response elements with material thermal state have not been considered in this study. We now consider the cost associated with the regeneration of the response matrices in order to incorporate thermal feedback.

It was found in preliminary analysis for this problem that approximately 0.01 sec per node is required by our code to construct the response matrices. Thus, to regenerate these matrices each timestep for the very coarse mesh problem with 49 nodes requires approximately 0.5 sec. It was also found that the iteration speed of our code is approximately 0.0004 sec per node per iteration. This gives an approximate time of 0.02 sec per iteration for the very coarse mesh problem. Therefore, the coefficient generation time is roughly equivalent to 25 spatial iterations.

In examining results of the ramp perturbation TWIGL problem of Sec. 4.4.1, we found that, with use of exponential extrapolation, typically 10 to 30 iterations, and rarely more than 100 iterations, were required per timestep for adequate spatial convergence. Thus regeneration of the response matrices for each timestep could conceivably consume as much computational time as the spatial iterations themselves.

In order to reduce the computational burden associated with the regeneration of the response matrices for each timestep, we have considered an alternative scheme for determining the frequency with which the response matrices should be modified.

In general, the thermal properties of the reactor vary relatively slowly in comparison with the timestep size necessary for an accurate treatment of the flux behavior. In particular, for this problem the power must increase many orders of magnitude before feedback effects become important. Thus, we use a scheme in which the response matrices are modified to account for changes in thermal feedback only when those changes are estimated to be significant. We update the response matrices for changes in thermal feedback when

$$a_{\Sigma} \left| \sqrt{T_{max}} - \sqrt{T^{*}_{max}} \right| > \delta$$

where T_{max} is the maximum region temperature, T^{*}_{max} is the temperature at which the last thermal update was made, and δ is a fixed parameter. For this calculation, δ was chosen as 0.001. This value was determined from a simple perturbation theory argument using typical LWR characteristics such that the reactivity worth of an update was predicted to be less than 1 cent. Clearly, the procedure we describe for updating the response matrices is only applicable to the simple feedback model used in this problem.

Timestep sizes were taken to be those which Shober[36] found to yield acceptably accurate results with his fully-implicit method. The

calculation was divided into six time domains. It should be recalled that spatial iteration acceleration parameters are reestimated at the beginning of each time domain. The time domains and the associated timestep sizes were as follows:

Time Domain	Time Interval (sec)	Timestep Size (sec)
1	$0 \leq t \leq 1.0$	.01
2	$1.0 \leq t \leq 1.3$	.001
3	$1.3 \leq t \leq 1.45$	.0005
4	$1.45 \leq t \leq 1.6$	.0005
5	$1.6 \leq t \leq 2.0$	.002
6	$2.0 \leq t \leq 3.0$	.01

A convergence parameter of 10^{-4} was imposed on the spatial iterations. Exponential extrapolation was used to improve the initial guess for the spatial iteration at each timestep.

A summary of transient results for the very coarse mesh calculation is given in Table 4.11. Results obtained by Werner,[39] Finnemann,[44] and Shober[36] with the coarse mesh layout are also presented. Entries in Table 4.11 which are not reported are either uncertain or unknown. Detailed results of the very coarse mesh solution are shown in Appendix 6. Total power versus time is shown in Fig. A6.6c. Average and maximum temperatures versus time are displayed in Fig. A6.6d. Power and temperature distributions for the initial condition and for portions of the transient in which the total power is most rapidly varying are given in Figs. A6.6e-h. The times reported are 0.0, 1.4, 2.0, and 3.0 sec.

Table 4.11 Summary of Results for the LRA Two-dimensional BWR Kinetics Benchmark Problem

	Werner (Coarse Mesh)	Finnemann (Coarse Mesh)	Shober (Coarse Mesh)	Sims (Very Coarse Mesh)
Number of time steps	1200	–	1300	1300
Execution time (min)	2*	–	6.7	16.9
Time to first peak (sec)	1.455	1.4425	1.402	1.432
Average power at first peak (w)	5712	5489	5627	5760
Time to second peak (sec)	2.0	–	2.0	2.0
Average power at second peak (w)	850	–	838	840
Average temperature at t = 3.0 sec	–	1096	1162	1142
Maximum temperature at t = 3.0 sec	–	2979	3286	3163

*IBM 360/91

In general, the results obtained with the various methods are in relatively close agreement. The accuracy of our very coarse mesh calculation appears to be roughly equivalent to that of the coarse mesh calculations. However, our computation time is significantly longer than that reported by Werner and Shober even though we have used the very coarse mesh rather than the coarse mesh layout. We approach this situation with a discussion of some of the numerical details of our calculation.

We give a summary of the computational results of the very coarse mesh calculation in Table 4.12. Results are reported in terms of average number of iterations per timestep and total number of thermal updates for each time domain. The number of iterations per timestep is presented graphically for each time domain in Figs. A6.6i-n of Appendix 6. In these figures, indications are given for the timesteps at which thermal updates were performed.

During the last time domain, which includes a third of the total transient time, the reactor power is relatively slowly varying. Thus we would not expect this portion of the transient to be difficult to treat numerically. However, out of a total of 1300 timesteps, we find that over 50% of the computational effort was spent in the 100 timesteps of the last time domain. This result can be attributed to the stepwise introduction of thermal feedback which, as can be seen in the figures A6.6 of Appendix 6, causes large oscillations in the number of iterations per timestep when the larger timestep sizes are used. This effect is

Table 4.12 Summary of Computational Results for the LRA Two-dimensional BWR Kinetics Benchmark Problem

Time Domain	Number of Timesteps	Timestep Size	Average Number of Iterations per Timestep	Percentage of Total Iterations	Number of Thermal Updates
1 (0 sec $\leq$ t $\leq$ 1.0 sec)	100	.01	37	7	0
2 (1.0 sec $\leq$ t $\leq$ 1.3 sec)	300	.001	10	5	1
3 (1.3 sec $\leq$ t $\leq$ 1.45 sec)	300	.0005	19	11	40
4 (1.45 sec $\leq$ t $\leq$ 1.6 sec)	300	.0005	21	12	12
5 (1.6 sec $\leq$ t $\leq$ 2.0 sec)	200	.002	26	10	30
6 (2.0 sec $\leq$ t $\leq$ 3.0 sec)	100	.01	292	55	24

especially severe in the last time domain in which a 10 ms timestep size was employed. The very large number of iterations per timestep for the last time domain in comparison with the other time domains indicates that this timestep size is too large to treat adequately the stepwise introduction of thermal feedback.

The perturbations introduced by the inclusion of thermal feedback in this stepwise fashion apparently cause mild transients to be superimposed on the overall solution behavior which are relatively difficult to handle numerically. With large timestep sizes, a relatively large number of iterations is required to follow the "prompt jump" associated with each of the thermal feedback perturbations. Also, as we previously discussed, abrupt changes in reactor properties destroy the effectiveness of the extrapolation procedure. The effects encountered here suggest that it would be preferable to treat the thermal feedback in a continuous fashion in order to minimize numerical difficulties. It should be noted, however, that even though treatment of the thermal feedback in a stepwise manner caused irregularities in the numerical behavior, significant distortions in the time-dependent behavior of the reactor power were not observed.

We feel that a substantial reduction in total execution time could be made for this problem with proper selection of timestep size for the last time domain. For instance, if we use the timestep size of the preceding time domain for the last time domain and assume that the same average number of iterations per timestep will result as in the preceding time domain, we find that the overall solution time would be reduced by approximately 30%. The execution time with these assmptions would

be 12 minutes rather than 17 minutes.

Clearly, when the difference in number of nodes is taken into account between the very coarse mesh (49 nodes) which we have used and the coarse mesh (121 nodes) used by Werner and Shober, this reduced time is still rather high. A reduction by a factor of 4 to 5 in running time is required for our scheme to give a solution speed roughly comparable to those reported by the other researchers. This suggests a number of areas for further investigation.

One area for additional research concerns analysis of the numerical properties of the nodal equations and selection of optimum iterative solution strategies for the implicitly time-differenced formulation. We have tested only one option for solution of the time-dependent equations and have not examined a sufficiently wide range of test cases to evaluate adequately its computational behavior.

Another area is to investigate alternative formulations of the nodal equations. Werner[23,24] and Shober[36] have chosen nonlinear nodal formulations in which the primary calculational effort is directed toward solving flux equations rather than the current equations we employ. With only the very crudest considerations, this shift in emphasis for the two-dimensional case would perhaps offer a factor of 4 in computational efficiency. This gain is derived from the fact that in two dimensions there are 4 average leakage currents per node as compared with only a single average flux. However, as Shober[36] indicates, coefficient generation for these alternative formulations can dominate in time requirements as compared with the spatial solution itself, and thus direct gains

in the computational efficiency of the spatial solution may not imply equivalent gains in the overall solution efficiency.

It should be emphasized that, in comparison with all of these nodal methods (even in their unrefined state), a finite difference code such as MEKIN is expensive to use. For this problem, Shober has found that a (6 × 6) finite-difference mesh per assembly is necessary to achieve a maximum error of 5% in the region power distribution for the initial condition. Thus 4356 spatial mesh points are required for the quarter-core problem. The computing time per timestep on the IBM 370/168 computer required by MEKIN is[20]

$$(3 \times 10^{-4} \text{ sec})(\text{NPTX})(\text{NGX} + 0.3 * \text{NDFX})$$

where NPTX is the number of spatial mesh points, NGX is the number of energy groups, and NDFX is the number of delayed precursor families. For this problem in which NPTX = 4356, NGX = 2, and NDFX = 2, MEKIN would require 3.4 seconds of computing time per timestep. For the 1300 timesteps we have used, MEKIN would require 74 minutes to execute compared with the 17 minutes for our very coarse mesh solution. Therefore we show an advantage in computational efficiency by more than a factor of 4 with what we expect to be roughly equivalent accuracy. Moreover, MEKIN uses an explicit time integration scheme which typically requires a substantially smaller timestep size in order to achieve equivalent accuracy in comparison with the fully-implicit scheme which we employ. Therefore the computational advantage of our nodal method in comparison with MEKIN may be significantly greater than the factor of 4 derived above. With consideration of the difference

in time integration schemes, it is not unreasonable to expect at least an order of magnitude gain in computational efficiency.

In summary, we have shown that a relatively accurate solution of this difficult problem can be obtained with our nodal method with very large mesh spacings. In comparison with the finite difference method, large gains in computational efficiency can be achieved. Problems were encountered in the expense of generating coefficients because of the inclusion of thermal feedback. Also, computational efficiency was found to be lacking in comparison with other currently proposed nodal schemes. Further investigation is called for in both of these areas.

4.5 Summary

In this chapter, the two-dimensional, spatially-discretized, multigroup nodal equations with continuous time dependence were reduced to a set of discrete time-dependent equations by finite difference approximations of the time behavior. A solution method for one- and two-group, two-dimensional problems which is immediately applicable to three-dimensional calculations was developed and tested.

Results demonstrated that accurate time-dependent solutions can be obtained with large mesh sizes in relatively short computing times. It was shown that large gains in computational efficiency can be made in comparison with conventional finite difference methods.

A problem was identified concerning excessive costs associated with coefficient generation when feedback effects are included. Less costly schemes for inclusion of feedback effects need to be devised for application to the general case of coupled neutronic-thermal hydraulic analysis.

A comparison with other currently proposed nodal schemes shows our method to be competitive in accuracy but lacking somewhat in computational efficiency. Additional work is needed on the formulation and optimization of solution techniques for the time-dependent nodal equations which have been developed here.

Chapter 5

SUMMARY

5.1 Overview of Thesis Results

The overall objective of this thesis was to develop an economical computational method for multidimensional transient analysis of nuclear power reactors. Specifically, nodal methods were investigated. This particular approach was prompted by the success of recently developed nodal schemes in multidimensional static calculations.[5]

In Chapter 2, a set of multigroup, two-dimensional, spatially-discretized nodal equations with continuous time dependence was derived. The response matrix approach[18] was used as a conceptual basis. Solutions of local response problems were obtained in terms of only average quantities by use of polynomial approximations with weighted residual procedures applied to an equivalent set of one-dimensional problems. Two approximations were used for spatially-dependent transverse leakage terms appearing in the one-dimensional equations. These were the "constant" approximation in which spatially-dependent terms were replaced by their average values and the "quadratic" approximation[21] in which spatial shape corrections were obtained from a fitting procedure applied to average values in neighboring nodes. The final result was a set of spatially-discretized, time-dependent nodal equations expressed in terms of nodal average fluxes and interface average partial currents.

In Chapter 3, the set of time-dependent nodal equations was reduced to the static case. Iterative solution techniques were developed for

two-dimensional problems and were evaluated with respect to computational efficiency. Extension of the solution techniques to three-dimensional dimensional calculations was also discussed. A number of one- and two-dimensional, two-group test problems were considered. It was found that in all cases the nodal method gave very accurate results with a mesh the size of a LWR assembly when used with the quadratic transverse leakage approximation. Only one exception, a "checkerboard" PWR core, was encountered in which unacceptable errors were obtained with use of the constant transverse leakage approximation with an assembly-size mesh. Although the quadratic approximation was found to give consistently better results, the constant approximation for the transverse leakage permits the use of solution techniques with straightforward extensions to three dimensions which are more efficient. Gains in computational efficiency of an order of magnitude were demonstrated for the nodal method in comparison with conventional finite difference methods for two-dimensional static calculations.

In Chapter 4, the set of nodal equations with continuous time dependence was discretized in time by use of finite difference approximations. A fully implicit time-differencing scheme was employed for the principal part of the spatial operator. Shape correction terms associated with the transverse leakage approximation were treated explicitly in order to avoid complications in the iterative solution of the spatial problem at each timestep. Approximations were considered for the delayed precursor shape in order to reduce the number of precursor associated unknowns. Results of two-dimensional, two-group test problems

demonstrated that accurate transient solutions can be obtained with very large mesh sizes. Comparisons with finite difference codes such as TWIGL[41-43] and MEKIN[20] indicated that the nodal method can maintain the order of magnitude gain in computational efficiency in transient computations which was shown for static calculations.

In summary, the nodal method developed in this thesis has been shown to be highly accurate and relatively efficient for two-dimensional, few-group, static and transient reactor calculations. In comparison with finite difference methods, an order of magnitude improvement in computational efficiency has been shown for the nodal scheme. Thus, we find this nodal method to be an economical alternative to the standard finite difference methods currently employed for design and analysis of nuclear power reactors.

5.2 Recommendations for Future Work

Work is required in the following areas:

i. optimization of currently employed solution methods with respect to linear[35] and nonlinear[3] acceleration techniques;

ii. investigation of nonlinear schemes for treating the transverse leakage shape corrections in order to reduce the complexity of the spatial problem to be solved in the response matrix approach;

iii. application of alternative time-integration schemes such as semi-implicit and splitting methods as well as the use of transformations in time for reduction of temporal truncation error[4,6];

iv. development of schemes for economical updating of response parameters in the response matrix approach when thermal-hydraulic feedback is considered;

v. analysis of the numerical behavior of the currently employed time-dependent solution scheme with particular emphasis on the relationship of iterative convergence and solution accuracy;

vi. extension to three dimensions;

vii. investigation of nonlinear solution techniques which shift the the calculational emphasis from current equations to flux equations.[23, 24, 36]

REFERENCES

1. W. M. Stacey, Jr., "Space- and Energy-Dependent Neutronics in Reactor Transient Analysis," Reactor Technology 14, 169 (1971).

2. A. F. Henry, "Review of Computational Methods for Space-Dependent Kinetics," Dynamics of Nuclear Systems, David L. Hetrick (Ed.), University of Arizona Press, Tucson, Arizona (1972).

3. R. Roechlich, "Current Problems in Multidimensional Reactor Calculations," Proc. Conf. Mathematical Models and Computational Techniques for Analysis of Nuclear Systems, CONF-730414, Vol. 2, p. VII-1 (1973).

4. J. W. Stewart, "Recent Development of Methods for Multidimensional Reactor Dynamics," Proc. Conf. Mathematical Models and Computational Techniques for Analysis of Nuclear Systems, CONF-730414, Vol. 2, p. IX-1 (1973).

5. M. R. Wagner, "Current Trends in Multidimensional Static Reactor Calculations," Proc. Conf. on Computational Methods in Nuclear Engineering, CONF-750413, Vol. 1, p. I-1 (1975).

6. D. R. Ferguson, "Multidimensional Reactor Dynamics Today: An Overview," Proc. Conf. on Computational Methods in Nuclear Engineering, CONF-750413, Vol. 2, p. VI-49 (1975).

7. A. F. Henry, Nuclear-Reactor Analysis, M.I.T. Press, Cambridge, Mass. (1975).

8. L. A. Hageman and C. J. Pfeifer, "The Utilization of the Neutron Diffusion Program PDQ-5," WAPD-TM-395, Bettis Atomic Power Laboratory (1965).

9. D. R. Vondy, T. B. Fowler, and G. W. Cunningham, "VENTURE: A Code Block for Solving Multigroup Neutronics Problems Applying the Finite-Difference Diffusion Theory Approximation to Neutron Transport," ORNL-5062, Oak Ridge National Laboratory (1975).

10. R. S. Varga, Matrix Iterative Analysis, Prentice-Hall, Englewood Cliffs, N.J. (1962).

11. E. L. Wachspress, Iterative Solution of Elliptic Systems and Applications to the Neutron Diffusion Equations of Reactor Physics, Prentice-Hall, Englewood Cliffs, N.J. (1966).

12. D. M. Young, Iterative Solution of Large Linear Systems, Academic Press, New York, N.Y. (1971).

13. C. M. Kang and K. F. Hansen, "Finite Element Methods for Reactor Analysis," Nucl. Sci. Eng. 51, 456 (1973).

14. G. Strang and G. J. Fix, An Analysis of the Finite Element Method, Prentice-Hall, Englewood Cliffs, N.J. (1973).

15. W. M. Stacey, Jr., Variational Methods in Nuclear Reactor Physics, Academic Press, New York, N.Y. (1974).

16. A. F. Henry, "Refinements in Accuracy of Coarse-Mesh Finite-Difference Solutions of the Group Diffusion Equations," Seminar on Nuclear Reactor Calculations, IAEA/SM-154/21, p. 447 (1972).

17. A. Leonard, "Collision Probabilities and Response Matrices: An Overview," Proc. Conf. on Computational Methods in Nuclear Engineering, CONF-750413, Vol. 2, p. III-15 (1975).

18. Z. Weiss, "Some Basic Properties of Response Matrix Equations," Trans. Am. Nucl. Soc. 23, 198 (1976).

19. A. Ancona, M. Becker, D. R. Harris, A. DaC. Menezes, M. A. Robinson, and D. M. Ver Planck, "Unified Analysis of Nodal Methods," Trans. Am. Nucl. Soc. 24, 444 (1976).

20. R. W. Bowring, J. W. Stewart, R. A. Shober, and R. N. Sims, "MEKIN: MIT-EPRI Nuclear Reactor Core Kinetics Code," CCM-1, Electric Power Research Institute RP 227 (1975).

21. F. Bennewitz, H. Finnemann, and M. R. Wagner, "Higher Order Corrections in Nodal Reactor Calculations," Trans. Am. Nucl. Soc. 22, 250 (1975).

22. M. R. Wagner, "Nodal Synthesis Method and Imbedded Flux Calculations," Trans. Am. Nucl. Soc. 18, 152 (1974).

23. A. Birkhofer, S. Langenbuch, and W. Werner, "Coarse-Mesh Method for Space-Time Kinetics," Trans. Am. Nucl. Soc. 18, 153 (1974).

24. S. Langenbuch, W. Maurer, and W. Werner, "Simulation of Transients with Space-Dependent Feedback by Coarse Mesh Flux Expansion Method," Proc. Joint NEACRP/CSNI Specialists' Meeting on New Developments in Three-Dimensional Neutron Kinetics and Review of Kinetics Benchmark Calculations, MRR-145, Laboratorium für Reaktorregelung und Anlangensieherung, p. 173 (1975).

25. A. Müller and M. R. Wagner, "Use of Collision Probability Methods for Multidimensional Flux Calculations," Trans. Am. Nucl. Soc. 15, 280 (1972).

26. T. J. Burns and J. J. Dorning, "A Partial Current Balance Method for Space-, and Energy-Dependent Reactor Calculations," Proc. Conf. on Mathematical Models and Computational Techniques for Analysis of Nuclear Systems, CONF-730414, Vol. 2, p. VII-162 (1973).

27. T. J. Burns and J. J. Dorning, "The Partial Current Balance Method: A New Computational Method for the Solution of Multi-dimensional Neutron Diffusion Problems," Proc. Joint NEACRP/CSNI Specialists' Meeting on New Developments in Three-Dimensional Neutron Kinetics and Review of Kinetics Benchmark Calculations, MRR-145, Laboratorium für Reaktorregelung und Anlangensieherung, p. 111 (1975).

28. T. J. Burns and J. J. Dorning, "Multidimensional Applications of an Integral Balance Technique for Neutron Diffusion Calculations," Proc. Conf. on Computational Methods in Nuclear Engineering, CONF-750413, Vol. 2, p. VI-69 (1975).

29. H. Finnemann, "A Consistent Nodal Method for the Analysis of Space-Time Effects in Large LWR's," Proc. Joint NEACRP/CSNI Specialists' Meeting on New Developments in Three-Dimensional Neutron Kinetics and Review of Kinetics Benchmark Calculations, MRR-145, Laboratorium für Reaktorregelung und Anlangensieherung, p. 131 (1975).

30. F. Bennewitz, H. Finnemann, and H. Moldaschl, "Solution of the Multidimensional Neutron Diffusion Equation by Nodal Expansion," Proc. Conf. on Computational Methods in Nuclear Engineering, CONF-750413, Vol. 1, p. I-99 (1975).

31. H. Finnemann and M. R. Wagner, "A New Computational Technique for the Solution of Multidimensional Neutron Diffusion Problems," presented at the International Meeting of Specialists on "Methods of Neutron Transport Theory in Reactor Calculations," Bologna, Italy, November 3-5, 1975.

32. B. A. Finlayson, The Method of Weighted Residuals and Variational Principles, Academic Press, New York, N.Y. (1972).

33. P. C. Kalambokas and A. F. Henry, "The Replacement of Reflectors by Albedo Type Boundary Conditions," Proc. Conf. on Computational Methods in Nuclear Engineering, CONF-750413, Vol. 1, p. I-25 (1975).

34. L. A. Hageman, "Numerical Methods and Techniques Used in the Two-Dimensional Neutron-Diffusion Program PDQ-5," WAPD-TM-364, Bettis Atomic Power Laboratory (1963).

35. L. A. Hageman, "The Estimation of Acceleration Parameters for the Chebyshev Polynomial and the Successive Overrelaxation Iteration Methods," WAPD-TM-1038, Bettis Atomic Power Laboratory (1972).

36. R. A. Shober and A. F. Henry, "Nonlinear Methods for Solving the Diffusion Equation," MIT Report, MITNE-196 (November 1976).

37. G. K. Kristiansen, "Investigation of the Accuracy of Centerpoint-, Cornerpoint-, and Finite-Element-Methods for Solution of the Neutron Diffusion Equation," NEACRP-L-149, Danish Atomic Energy Commission (1976).

38. D. R. Vondy, T. B. Fowler, G. W. Cunningham, and D. B. Selby, "Two- and Three-Dimensional Reactor Benchmark Problems," Oak Ridge National Laboratory (August 1976).

39. W. Werner, private communications (1976).

40. W. M. Stacey, Jr., Space-Time Nuclear Reactor Kinetics, Academic Press, New York, N.Y. (1969).

41. L. A. Hageman and J. B. Yasinsky, "Comparison of Alternating-Direction Time-Differencing Methods and Other Implicit Methods for the Solution of the Neutron Group Diffusion Equations," Nucl. Sci. Eng. 38, 8 (1969).

42. J. B. Yasinsky and L. A. Hageman, "On the Solution of the Time-Dependent Group Diffusion Equations by an Implicit Time Differenced Iterative Method," Proc. Conf. on the Effective Use of Computers in the Nuclear Industry, CONF-690401, p. 55 (1969).

43. J. B. Yasinsky, M. Natelson, and L. A. Hageman, "TWIGL – A Program to Solve the Two-Dimensional, Two-Group, Space-Time Neutron Diffusion Equations with Temperature Feedback," WAPD-TM-743, Bettis Atomic Power Laboratory (1968).

44. W. Werner, H. Finnemann, and S. Langenbuch, "Two- and Three-Dimensional BWR Kinetics Problem," Trans. Am. Nucl. Soc. 23, 215 (1976).

45. R. N. Sims, "Description of the Two-Dimensional Nodal Codes NRMS, a Multigroup Statics Code, and NRMT, a One- and Two-Group Transient Code," MIT Report, MITNE-201 (March 1977).

Appendix 1

ONE-DIMENSIONAL AVERAGE FLUX EXPANSION FUNCTIONS

The polynomial approximation for the one-dimensional average flux [Sec. 2.3.3.1a, Eq. (2.10)] in node (ij), space direction u, and energy group g is

$$\phi^{u}_{g,ij}(u,t) \approx \phi_{g,ij}(t)\ \rho^{\phi,u}_{g,ij}(u,t) + J^{in,u-}_{g,ij}(t)\ \rho^{in,u-}_{g,ij}(u,t)$$
$$+ J^{out,u-}_{g,ij}(t)\ \rho^{out,u-}_{g,ij}(u,t) + J^{in,u+}_{g,ij}(t)\ \rho^{in,u+}_{g,ij}(u,t)$$
$$+ J^{out,u+}_{g,ij}(t)\ \rho^{out,u+}_{g,ij}(u,t)$$

where the ρ's are quartic polynomials chosen such that the conditions implied by the coefficients are satisfied. We introduce the operator notation

$$P^{in,u-}_{g,ij}\,\cdot \equiv \left[\frac{1}{4} - \frac{1}{2} D_{g,ij}(t)\,\frac{\partial}{\partial u}\right]_{u=u_{\ell}} \cdot$$

$$P^{out,u-}_{g,ij}\,\cdot \equiv \left[\frac{1}{4} + \frac{1}{2} D_{g,ij}(t)\,\frac{\partial}{\partial u}\right]_{u=u_{\ell}} \cdot$$

$$P^{in,u+}_{g,ij}\,\cdot \equiv \left[\frac{1}{4} + \frac{1}{2} D_{g,ij}(t)\,\frac{\partial}{\partial u}\right]_{u=u_{\ell+1}} \cdot$$

$$P^{out,u+}_{g,ij}\,\cdot \equiv \left[\frac{1}{4} - \frac{1}{2} D_{g,ij}(t)\,\frac{\partial}{\partial u}\right]_{u=u_{\ell+1}} \cdot$$

$$Q^{u}_{ij}\,\cdot \equiv \frac{1}{h^{\ell}_{u}} \int_{u_{\ell}}^{u_{\ell+1}} du\ \cdot\ . \qquad \text{(A1.1)}$$

If we denote the polynomial approximation for $\phi^{u}_{g,ij}(u,t)$ by $\psi^{u}_{g,ij}(u,t)$, then the restraints on ψ are

$$P^{in,u-}_{g,ij} \cdot \psi^{u}_{g,ij}(u,t) = J^{in,u-}_{g,ij}(t)$$

$$P^{out,u-}_{g,ij} \cdot \psi^{u}_{g,ij}(u,t) = J^{out,u-}_{g,ij}(t)$$

$$P^{in,u+}_{g,ij} \cdot \psi^{u}_{g,ij}(u,t) = J^{in,u+}_{g,ij}(t)$$

$$P^{out,u+}_{g,ij} \cdot \psi^{u}_{g,ij}(u,t) = J^{out,u+}_{g,ij}(t)$$

$$Q^{u}_{ij} \cdot \psi^{u}_{g,ij}(u,t) = \phi_{g,ij}(t). \qquad \text{(A1.2)}$$

These restraints require that the ρ's satisfy the following conditions, presented here in tabular form:

	$\rho^{in,u-}_{g,ij}(u,t)$	$\rho^{out,u-}_{g,ij}(u,t)$	$\rho^{in,u+}_{g,ij}(u,t)$	$\rho^{out,u+}_{g,ij}(u,t)$	$\rho^{\phi}_{g,ij}(u,t)$
$P^{in,u-}_{g,ij}\cdot$	1	0	0	0	0
$P^{out,u-}_{g,ij}\cdot$	0	1	0	0	0
$P^{in,u+}_{g,ij}\cdot$	0	0	1	0	0
$P^{out,u+}_{g,ij}\cdot$	0	0	0	1	0
$Q^{u}_{ij}\cdot$	0	0	0	0	1

(A1.3)

In order to give specific expressions for the ρ's, we first introduce quartic polynomial basis functions denoted as q's. These basis functions are defined by the conditions presented in the following table:

	$q_\ell^{u-,0}(u)$	$q_\ell^{u-,1}(u)$	$q_\ell^{u+,0}(u)$	$q_\ell^{u+,1}(u)$	$q_\ell^{u0,0}(u)$
$q(u_\ell)$	1	0	0	0	0
$\left.\frac{dq(u)}{du}\right\|_{u=u_\ell}$	0	1	0	0	0
$q(u_{\ell+1})$	0	0	1	0	0
$\left.\frac{dq(u)}{du}\right\|_{u=u_{\ell+1}}$	0	0	0	1	0
$\frac{1}{h_\ell^u}\int_{u_\ell}^{u_{\ell+1}} duq(u)$	0	0	0	0	1

(A1.4)

We define the spatial variable z as

$$z \equiv \frac{u - u_\ell}{h_\ell^u}. \tag{A1.5}$$

With this definition, the q's are given explicitly by

$$q_\ell^{u-,0}(u) = 1 - 18z^2 + 32z^3 - 15z^4$$

$$q_\ell^{u-,1}(u) = z - \frac{9}{2}z^2 + 6z^3 - \frac{5}{2}z^4$$

$$q_\ell^{u+,0}(u) = -12z^2 + 28z^3 - 15z^4$$

$$q_\ell^{u+,1}(u) = \frac{3}{2}z^2 - 4z^3 + \frac{5}{2}z^4$$

$$q_\ell^{u0,0}(u) = 30z^2 - 60z^3 + 30z^4. \tag{A1.6}$$

These basis functions on the unit interval are shown graphically in Fig. A1.1. In terms of the q's, the ρ's are

$$\rho_{g,ij}^{in,u-}(u,t) = 2q_\ell^{u-,0}(u) - \frac{h_\ell^u}{D_{g,ij}(t)} q_\ell^{u-,1}(u)$$

$$\rho_{g,ij}^{out,u-}(u,t) = 2q_\ell^{u-,0}(u) + \frac{h_\ell^u}{D_{g,ij}(t)} q_\ell^{u-,1}(u)$$

$$\rho_{g,ij}^{in,u+}(u,t) = 2q_\ell^{u+,0}(u) + \frac{h_\ell^u}{D_{g,ij}(t)} q_\ell^{u+,1}(u)$$

$$\rho_{g,ij}^{out,u+}(u,t) = 2q_\ell^{u+,0}(u) - \frac{h_\ell^u}{D_{g,ij}(t)} q_\ell^{u+,1}(u)$$

$$\rho_{g,ij}^{\phi,u}(u,t) = q_\ell^{u0,0}(u). \tag{A1.7}$$

Equations (A1.5)-(A1.7) completely define the one-dimensional average flux expansion coefficients.

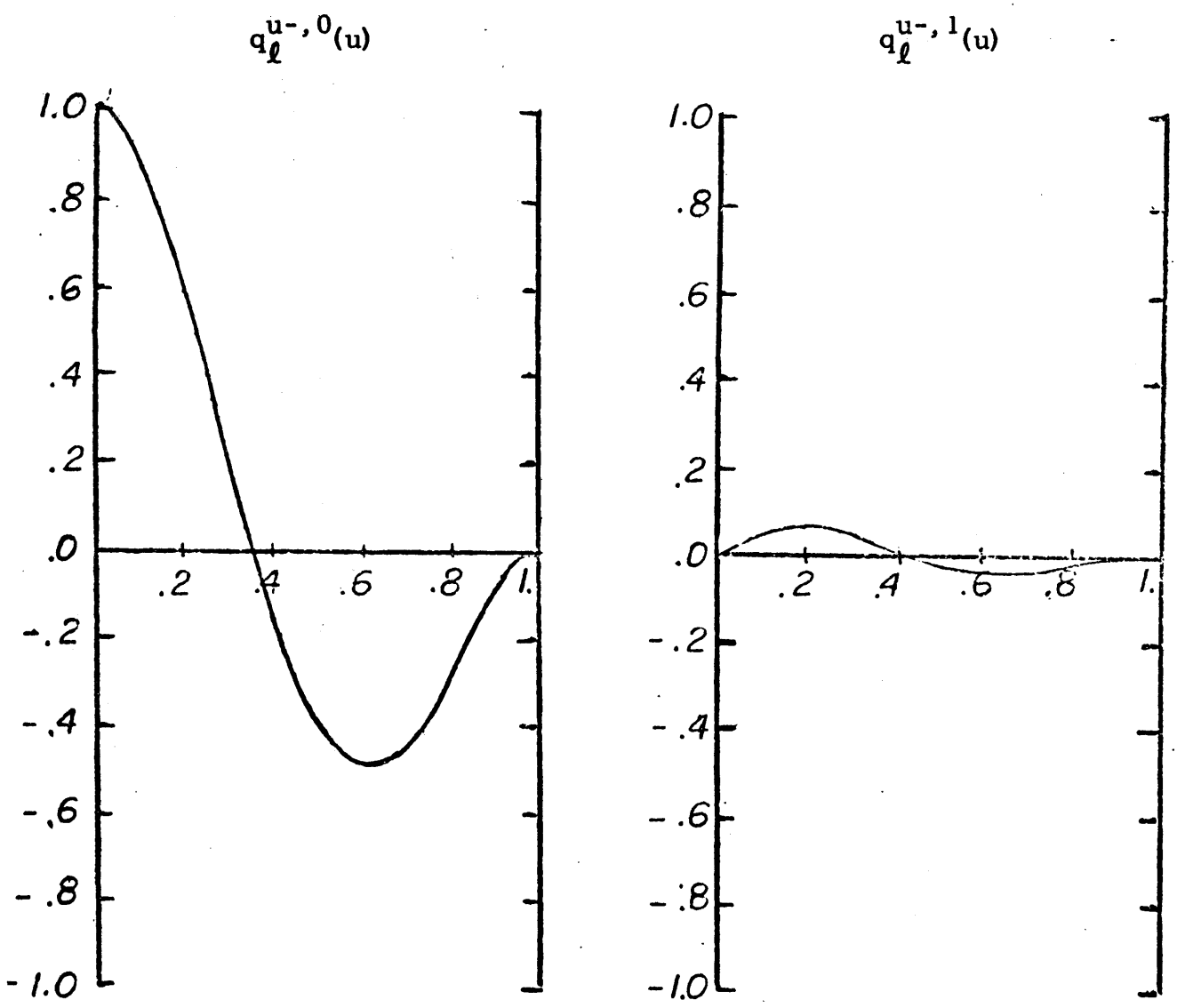

Figure A1.1 Basis Functions for the One-dimensional Average Flux Expansion

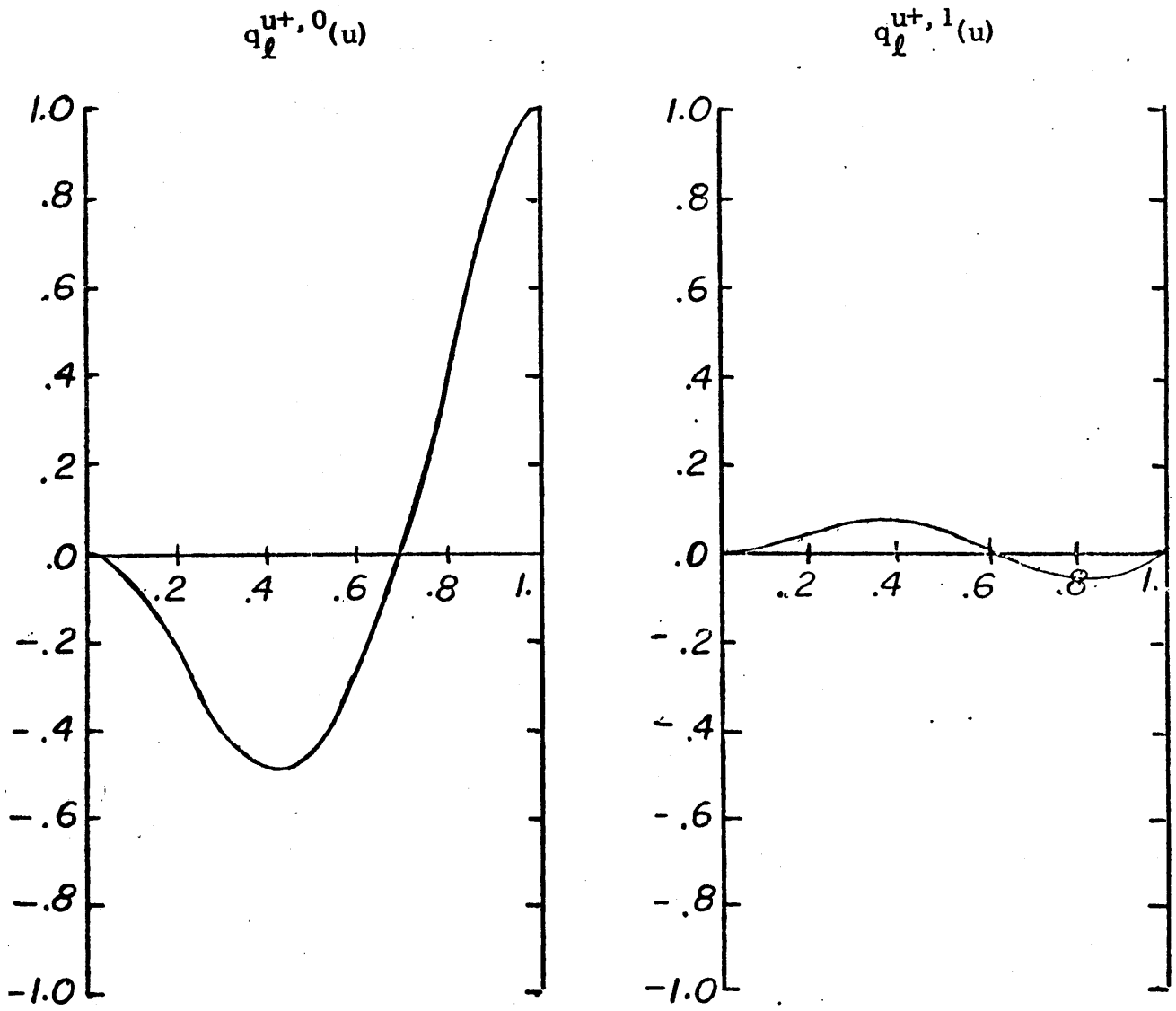

Figure A1.1, contd.

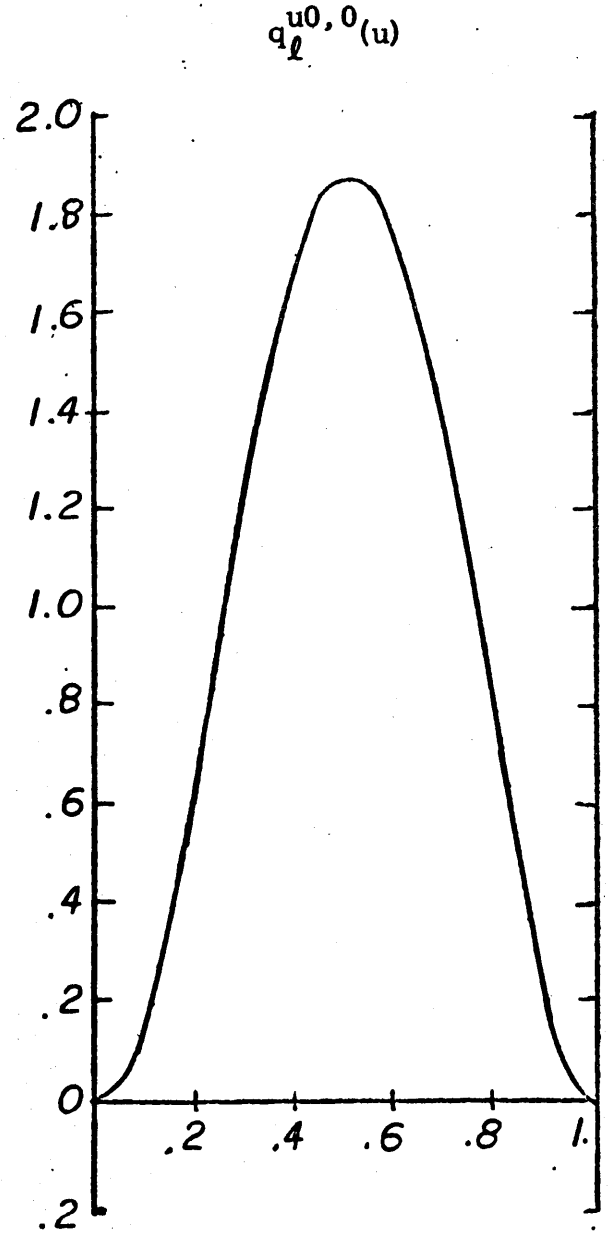

Figure A1.1, contd.

Appendix 2

"QUADRATIC" TRANSVERSE LEAKAGE EXPANSION FUNCTIONS

The polynomial approximation of the transverse leakage, Eqs. (2.3a) and (2.4), discussed in Sec. 2.3.3.1c, can be written as

$$L^{u}_{g,\ell\ell'}(u,t) \approx \tilde{L}^{u}_{g,\ell-1\ell'}(t)\,\rho^{u}_{\ell\ell-1}(u) + \tilde{L}^{u}_{g,\ell\ell'}(t)\,\rho^{u}_{\ell\ell}(u) + \tilde{L}^{u}_{g,\ell+1\ell'}(t)\,\rho^{u}_{\ell\ell+1}(u) \tag{A2.1}$$

where the $\tilde{L}$'s are average total leakages in the direction transverse to coordinate u in three adjacent nodes in the u direction, and the ρ's are quadratic expansion functions dependent only on the grid spacing in the u direction. In order to preserve the integral interpretation of the average transverse leakages (or the corresponding average transverse partial currents), the following conditions presented here in tabular form must be obeyed by the expansion functions:

	$\rho^{u}_{\ell\ell-1}(u)$	$\rho^{u}_{\ell\ell}(u)$	$\rho^{u}_{\ell\ell+1}(u)$
$\frac{1}{h^{u}_{\ell-1}} \int_{u_{\ell-1}}^{u_{\ell}} du\ \rho(u)$	1	0	0
$\frac{1}{h^{u}_{\ell}} \int_{u_{\ell}}^{u_{\ell+1}} du\ \rho(u)$	0	1	0
$\frac{1}{h^{u}_{\ell+1}} \int_{u_{\ell+1}}^{u_{\ell+1}} du\ \rho(u)$	0	0	1

(A2.2)

We define the spatial variable z as

$$z \equiv \frac{u - u_\ell}{h^u_\ell}. \tag{A2.3}$$

With this definition, we express the general form of the ρ's as

$$\rho^u_{\ell\ell-1}(u) = a^u_{\ell\ell-1} + b^u_{\ell\ell-1} z + c^u_{\ell\ell-1} z^2$$

$$\rho^u_{\ell\ell}(u) = a^u_{\ell\ell} + b^u_{\ell\ell} z + c^u_{\ell\ell} z^2$$

$$\rho^u_{\ell\ell+1}(u) = a^u_{\ell\ell+1} + b^u_{\ell\ell+1} z + c^u_{\ell\ell+1} z^2. \tag{A2.4}$$

We denote the mesh spacings as

$$h_m \equiv h^u_{\ell-1}$$

$$h \equiv h^u_\ell$$

$$h_p = h^u_{\ell+1} \tag{A2.5}$$

and introduce the normalizing parameter d defined as

$$d^u_\ell \equiv h^4\left(\tfrac{1}{6} h_m h_p\right) + h^3\left(\tfrac{1}{3} h_m^2 h_p + \tfrac{1}{3} h_m h_p^2\right)$$

$$+ h^2\left(\tfrac{1}{6} h_m^3 h_p + \tfrac{1}{2} h_m^2 h_p + \tfrac{1}{6} h_m h_p^3\right) + h\left(\tfrac{1}{6} h_m^3 h_p^2 + \tfrac{1}{6} h_m^2 h_p^3\right). \tag{A2.6}$$

By applying the conditions of Eq. (A2.2) to the expansions of Eq. (A2.4), we find that the polynomial coefficients (a's, b's, and c's) are

$$d^u_{\ell} a^u_{\ell\ell-1} = h^4\left(\tfrac{1}{6} h_m h_p\right) + h^3\left(\tfrac{1}{3} h_m h_p^2\right) + h^2\left(\tfrac{1}{6} h_m h_p^3\right)$$

$$d^u_{\ell} b^u_{\ell\ell-1} = h^4\left(-\tfrac{2}{3} h_m h_p\right) + h^3\left(-h_m h_p^2\right) + h^2\left(-\tfrac{1}{3} h_m h_p^3\right)$$

$$d^u_{\ell} c^u_{\ell\ell-1} = h^4\left(\tfrac{1}{2} h_m h_p\right) + h^3\left(\tfrac{1}{2} h_m h_p^2\right)$$

$$d^u_{\ell} a^u_{\ell\ell} = h^3\left(\tfrac{1}{2} h_m^2 h_p\right) + h^2\left(\tfrac{1}{3} h_m^3 h_p + \tfrac{1}{2} h_m^2 h_p^2\right)$$

$$+ h\left(\tfrac{1}{6} h_m^3 h_p^2 + \tfrac{1}{6} h_m^2 h_p^3\right)$$

$$d^u_{\ell} b^u_{\ell\ell} = h^4\left(h_m h_p\right) + h^3\left(h_m h_p^2\right) + h^2\left(-\tfrac{1}{3} h_m^3 h_p + \tfrac{1}{3} h_m h_p^3\right)$$

$$d^u_{\ell} c^u_{\ell\ell} = h^4\left(-h_m h_p\right) + h^3\left(-\tfrac{1}{2} h_m^2 h_p - \tfrac{1}{2} h_m h_p^2\right)$$

$$d^u_{\ell} a^u_{\ell\ell+1} = h^3\left(-\tfrac{1}{6} h_m^2 h_p\right) + h^2\left(-\tfrac{1}{6} h_m^3 h_p\right)$$

$$d^u_{\ell} b^u_{\ell\ell+1} = h^4\left(-\tfrac{1}{3} h_m h_p\right) + h^2\left(\tfrac{1}{3} h_m^3 h_p\right)$$

$$d^u_{\ell} c^u_{\ell\ell+1} = h^4\left(\tfrac{1}{2} h_m h_p\right) + h^3\left(\tfrac{1}{2} h_m^2 h_p^2\right). \qquad \text{(A2. 7)}$$

Relations (A2. 5)-(A2. 7) completely specify the transverse leakage polynomial expansion functions. Actually, because of the particular form chosen in Sec. 2. 3. 3. 1c for the transverse leakage approximation, only $\rho^u_{\ell\ell-1}$ and $\rho^u_{\ell\ell+1}$ are explicitly used. This is the case because the complete quadratic set $\rho^u_{\ell\ell-1}$, $\rho^u_{\ell\ell}$, and $\rho^u_{\ell\ell+1}$ is replaced by the equivalent complete quadratic set 1 $\left(=\rho^u_{\ell\ell-1} + \rho^u_{\ell\ell} + \rho^u_{\ell\ell+1}\right)$, $\rho^u_{\ell\ell-1}$ and $\rho^u_{\ell\ell+1}$.

The ρ's for a uniform mesh with unit interval width are shown graphically in Fig. A2.1. The reader should note that the polynomial coefficients, Eq. (A2.7), can be greatly simplified in the case of uniform mesh spacing.

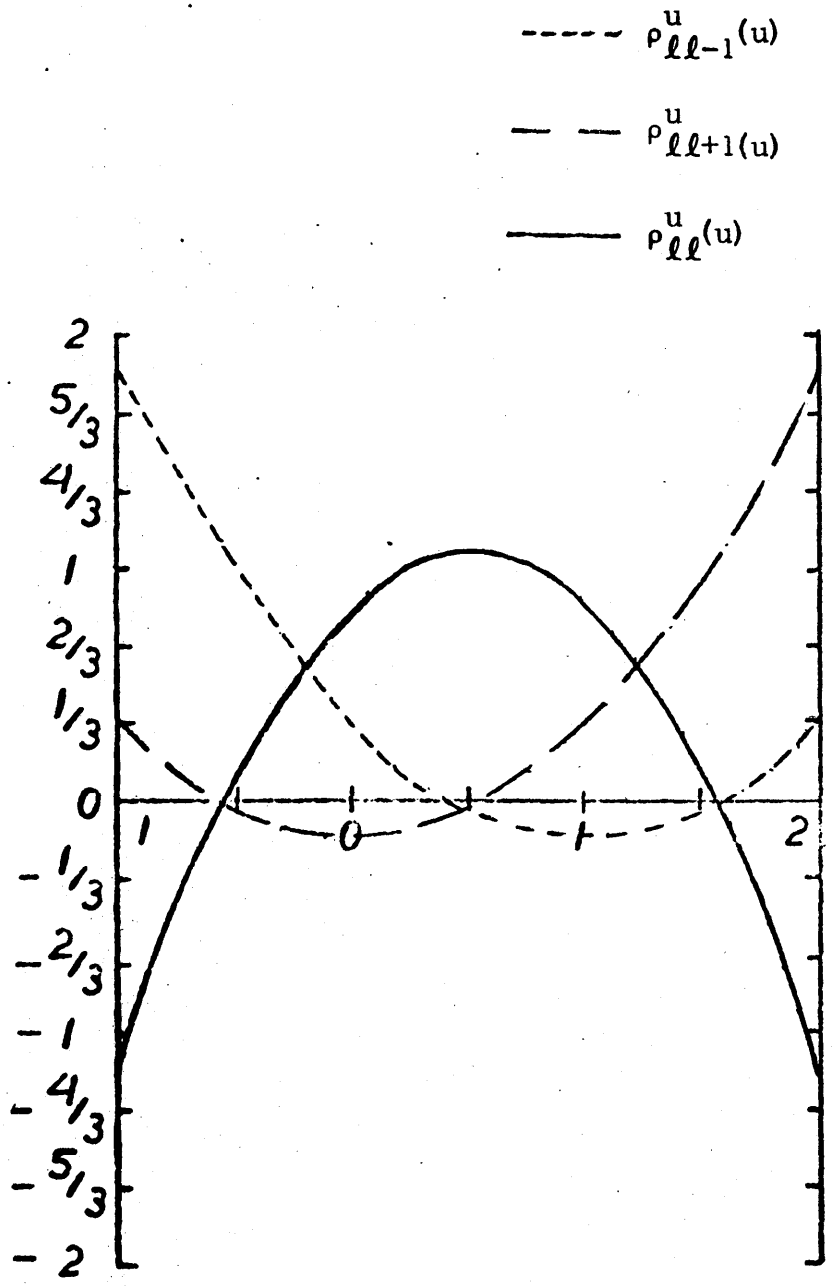

Figure A2.1 Basis Functions for the Quadratic Transverse Leakage Expansion

Appendix 3

WEIGHT FUNCTIONS

A quadratic moments weighted residual procedure is applied in each energy group and delayed family and in each coordinate direction of the one-dimensional average diffusion equations (Sec. 2.3.3.2) in order to determine the unknown coefficients of the polynomial expansions used to approximate the spatial dependence of fluxes and currents. The quadratic weight functions employed are members of the complete quadratic set defined on the interval $[u_\ell, u_{\ell+1}]$ by requiring unit or zero function values at the end points and midpoint of the interval. Specifically, we define the quadratic basis functions, q's, as

$$
\begin{aligned}
q_\ell^{u,0}(u) &\equiv a_\ell^{u,0} + b_\ell^{u,0} z + c_\ell^{u,0} z^2 \\
q_\ell^{u,\frac{1}{2}}(u) &\equiv a_\ell^{u,\frac{1}{2}} + b_\ell^{u,\frac{1}{2}} z + c_\ell^{u,\frac{1}{2}} z^2 \\
q_\ell^{u,1}(u) &\equiv a_\ell^{u,1} + b_\ell^{u,1} z + c_\ell^{u,1} z^2
\end{aligned}
\qquad \text{(A3.1)}
$$

where the spatial variable z is defined as

$$
z \equiv \frac{u - u_\ell}{h_\ell^u}. \qquad \text{(A3.2)}
$$

The coefficients of these polynomials are completely determined by the conditions presented in the following tabular form:

	$q_\ell^{u,0}(u)$	$q_\ell^{u,\frac{1}{2}}(u)$	$q_\ell^{u,1}(u)$
$q(u_\ell)$	1	0	0
$q\left(u_\ell + \frac{1}{2} h_\ell^u\right)$	0	1	0
$q(u_{\ell+1})$	0	0	1

(A3. 3)

By applying the conditions of Eqs. (A3. 3), we find the polynomial coefficients (a's, b's, and c's of (A3. 1)) are

$$a_\ell^{u,0} = 1 \qquad a_\ell^{u,\frac{1}{2}} = 0 \qquad a_\ell^{u,1} = 0$$

$$b_\ell^{u,0} = -3 \qquad b_\ell^{u,\frac{1}{2}} = 4 \qquad b_\ell^{u,1} = -1$$

$$c_\ell^{u,0} = 2 \qquad c_\ell^{u,\frac{1}{2}} = -4 \qquad c_\ell^{u,1} = 2. \qquad \text{(A3. 4)}$$

Equations (A3. 1), (A3. 2), and (A3. 4) completely specify the quadratic set which is complete on the interval $[u_\ell, u_{\ell+1}]$. These functions on the unit interval are shown graphically in Fig. A3. 1.

Actually, only $q_\ell^{u,0}$ and $q_\ell^{u,1}$ are explicitly used in the weighted residual procedure. This is the case because the complete quadratic set $q_\ell^{u,0}$, $q_\ell^{u,\frac{1}{2}}$, and $q_\ell^{u,1}$ is replaced by the equivalent complete quadratic set 1 $\left(= q_\ell^{u,0} + q_\ell^{u,\frac{1}{2}} + q_\ell^{u,1}\right)$, $q_\ell^{u,0}$, and $q_\ell^{u,1}$ on the interval $[u_\ell, u_{\ell+1}]$. The weight functions of Sec. 2. 3. 3. 3, denoted as w's, are

$$w_{n,ij}^u(u) \equiv q_\ell^{u,n}(u); \qquad n = 0, 1. \qquad \text{(A3. 5)}$$

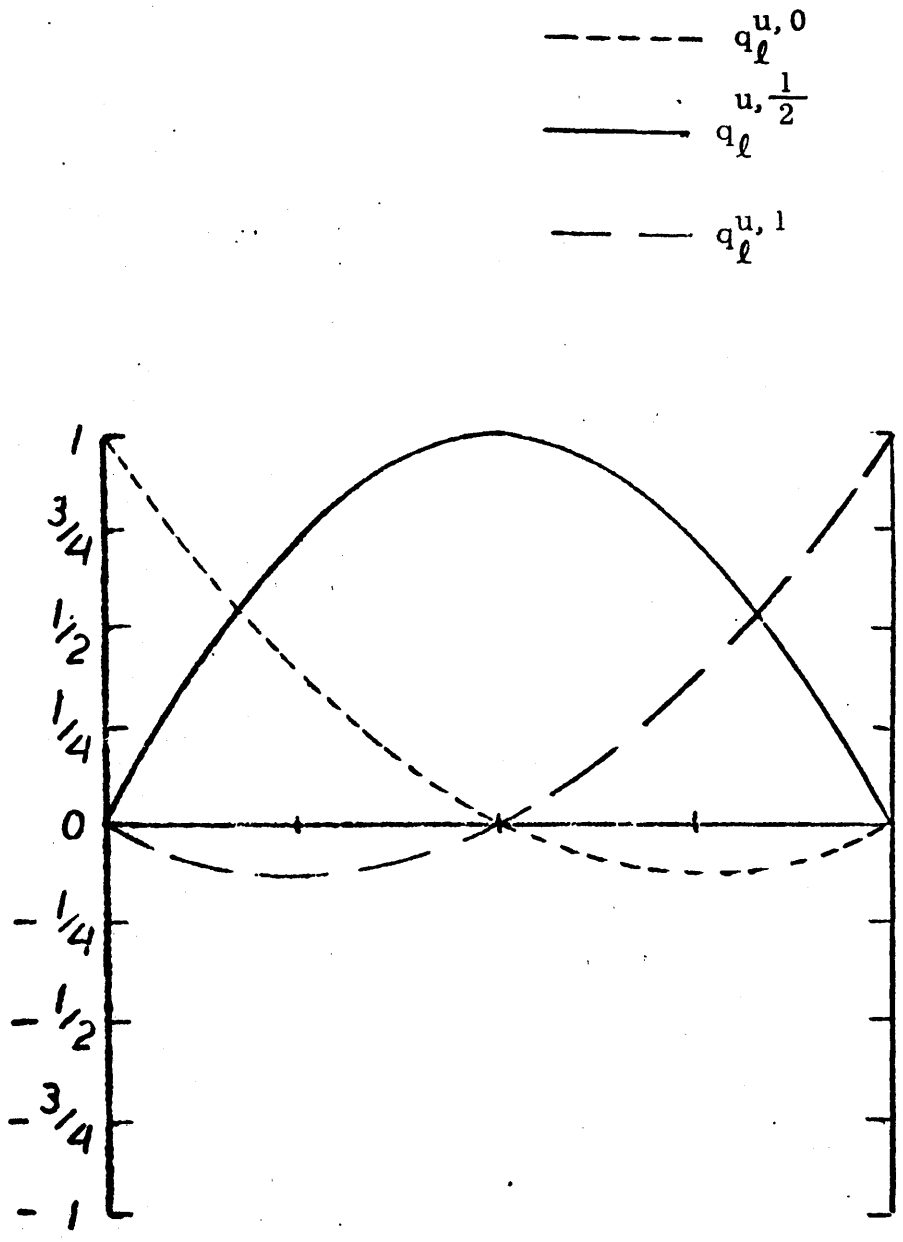

Figure A3.1 Weight Functions for the One-dimensional Weighted Residual Procedure

Appendix 4

EVALUATION OF WEIGHTED INTEGRALS

The weighted integrals appearing in Sec. 2.3.3.3 are evaluated here. These integrals result from application of a quadratic moments weighted residual procedure in each node to each energy group and delayed family and to each coordinate direction of the one-dimensional average diffusion equations in order to determine unknown coefficients associated with polynomial approximations of flux, precursor, and transverse leakage spatial shapes. The polynomial approximations are discussed and explicitly defined in Sec. 2.3.3.1a and App. 1 for the one-dimensional average fluxes, Sec. 2.3.3.1b for the one-dimensional average delayed precursors, and Sec. 2.3.3.1c and App. 2 for the transverse leakage. The weighted residual weight functions are explicitly defined in App. 3.

Weighted integrals associated with the one-dimensional average flux expansions are

$$\left\langle w^u_{0,ij} \middle| \frac{d^2}{du^2} \rho^{in,u-}_{g,ij}(t) \right\rangle = \left\langle w^u_{1,ij} \middle| \frac{d^2}{du^2} \rho^{in,u+}_{g,ij}(t) \right\rangle = \frac{1}{h^u_\ell} \left(-6 + \frac{h^u_\ell}{D_{g,ij}(t)} \right)$$

$$\left\langle w^u_{0,ij} \middle| \frac{d^2}{du^2} \rho^{out,u-}_{g,ij}(t) \right\rangle = \left\langle w^u_{1,ij} \middle| \frac{d^2}{du^2} \rho^{out,u+}_{g,ij} \right\rangle = \frac{1}{h^u_\ell} \left(-6 - \frac{h^u_\ell}{D_{g,ij}(t)} \right)$$

$$\left\langle w^u_{0,ij} \middle| \frac{d^2}{du^2} \rho^{in,u+}_{g,ij}(t) \right\rangle = \left\langle w^u_{1,ij} \middle| \frac{d^2}{du^2} \rho^{in,u-}_{g,ij}(t) \right\rangle = \frac{1}{h^u_\ell} (-2)$$

$$\left\langle w^u_{0,ij} \middle| \frac{d^2}{du^2} \rho^{out,u+}_{g,ij} \right\rangle = \left\langle w^u_{1,ij} \middle| \frac{d^2}{du^2} \rho^{out,u-}_{g,ij}(t) \right\rangle = \frac{1}{h^u_\ell} (-2)$$

$$\langle w^u_{0,ij} | \frac{d^2}{du^2} \rho^{\phi,u}_{g,ij}(t) \rangle = \langle w^u_{1,ij} | \frac{d^2}{du^2} \rho^{\phi,u}_{g,ij}(t) \rangle = \frac{1}{h^u_\ell} \quad (4)$$

$$\langle w^u_{0,ij} | \rho^{in,u-}_{g,ij}(t) \rangle = \langle w^u_{1,ij} | \rho^{in,u+}_{g,ij}(t) \rangle = h^u_\ell \left(\frac{31}{105} - \frac{3}{280} \frac{h^u_\ell}{D_{g,ij}(t)} \right)$$

$$\langle w^u_{0,ij} | \rho^{out,u-}_{g,ij}(t) \rangle = \langle w^u_{0,ij} | \rho^{out,u+}_{g,ij}(t) \rangle = h^u_\ell \left(\frac{31}{105} + \frac{3}{280} \frac{h^u_\ell}{D_{g,ij}(t)} \right)$$

$$\langle w^u_{0,ij} | \rho^{in,u+}_{g,ij}(t) \rangle = \langle w^u_{1,ij} | \rho^{in,u-}_{g,ij}(t) \rangle = h^u_\ell \left(-\frac{11}{105} + \frac{1}{168} \frac{h^u_\ell}{D_{g,ij}(t)} \right)$$

$$\langle w^u_{0,ij} | \rho^{out,u+}_{g,ij}(t) \rangle = \langle w^u_{1,ij} | \rho^{out,u-}_{g,ij}(t) \rangle = h^u_\ell \left(-\frac{11}{105} - \frac{1}{168} \frac{h^u_\ell}{D_{g,ij}(t)} \right)$$

$$\langle w^u_{0,ij} | \rho^{\phi,u}_{g,ij}(t) \rangle = \langle w^u_{1,ij} | \rho^{\phi,u}_{g,ij}(t) \rangle = h^u_\ell \left(\frac{1}{14} \right). \quad (A4.1)$$

Weighted integrals of the flat component of the transverse leakage as well as the shape function associated with the flat approximation of the one-dimensional average delayed precursors are integrals of the weight functions themselves and are evaluated as

$$\langle w^u_{0,ij} | 1 \rangle = \langle w^u_{1,ij} | 1 \rangle = \frac{1}{6} h^u_\ell. \quad (A4.2)$$

We now evaluate weighted integrals associated with the transverse leakage expansion. The expansion function notation of App. 2 is used. First we introduce the mesh spacing notation

$$h_m \equiv h^u_{\ell-1}$$

$$h \equiv h^u_{\ell}$$

$$h_p \equiv h^u_{\ell+1}$$

and the normalizing factor, d, which is defined as

$$d \equiv h^4\left(\tfrac{1}{6} h_m h_p\right) + h^3\left(\tfrac{1}{3} h_m^2 h_p + \tfrac{1}{3} h_m h_p^2\right)$$

$$+ h^2\left(\tfrac{1}{6} h_m^3 h_p + \tfrac{1}{2} h_m^2 h_p^2 + \tfrac{1}{6} h_m h_p^3\right) + h\left(\tfrac{1}{6} h_m^3 h_p^2 + \tfrac{1}{6} h_m^2 h_p^3\right).$$

With these definitions, the weighted integrals of the transverse leakage expansion functions are

$$\langle w^u_{0,ij} | \rho^u_{\ell,\ell-1} \rangle = \frac{h}{d}\left\{h^4\left(\tfrac{7}{360} h_m h_p\right) + h^3\left(\tfrac{17}{360} h_m h_p^2\right) + h^2\left(\tfrac{1}{36} h_m h_p^3\right)\right\}$$

$$\langle w^u_{0,ij} | \rho^u_{\ell\ell} \rangle = \frac{h}{d}\left\{h^4\left(\tfrac{1}{60} h_m h_p\right) + h^3\left(\tfrac{11}{120} h_m^2 h_p + \tfrac{1}{120} h_m h_p^2\right)\right.$$

$$\left. + h^2\left(\tfrac{1}{18} h_m^3 h_p + \tfrac{1}{12} h_m^2 h_p^2\right) + h\left(\tfrac{1}{36} h_m^3 h_p^2 + \tfrac{1}{36} h_m^2 h_p^3\right)\right\}$$

$$\langle w^u_{0,ij} | \rho^u_{\ell\ell+1} \rangle = \frac{h}{d}\left\{h^4\left(-\tfrac{1}{120} h_m h_p\right) + h^3\left(-\tfrac{13}{360} h_m^2 h_p\right) + h^2\left(-\tfrac{1}{36} h_m^3 h_p\right)\right\}$$

$$\langle w^u_{1,ij} | \rho^u_{\ell,\ell-1} \rangle = \frac{h}{d}\left\{h^4\left(-\tfrac{1}{120} h_m h_p\right) + h^3\left(-\tfrac{13}{360} h_m h_p^2\right) + h^2\left(-\tfrac{1}{36} h_m h_p^3\right)\right\}$$

$$\langle w^u_{1,ij} | \rho^u_{\ell\ell} \rangle = \frac{h}{d}\left\{h^4\left(\tfrac{1}{60} h_m h_p\right) + h^3\left(\tfrac{1}{120} h_m^2 h_p + \tfrac{11}{120} h_m h_p^2\right)\right.$$

$$\left. + h^2\left(\tfrac{1}{12} h_m^2 h_p^2 + \tfrac{1}{18} h_m h_p^3\right) + h\left(\tfrac{1}{36} h_m^3 h_p^2 + \tfrac{1}{36} h_m^2 h_p^3\right)\right\}$$

$$\langle w^u_{1,ij} | \rho^u_{\ell\ell+1} \rangle = \frac{h}{d} \left\{ h^4 \left(\frac{7}{360} h_m h_p \right) + h^3 \left(\frac{17}{360} h_m^2 h_p \right) + h^2 \left(h_m^3 h_p \right) \right\} \tag{A4. 3a}$$

For the case of uniform mesh spacing, these evaluated expressions can be greatly reduced and are

$$\langle w^u_{0,ij} | \rho^u_{\ell\ell-1} \rangle = \langle w^u_{1,ij} | \rho^u_{\ell\ell+1} \rangle = h^u_\ell \left(\frac{17}{360} \right)$$

$$\langle w^u_{0,ij} | \rho^u_{\ell\ell} \rangle = \langle w^u_{1,ij} | \rho^u_{\ell\ell} \rangle = h^u_\ell \left(\frac{7}{45} \right)$$

$$\langle w^u_{0,ij} | \rho^u_{\ell\ell+1} \rangle = \langle w^u_{1,ij} | \rho^u_{\ell\ell-1} \rangle = h^u_\ell \left(-\frac{13}{360} \right). \tag{A4. 3b}$$

Appendix 5

DESCRIPTION OF TEST PROBLEMS

A5.1 Kang's One-dimensional LWR Problem

A5.2 A One-dimensional Version of the IAEA PWR Problem

A5.3 The IAEA Two-dimensional PWR Benchmark Problem

A5.4 The LRA Two-dimensional BWR Benchmark Problem

A5.5 The Biblis Two-dimensional PWR Problem

A5.6 The TWIGL Two-dimensional Seed-Blanket Reactor Problem

Note: In tabulations of macroscopic cross sections, DB^2 terms are not included in the total removal cross sections.

A5.1 Kang's One-dimensional LWR Problem

Geometry:

Material Constants:

Group 1

Composition	D_1	Σ_{r1}	Σ_{21}	$\nu\Sigma_{f1}$
1	1.5	.0623	.06	0
2	1.2	.101	.1	0

Group 2

Composition	D_2	Σ_{r2}	Σ_{12}	$\nu\Sigma_{f2}$
1	.4	.2	0	.218
2	.15	.02	0	0

$\chi_1 = 1, \quad \chi_2 = 0$

A5.2 A One-dimensional Version of the IAEA PWR Problem

Geometry:

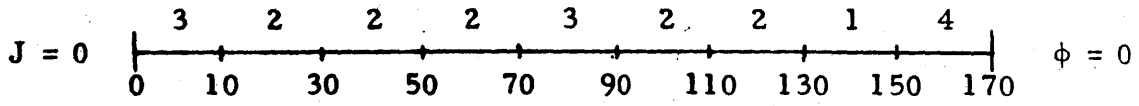

Material Constants:

Material constants are the same as those of the IAEA Two-dimensional PWR Benchmark Problem (A5. 3). For this one-dimensional problem, the buckling is not included.

A5.3 The IAEA Two-dimensional PWR Benchmark Problem

Geometry:

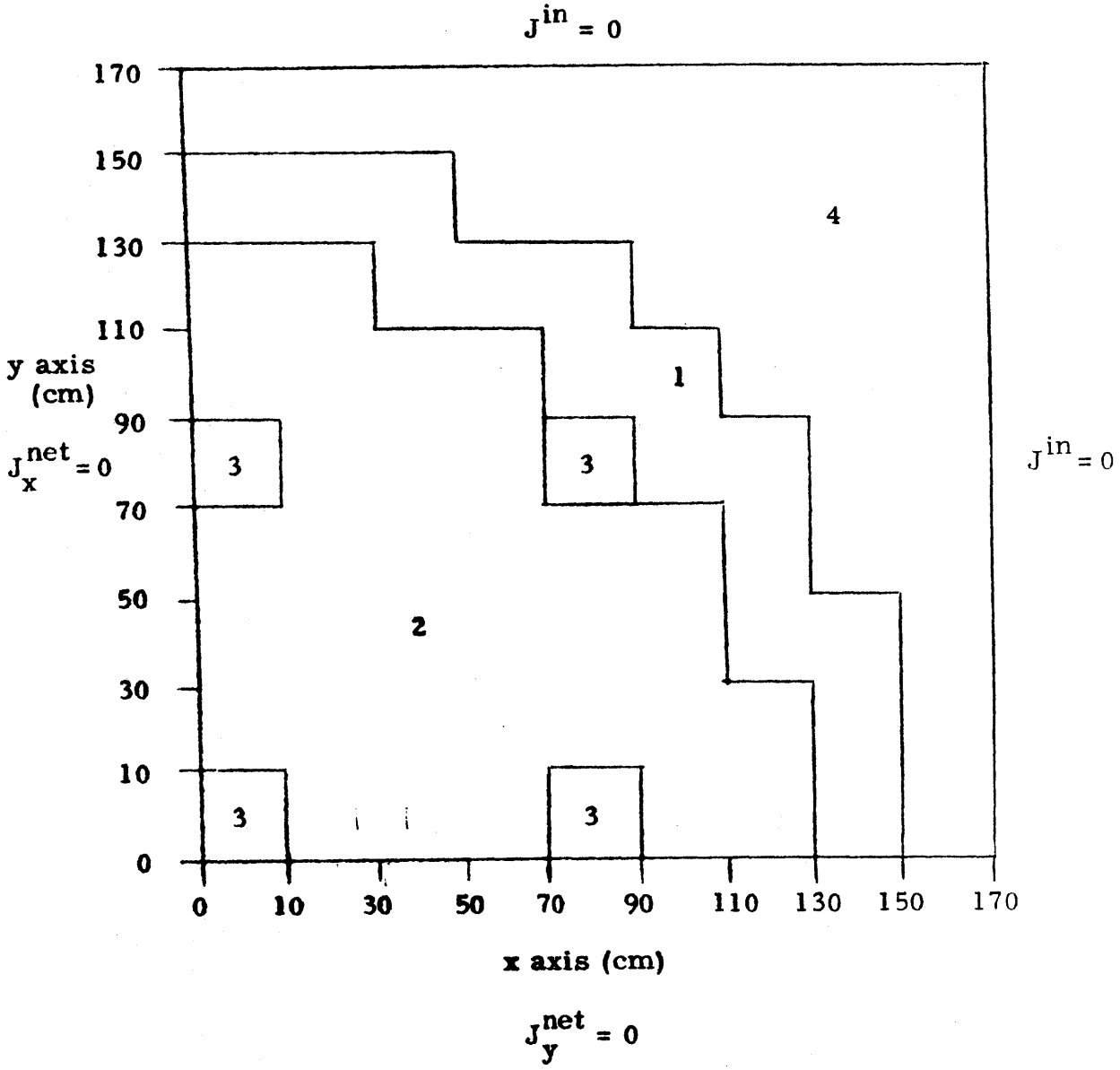

Material Constants:

Group 1

Composition	D_1 (cm)	Σ_{r1} (cm^{-1})	Σ_{21} (cm^{-1})	$\nu\Sigma_{f1}$ (cm^{-1})
1	1.5	.04	.02	0
2	1.5	.03	.02	0
3	1.5	.03	.02	0
4	2.0	.04	.04	0

Group 2

Composition	D_1 (cm)	Σ_{r2} (cm^{-1})	Σ_{12} (cm^{-1})	$\nu\Sigma_{f2}$ (cm^{-1})
1	.4	.08	0	.135
2	.4	.085	0	.135
3	.4	.13	0	.135
4	.3	.01	0	0

$\chi_1 = 1, \quad \chi_2 = 0$

$B_z^2 = .8 \times 10^{-4}$ cm^{-2} (in all compositions)

A5.4 The LRA Two-dimensional BWR Benchmark Problem

Geometry:

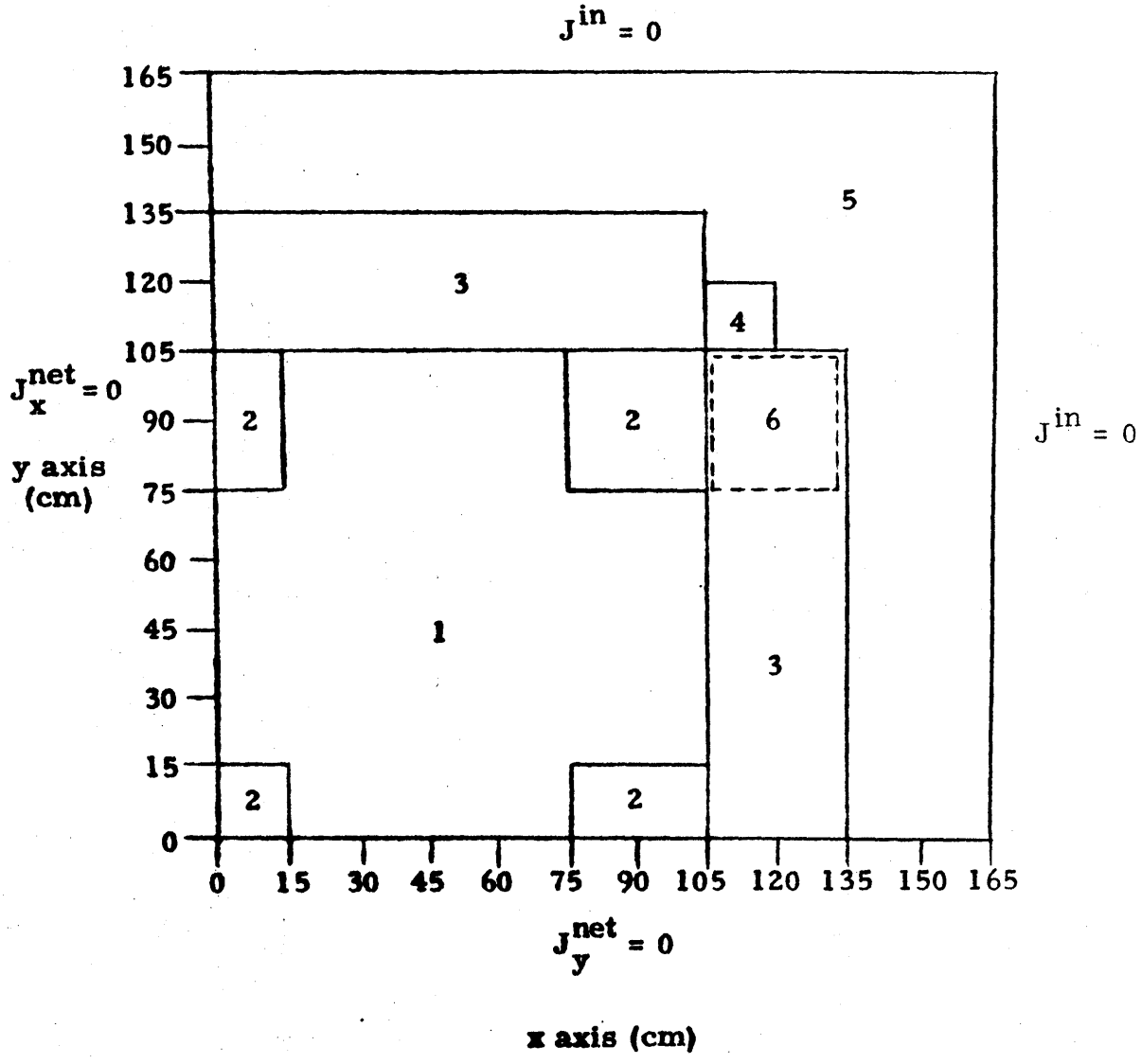

Material Constants:

Group 1

Composition	D_1 (cm)	Σ_{r1} (cm^{-1})	Σ_{21} (cm^{-1})	$\nu\Sigma_{f1}$ (cm^{-1})
1	1.255	.033582	.02533	.004602
2	1.268	.034851	.02767	.004609
3	1.259	.034172	.02617	.004663
4	1.234	.035172	.02805	.004668
5	1.257	.0481434	.04754	0
6		– same as 3 –		

Group 2

Composition	D_1 (cm)	Σ_{r2} (cm^{-1})	Σ_{12} (cm^{-1})	$\nu\Sigma_{f2}$ (cm^{-1})
1	.211	.1003	0	.1091
2	.1902	.07047	0	.08675
3	.2091	.08344	0	.1021
4	.1935	.06552	0	.08792
5	.1592	.01911	0	0
6		– same as 3 –		

$\chi_1 = 1, \quad \chi_2 = 0$

$\nu = 2.43$

$B_z^2 = 1 \times 10^{-4}\ cm^{-2}$ (in all compositions)

Kinetic Parameters:

Delayed Family	β	λ (sec^{-1})
1	.0054	.0654
2	.001087	1.35

$v_1 = 3 \times 10^7$ sec/cm, $v_2 = 3 \times 10^5$ sec/cm

Perturbation:

Ramp perturbation in Composition 6

$\Delta\Sigma_{a2} = -.010116\ cm^{-1}$

Ramp duration ($0 \leq t \leq 2.0$ sec)

Feedback Model:

Adiabatic Heatup –

$$\alpha_{ah}[\Sigma_{f1}(\underline{r}, t)\,\phi_1(\underline{r}, t) + \Sigma_{f2}(\underline{r}, t)\,\phi_2(\underline{r}, t)] = \frac{\partial}{\partial t}\,T(\underline{r}, t)$$

Doppler Feedback –

$$\Sigma_{a1}(\underline{r}, t) = \Sigma_{a1}(\underline{r}, t=0)\{1 + \alpha_{df}[\sqrt{T(\underline{r}, t)} - \sqrt{T_o}\,]\}$$

Thermal Parameters:

Energy conversion factor

$$\epsilon = .3204 \times 10^{-10} \text{ ws/f}$$

Mean power desnity at t = 0

$$d = 1.0 \times 10^{-6} \text{ w/cc}$$

Conversion factor in feedback model

$$\alpha_{ah} = 3.83 \times 10^{-11} \text{ °K cc}$$

Feedback constant

$$\alpha_{df} = 3.034 \times 10^{-3} \frac{1}{\sqrt{\text{°K}}}$$

Initial temperature distribution

$$T_o = T(\underline{r}, t = 0) = 300\text{°K}$$

A5.5 The Biblis Two-dimensional PWR Problem

Limitations concerning industrial confidentiality prohibit us from presenting a problem description. Overall features are described in the text of Chapter 3.

A5.6 The TWIGL Two-dimensional Seed-Blanket Reactor Problem

Geometry:

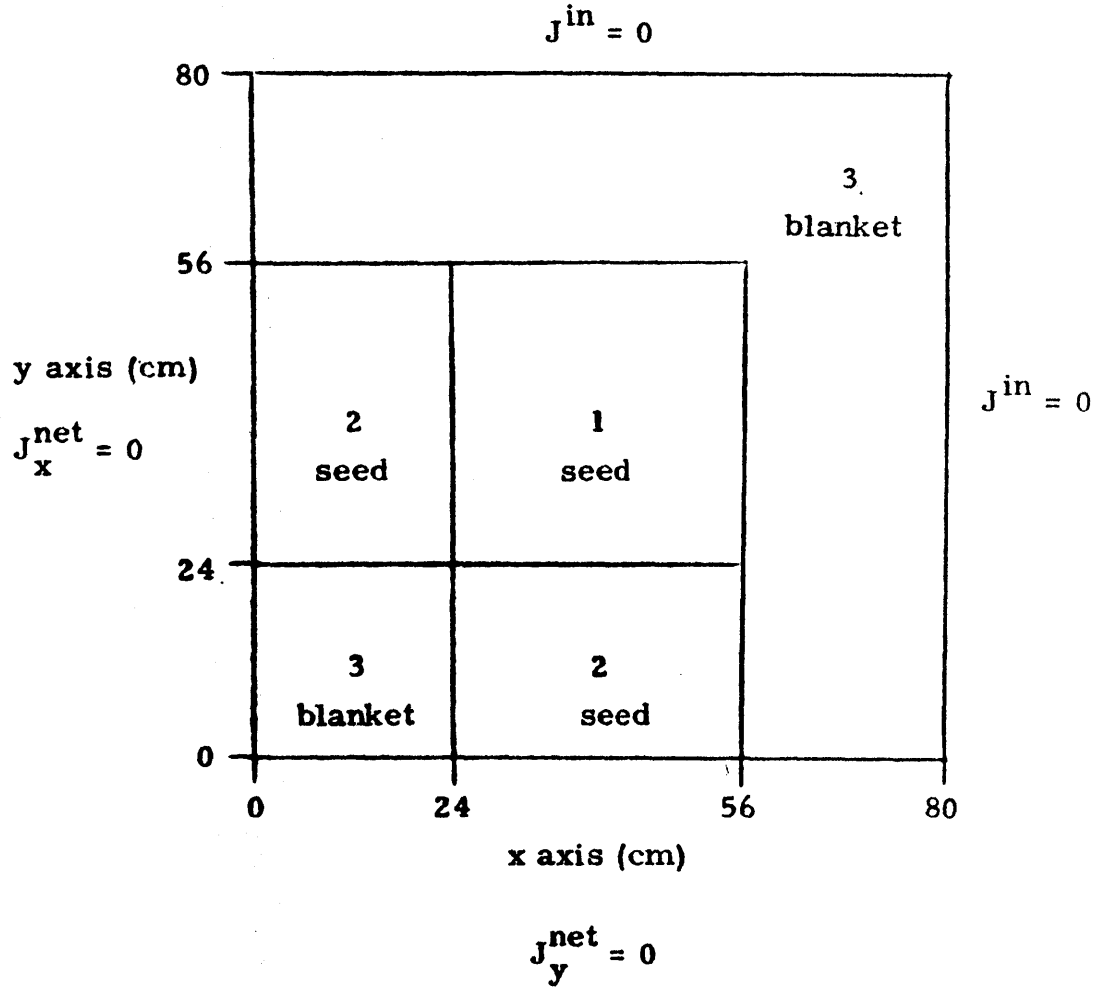

Material Constants:

Group 1

Composition	D_1 (cm)	Σ_{r1} (cm^{-1})	Σ_{21} (cm^{-1})	$\nu\Sigma_{f1}$ (cm^{-1})
seed	1.4	.02	.01	.007
blanket	1.3	.018	.01	.003

Group 2

Composition	D_2 (cm)	Σ_{r2} (cm^{-1})	Σ_{12} (cm^{-1})	$\nu\Sigma_{f2}$ (cm^{-1})
seed	.4	.15	0	.2
blanket	.5	.05	0	.06

$\chi_1 = 1, \quad \chi_2 = 0$

Kinetic Parameters:

Delayed Family	β	λ (sec^{-1})
1	.0075	.08

$1/v_1 = 1 \times 10^{-7}$ sec/cm, $1/v_2 = 5 \times 10^{-6}$ sec/cm

Perturbation:

Step perturbation in Region 1

$\Delta\Sigma_{r2} = -.0035\ cm^{-1}$

Problem duration ($0 \leq t \leq .5$ sec)

Ramp perturbation in Region 1

$\Delta\Sigma_{r2} = -.0035\ cm^{-1}$

Ramp duration ($0 \leq t \leq .2$ sec)

Problem duration ($0 \leq t \leq .5$ sec)

Appendix 6

RESULTS

A6.1 Kang's One-dimensional LWR Problem

A6.2 A One-dimensional Version of the IAEA PWR Problem

A6.3 The IAEA Two-dimensional PWR Benchmark Problem

A6.4 The LRA Two-dimensional BWR Static Benchmark Problem

A6.5 The TWIGL Two-dimensional Seed-Blanket Reactor Problem

A6.6 The LRA Two-dimensional BWR Kinetics Benchmark Problem

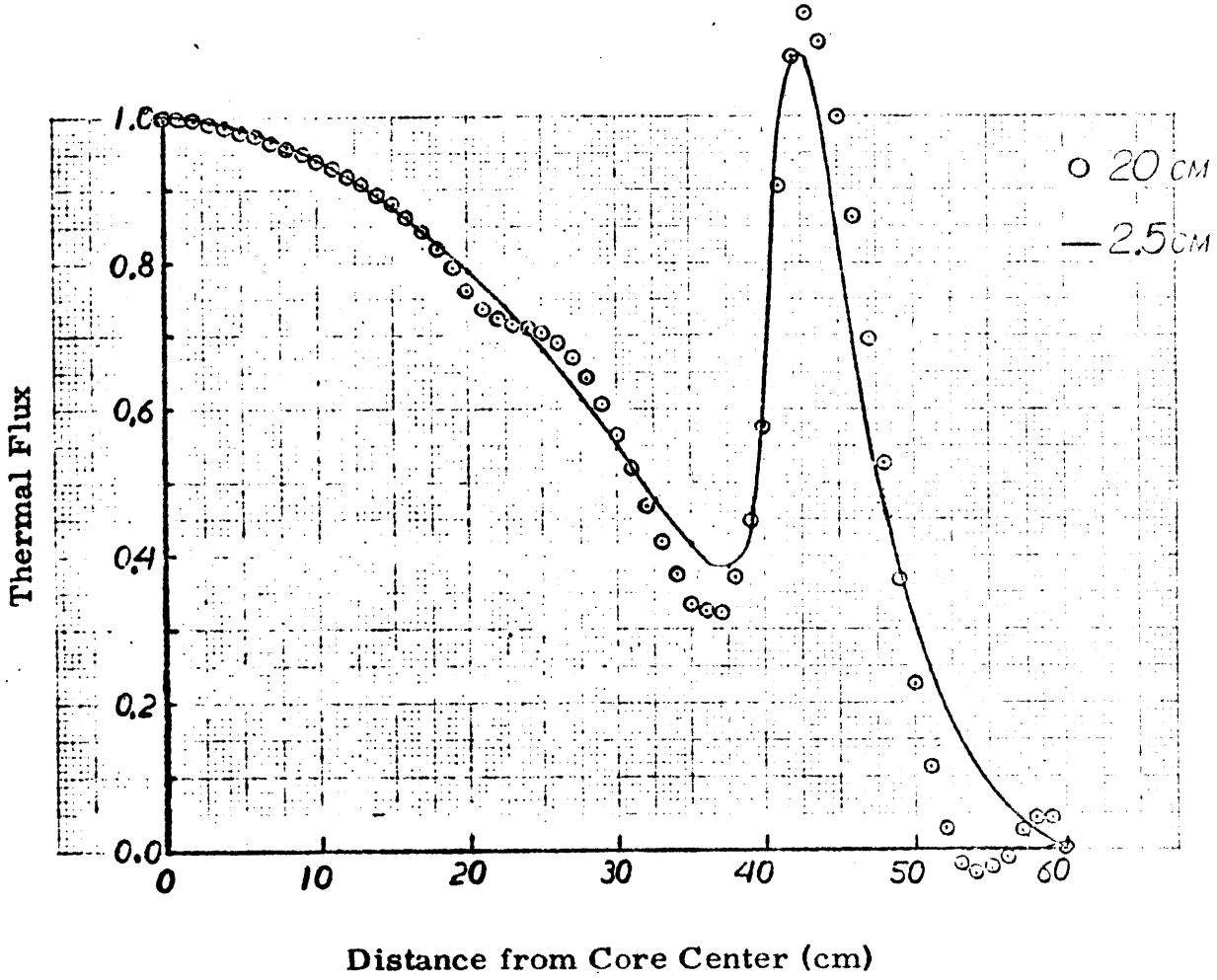

Figure A6. 1a Thermal Flux Plot for Kang's One-dimensional LWR Problem: 20 cm Mesh

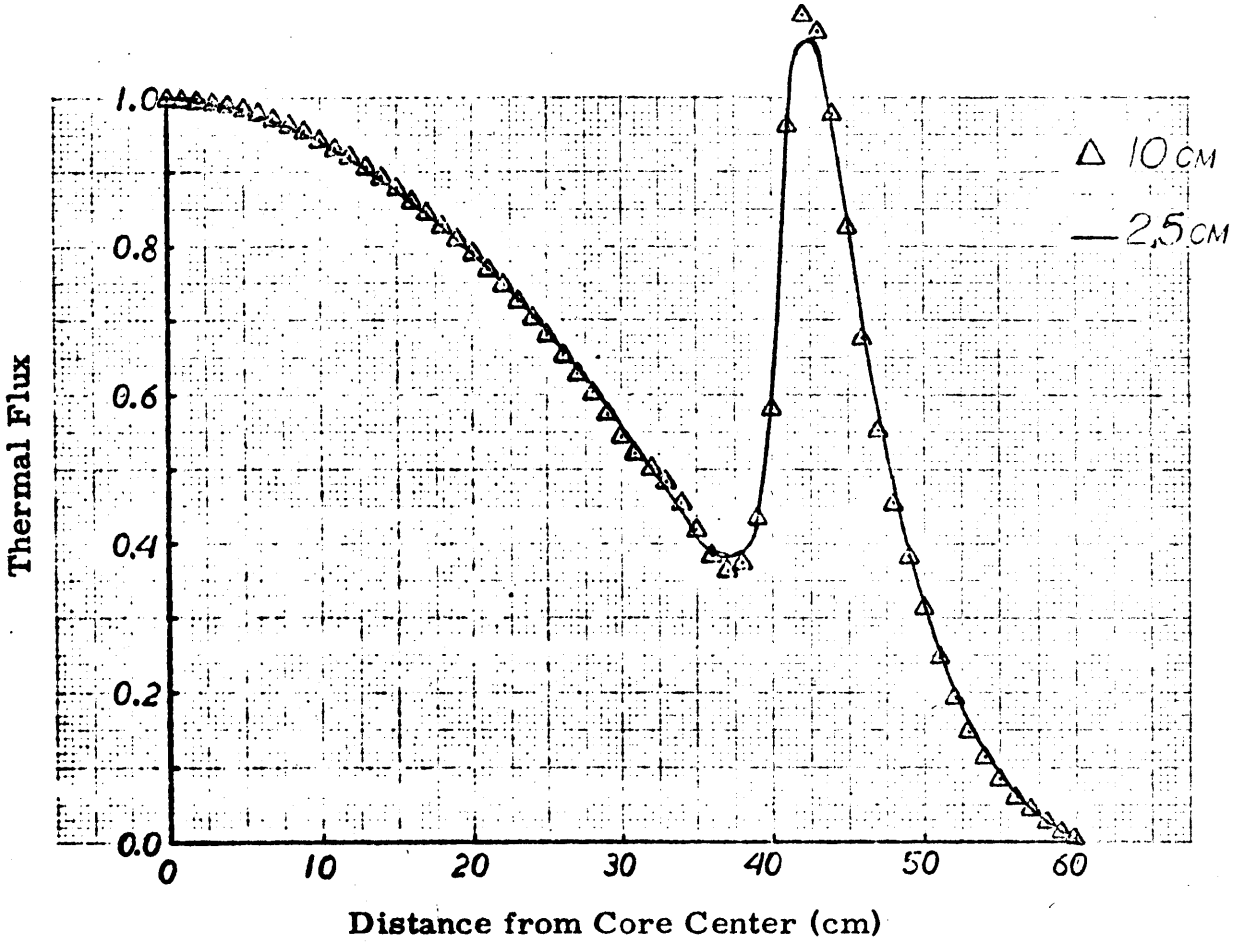

Figure A6.1b Thermal Flux Plot for Kang's One-dimensional LWR Problem: 10 cm Mesh

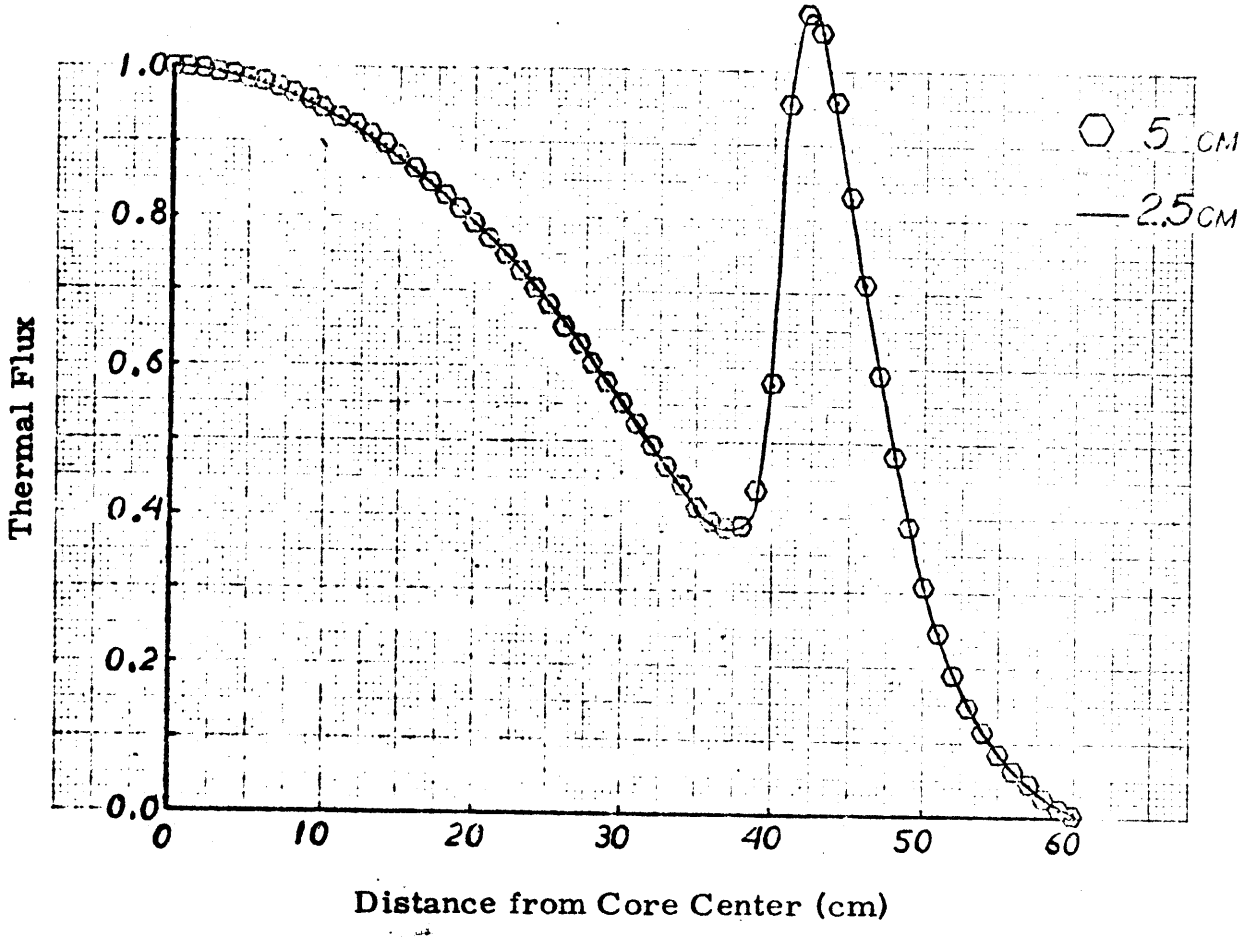

Figure A6.1c Thermal Flux Plot for Kang's One-dimensional LWR Problem: 5 cm Mesh

Figure A6.2a Power Distribution for the One-dimensional IAEA PWR Problem: Results of Uniform Mesh Refinement

(core centerline)

x-axis (cm)	assembly power fraction (Reference*)	(1) 20 cm	(2) 10 cm	(4) 5 cm	(8) 2.5 cm
0 – 10	(.017249)	.017752	.017298	.017249	.017248
10 – 30	(.081628)	.084103	.081910	.081628	.081623
30 – 50	(.109214)	.112250	.109527	.109213	.109207
50 – 70	(.093073)	.095181	.093320	.093075	.093069
70 – 90	(.055252)	.055438	.055255	.055251	.055252
90 – 110	(.168395)	.167709	.168323	.168400	.168398
110 – 130	(.241250)	.238163	.240951	.241253	.241256
130 – 150	(.233939)	.229403	.233415	.233931	.233945

(core-reflector interface)

nodes per assembly

*Shober analytic solution

Figure A6.2b Power Distribution for the One-dimensional IAEA PWR **Problem: Refinement of Reflector Treatment**

(core centerline)

x-axis (cm)			
0	(.017249)	.017308	.017480
10	(.081628)	.082060	.082850
30	(.109214)	.109740	.110716
50	(.093073)	.093470	.094146
70	(.055252)	.055183	.055307
90	(.168395)	.168372	.168242
110	(.241250)	.240726	.239454
130	(.233939)	.233139	.231804
150			

(core-reflector interface)

assembly power fraction			
	(Reference*)	20 cm ($0 \leq x \leq 130$) 10 cm ($130 \leq x \leq 170$)	20 cm ($0 \leq x \leq 150$) reflector replaced by analytic albedo

*Shober analytic solution

Figure A6. 3a Power Distribution for the Two-dimensional IAEA PWR Problem (Regular Core): Results of Uniform Mesh Refinement with the Constant Transverse Leakage Approximation

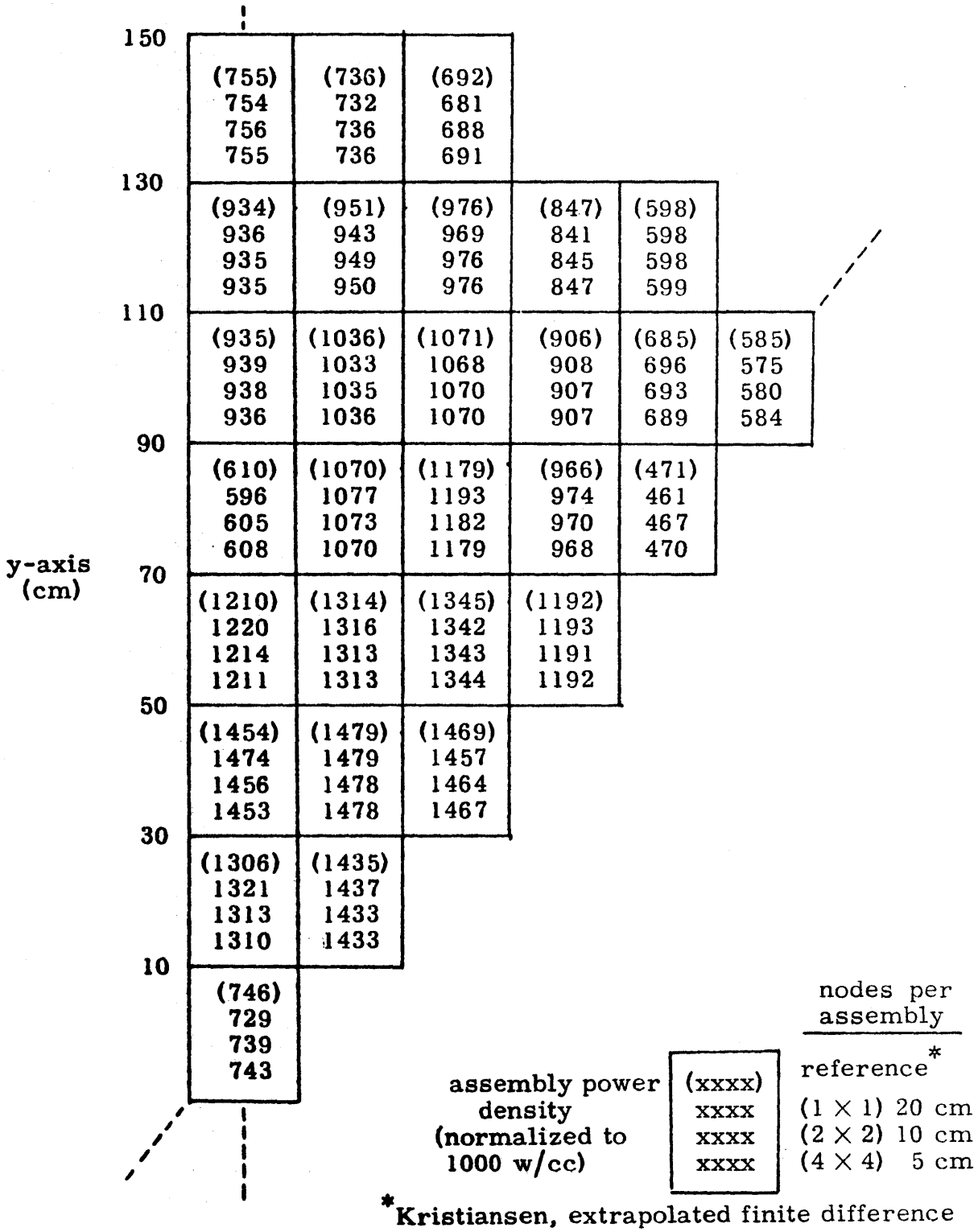

*Kristiansen, extrapolated finite difference

Figure A6.3b Power Distribution for the Two-dimensional IAEA PWR Problem (Regular Core): Results of Uniform Mesh Refinement with the Quadratic Transverse Leakage Approximation

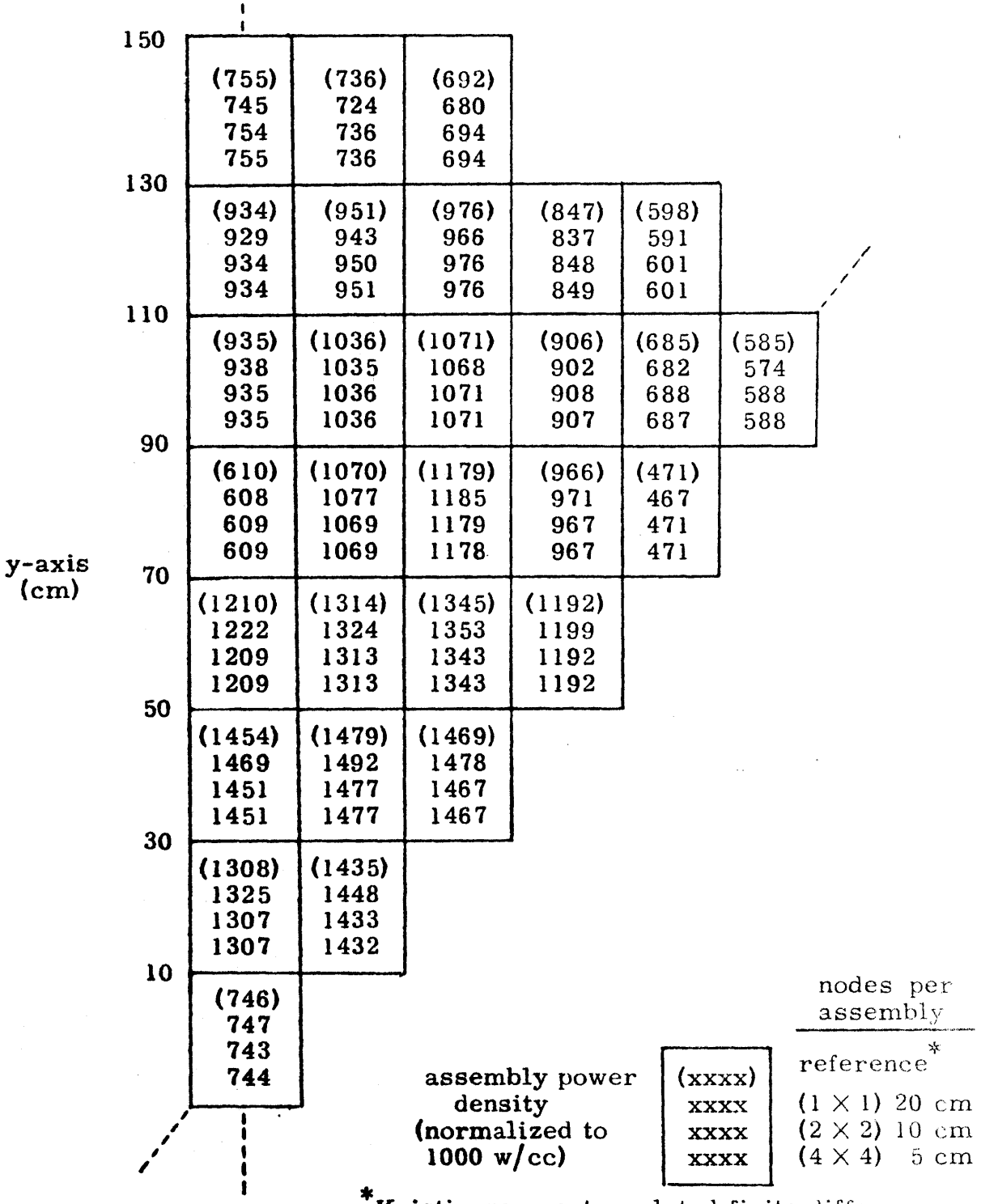

*Kristiansen, extrapolated finite difference

Figure A6.3c Power Distribution for the Two-dimensional IAEA PWR Problem (Irregular Core): Coarse Mesh Results

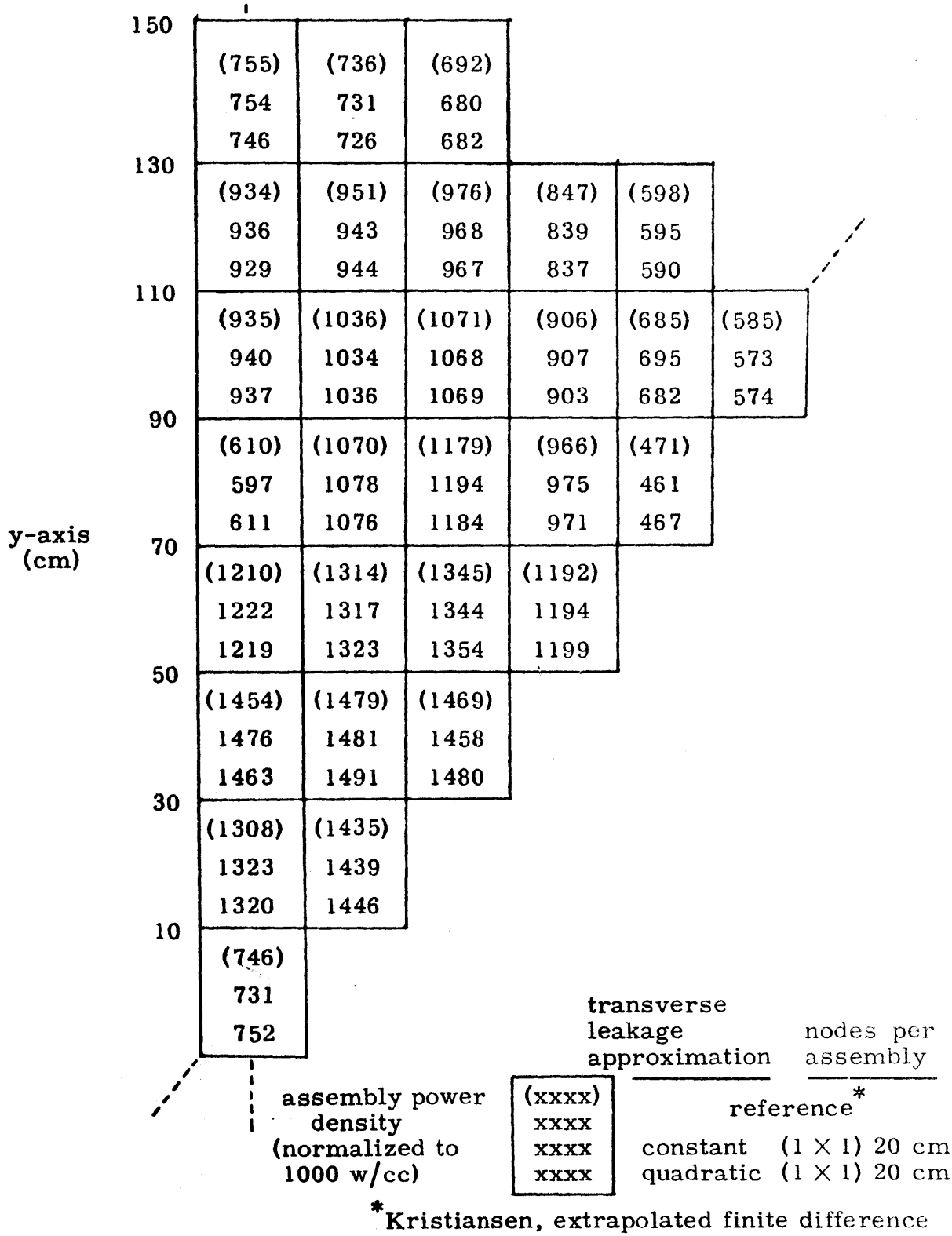

Figure A6.4 Power Distribution for the LRA BWR Static Problem (Rods Inserted): Coarse Mesh Results

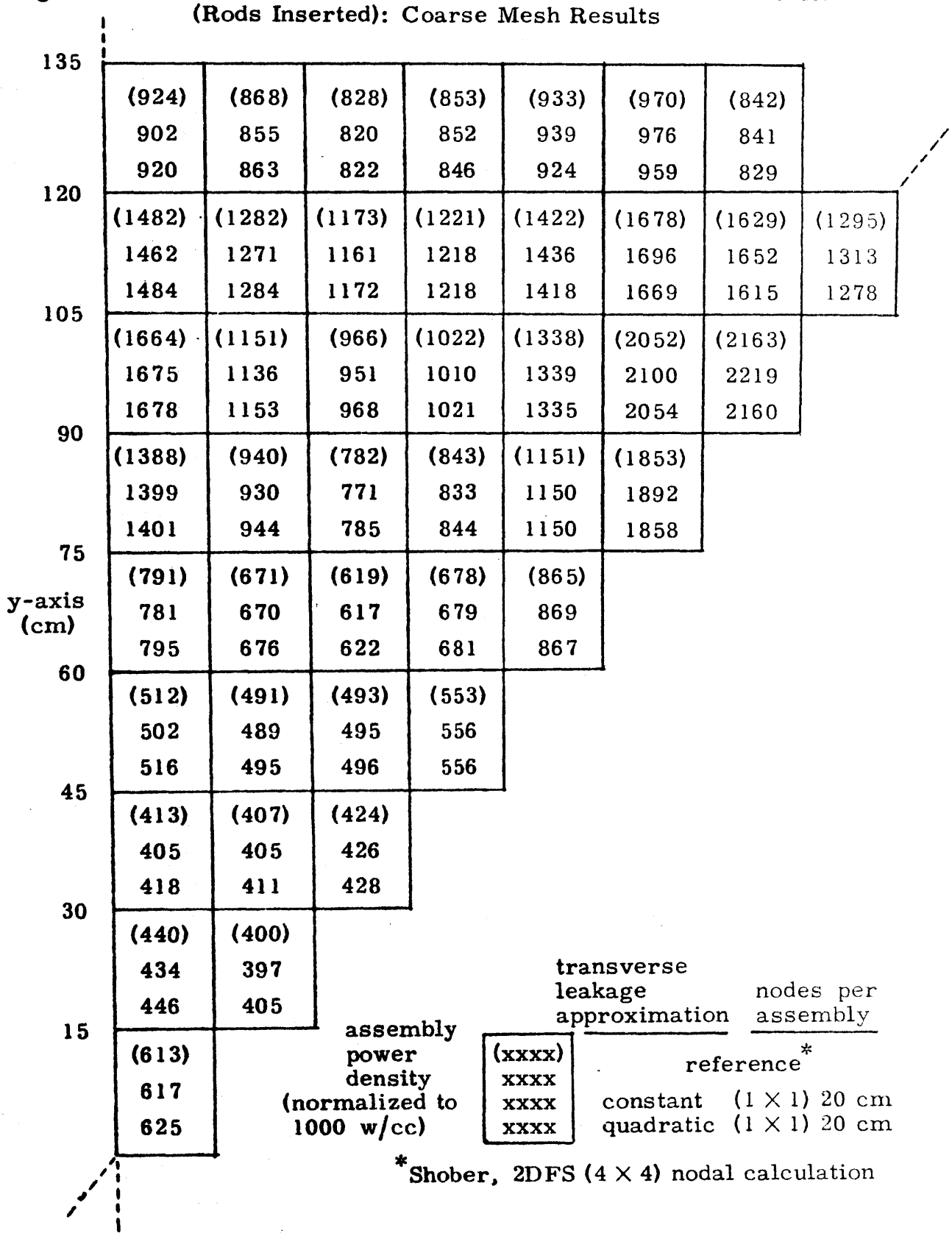

*Shober, 2DFS (4 × 4) nodal calculation

Fig. A6.5a Static Power Distribution Results for the TWIGL Two-dimensional Seed-Blanket Reactor Problem

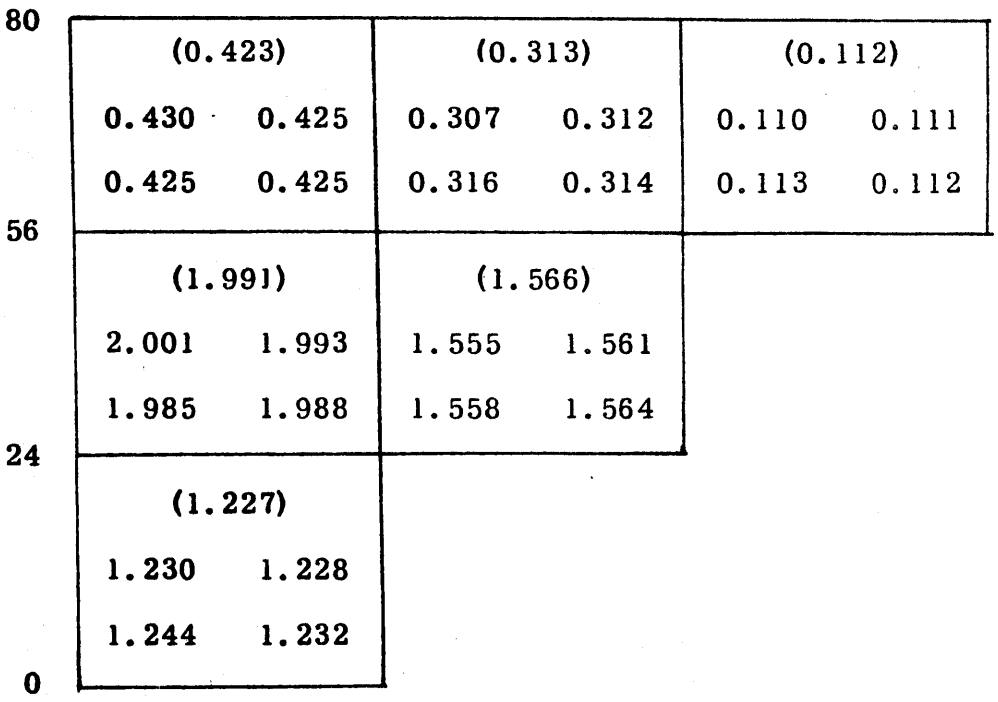

Mesh Layout

	Very Coarse Mesh	Coarse Mesh
Region average power density (normalized to 1 w/cc)	(x.xxx)	
	x.xxx	x.xxx
	x.xxx	x.xxx

Transverse Leakage Approximation
(Reference*)
constant
quadratic

*Reference, (6,8,6), quadratic, RC-Q nodal solution

Fig. A6.5b Asymptotic Power Distribution Results for the TWIGL Two-dimensional Seed-Blanket Reactor Problem

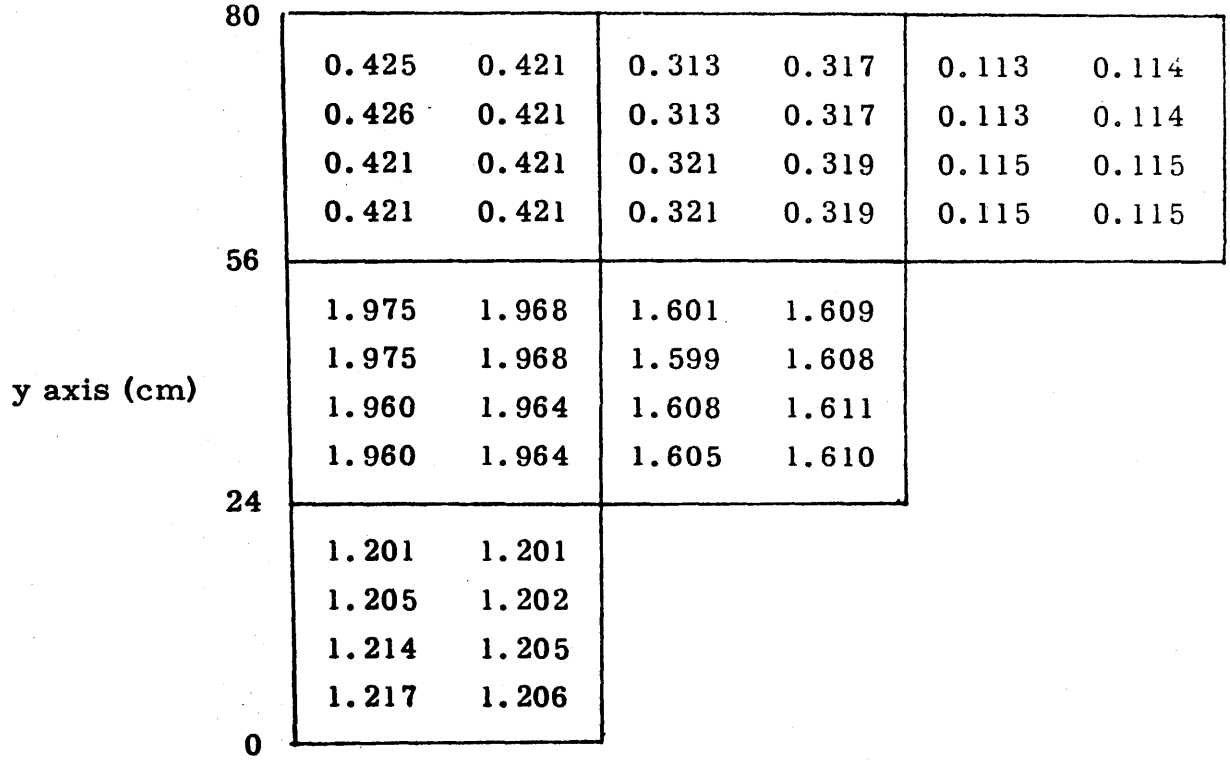

Mesh Division per Region	Very Coarse Mesh (1,1,1)	Coarse Mesh (2,2,2)	Transverse Leakage Approximation	Precursor Shape Approximation
Region average power density (normalized to 1 w/cc)	x.xxx	x.xxx	constant	constant
	x.xxx	x.xxx	constant	implicit
	x.xxx	x.xxx	quadratic	constant
	x.xxx	x.xxx	quadratic	implicit

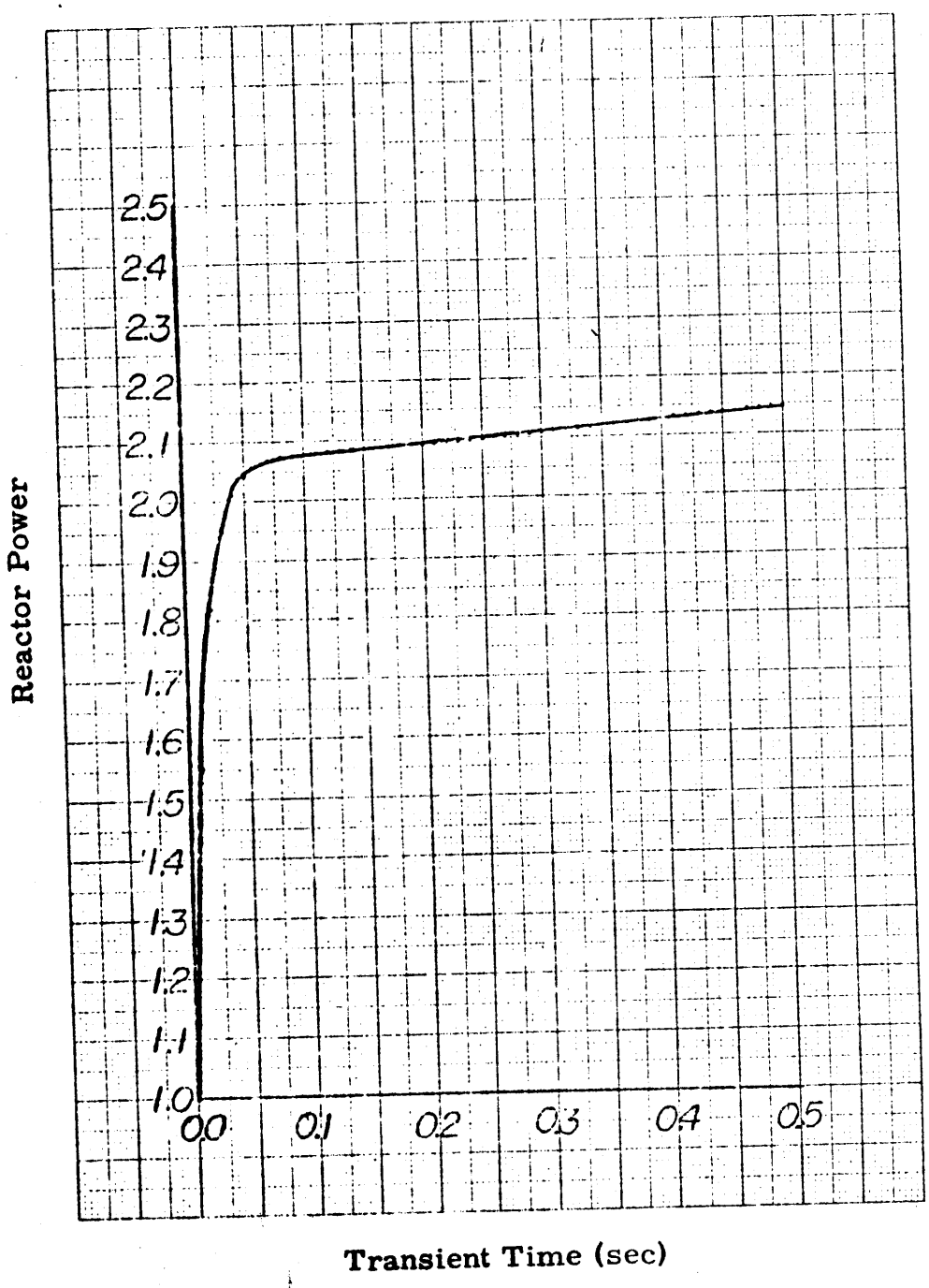

Figure A6. 5c Reactor Power versus Time for the TWIGL Two-dimensional Seed-Blanket Reactor Problem (Step Perturbation)

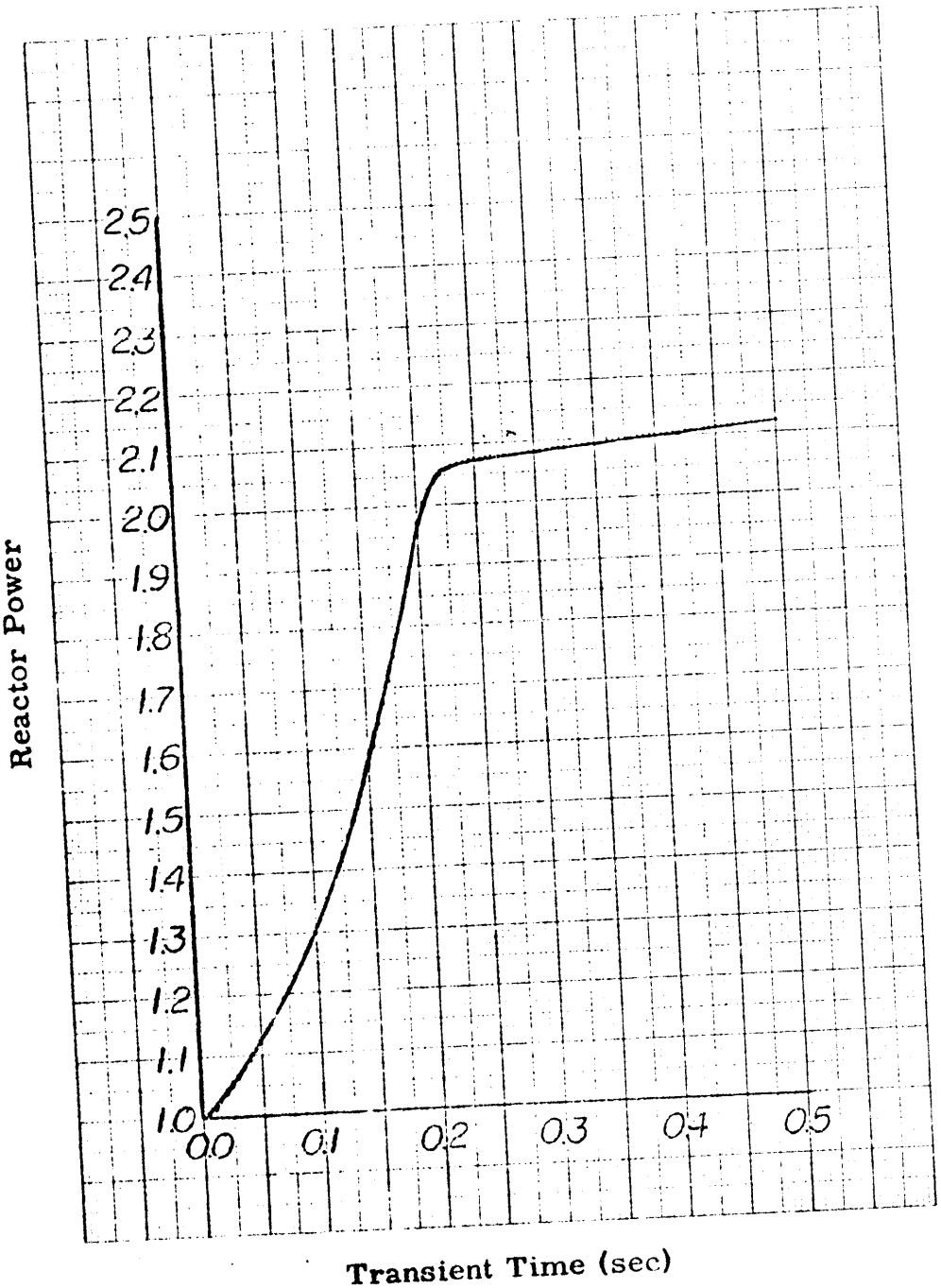

Figure A6. 5d Reactor Power versus Time for the TWIGL Two-dimensional Seed-Blanket Reactor Problem (Ramp Perturbation)

Figure A6.5e Iterations versus Timestep for the TWIGL Two-dimensional Seed-Blanket Reactor Problem (Step Perturbation): Very Coarse Mesh

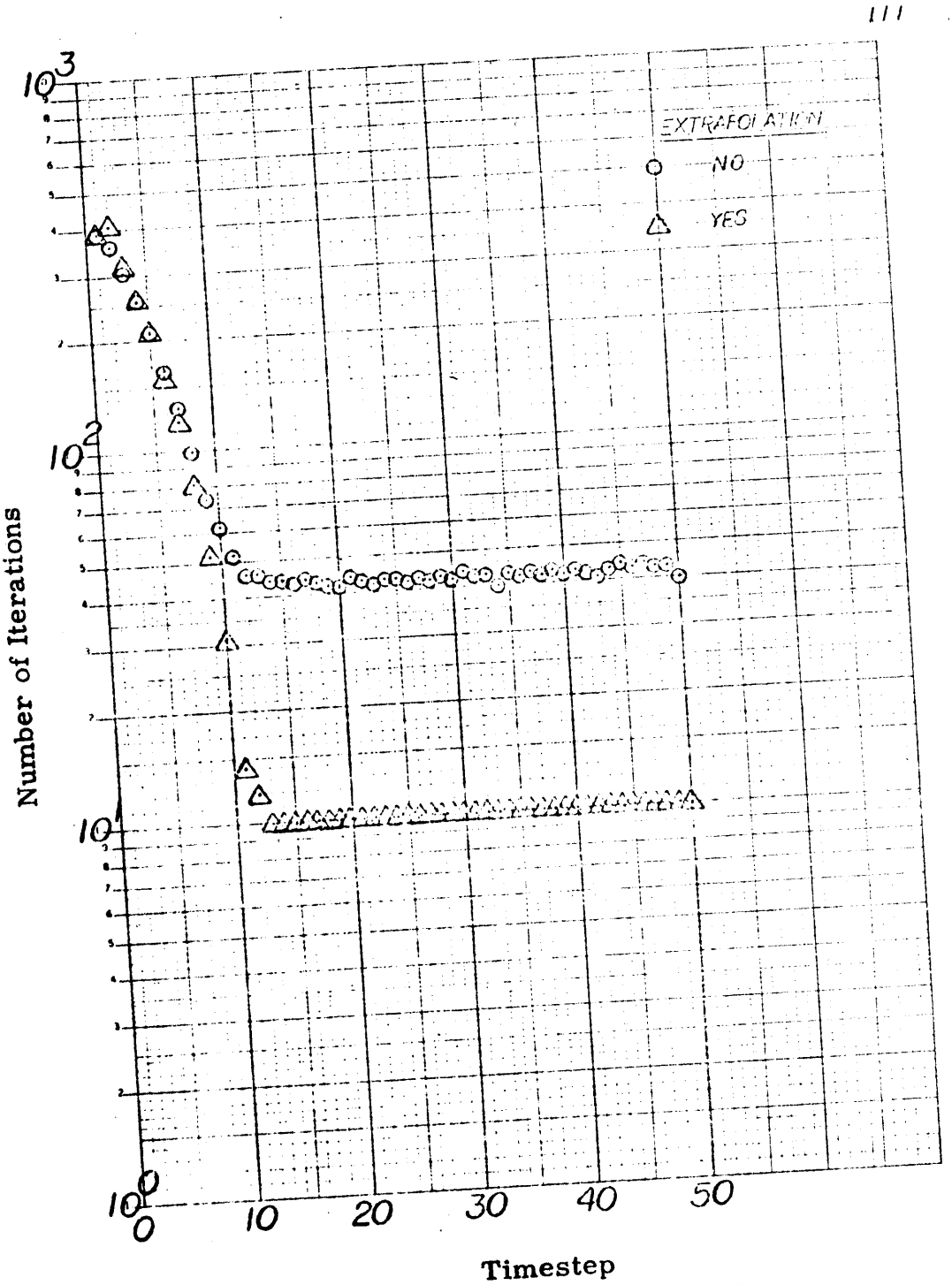

Figure A6.5f Iterations versus Timestep for the TWIGL Two-dimensional Seed-Blanket Reactor Problem (Step Perturbation): Coarse Mesh

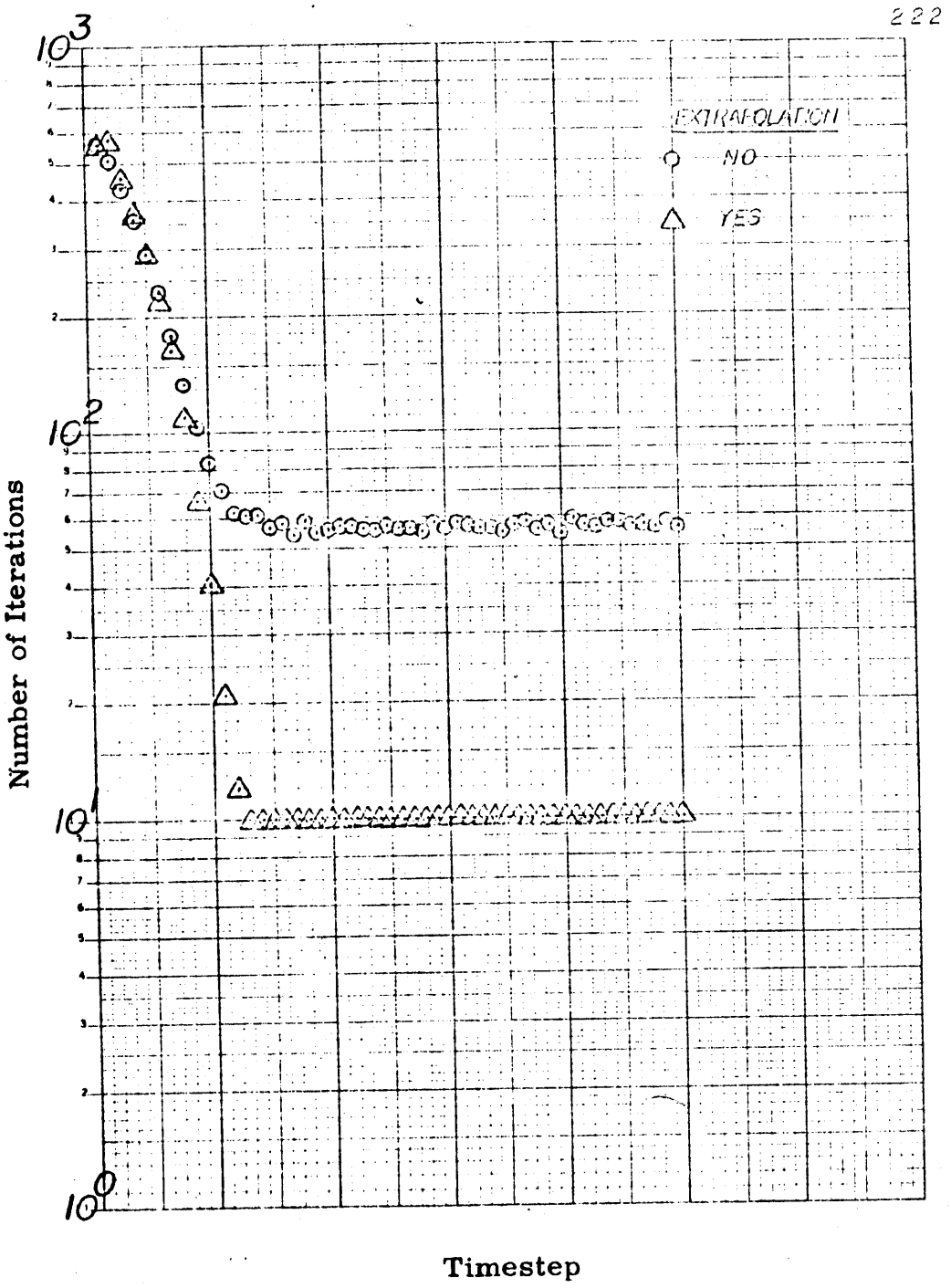

Figure A6.5g Iterations versus Timestep for the TWIGL Two-dimensional Seed-Blanket Reactor Problem (Ramp Perturbation): Very Coarse Mesh

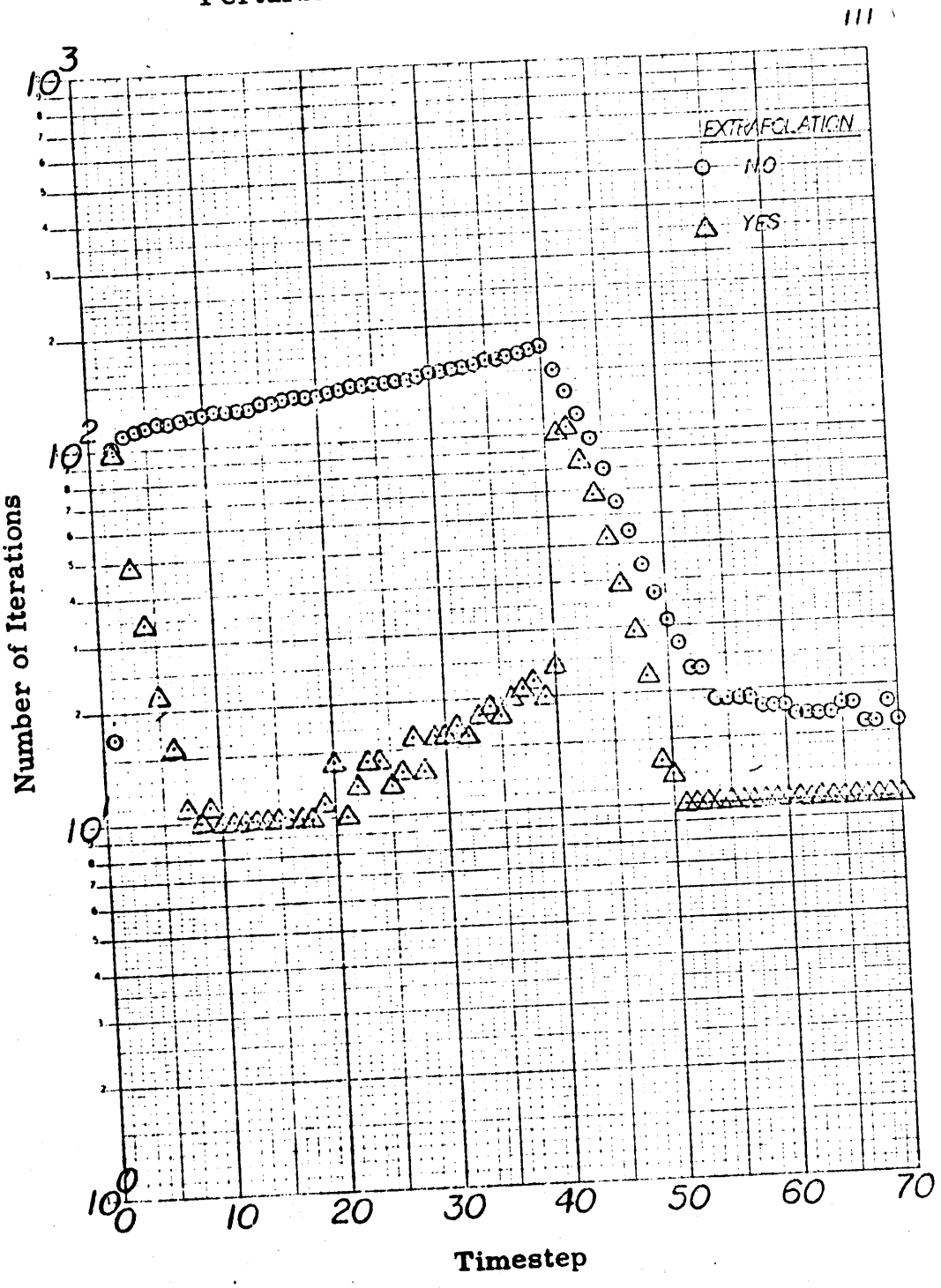

Figure A6.5h Iterations versus Timestep for the TWIGL Two-dimensional Seed-Blanket Reactor Problem (Ramp Perturbation): Coarse Mesh

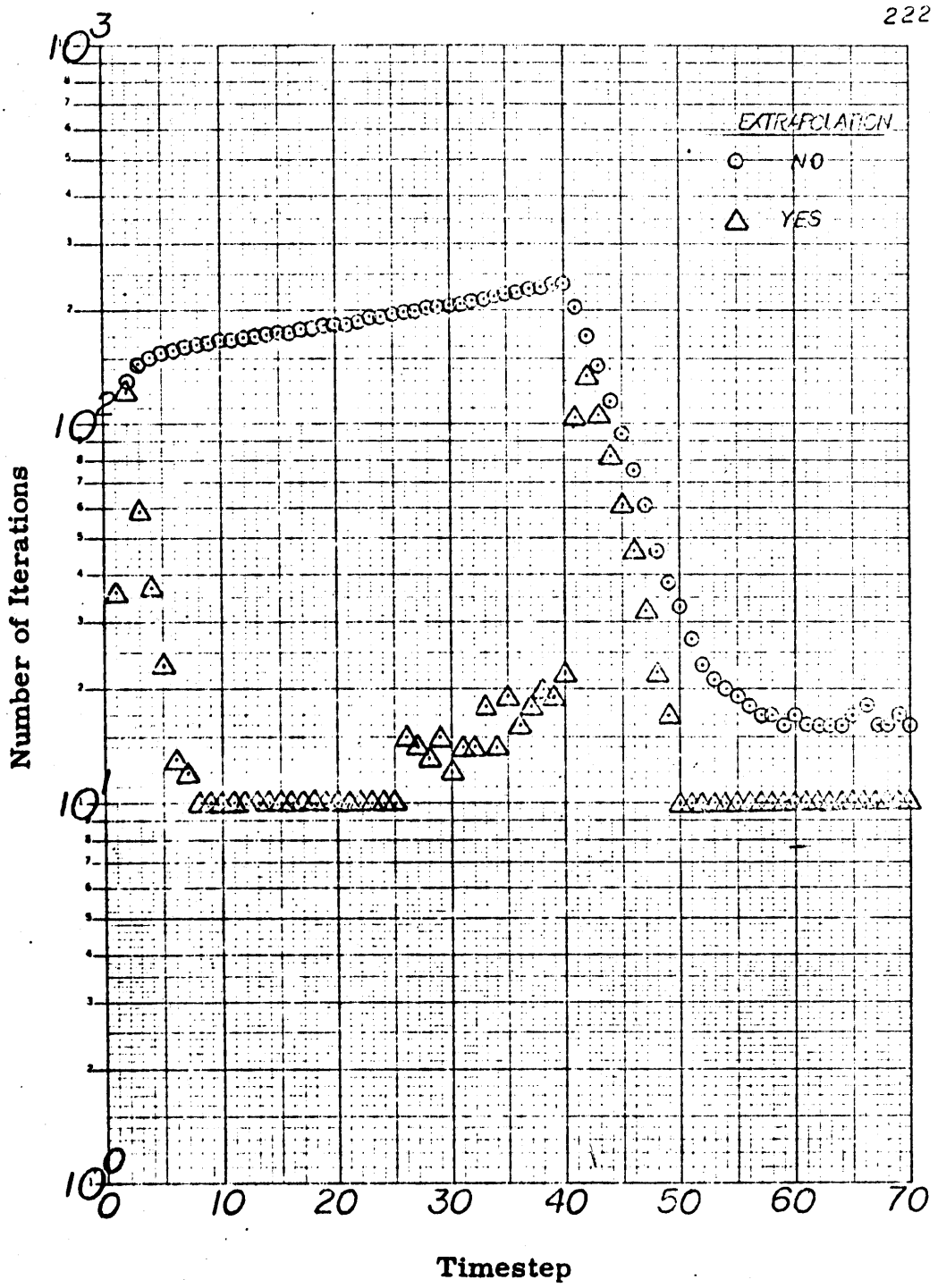

Figure A6.6a Power Distribution for the LRA BWR Static Problem (Rods Inserted): Very Coarse Mesh Results with the Quadratic Transverse Leakage Approximation

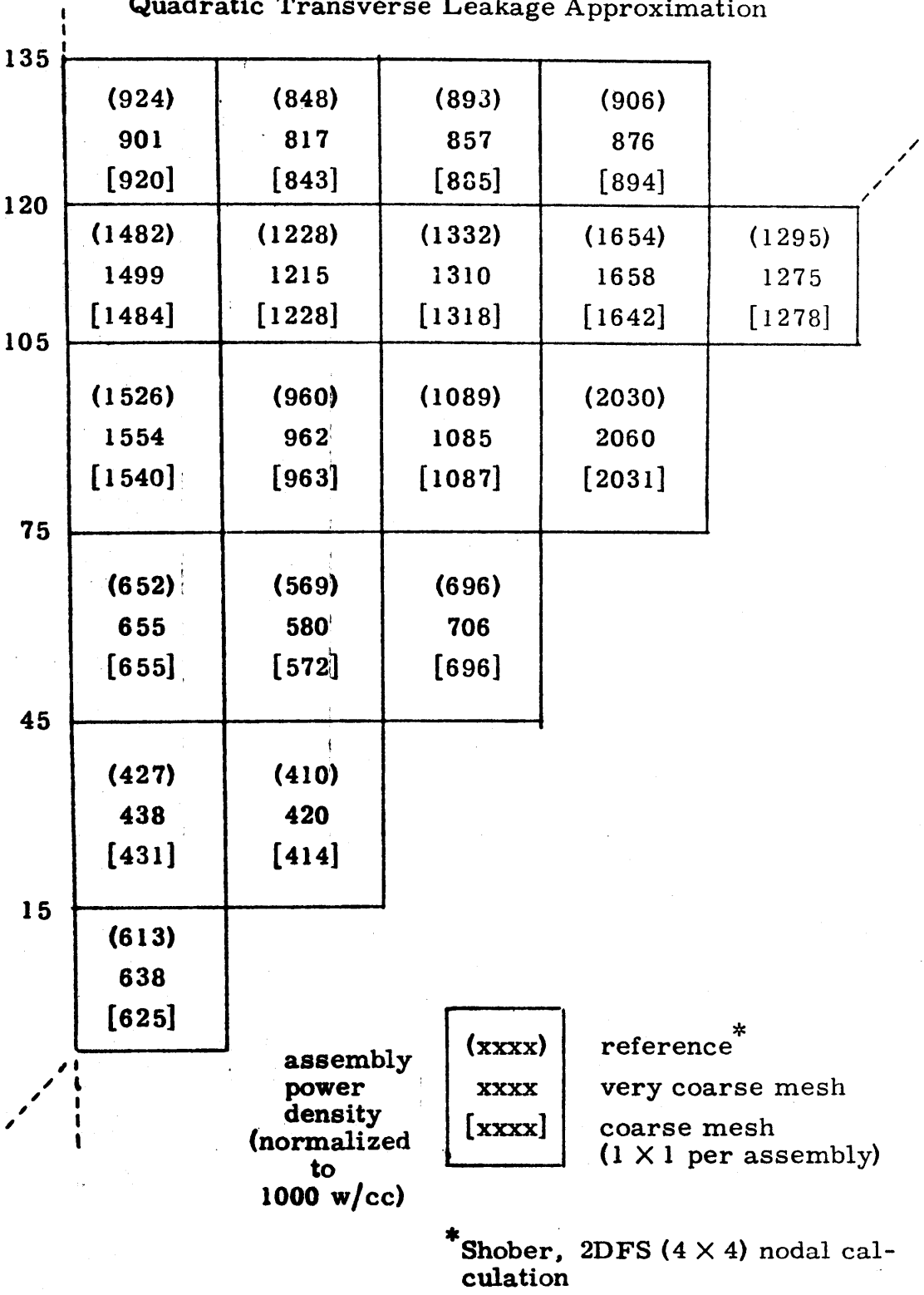

*Shober, 2DFS (4 X 4) nodal calculation

Figure A6. 6b Power Distribution for the LRA BWR Static Problem (Rods Withdrawn): Very Coarse Mesh Static Results with the Quadratic Transverse Leakage Approximation

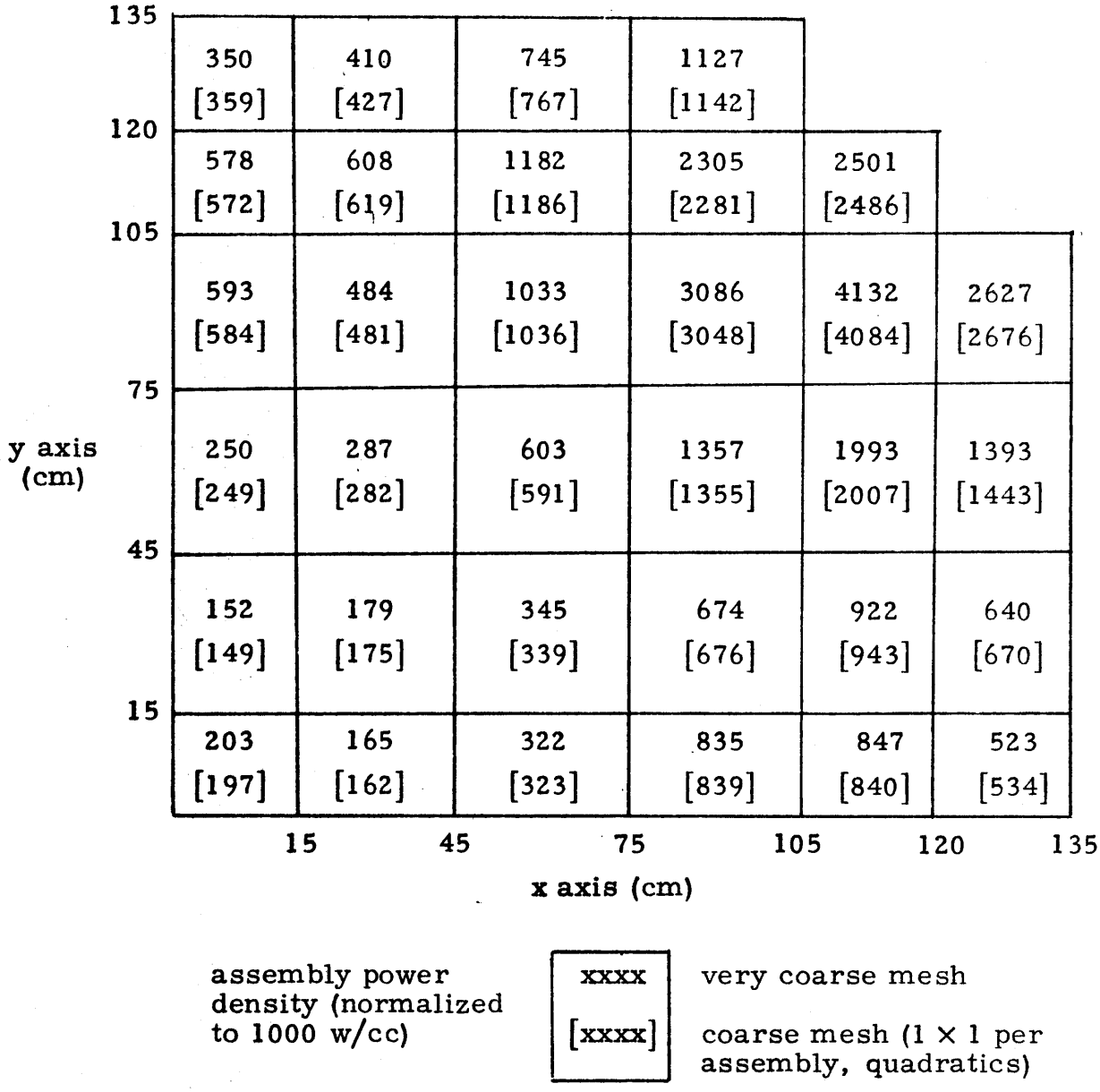

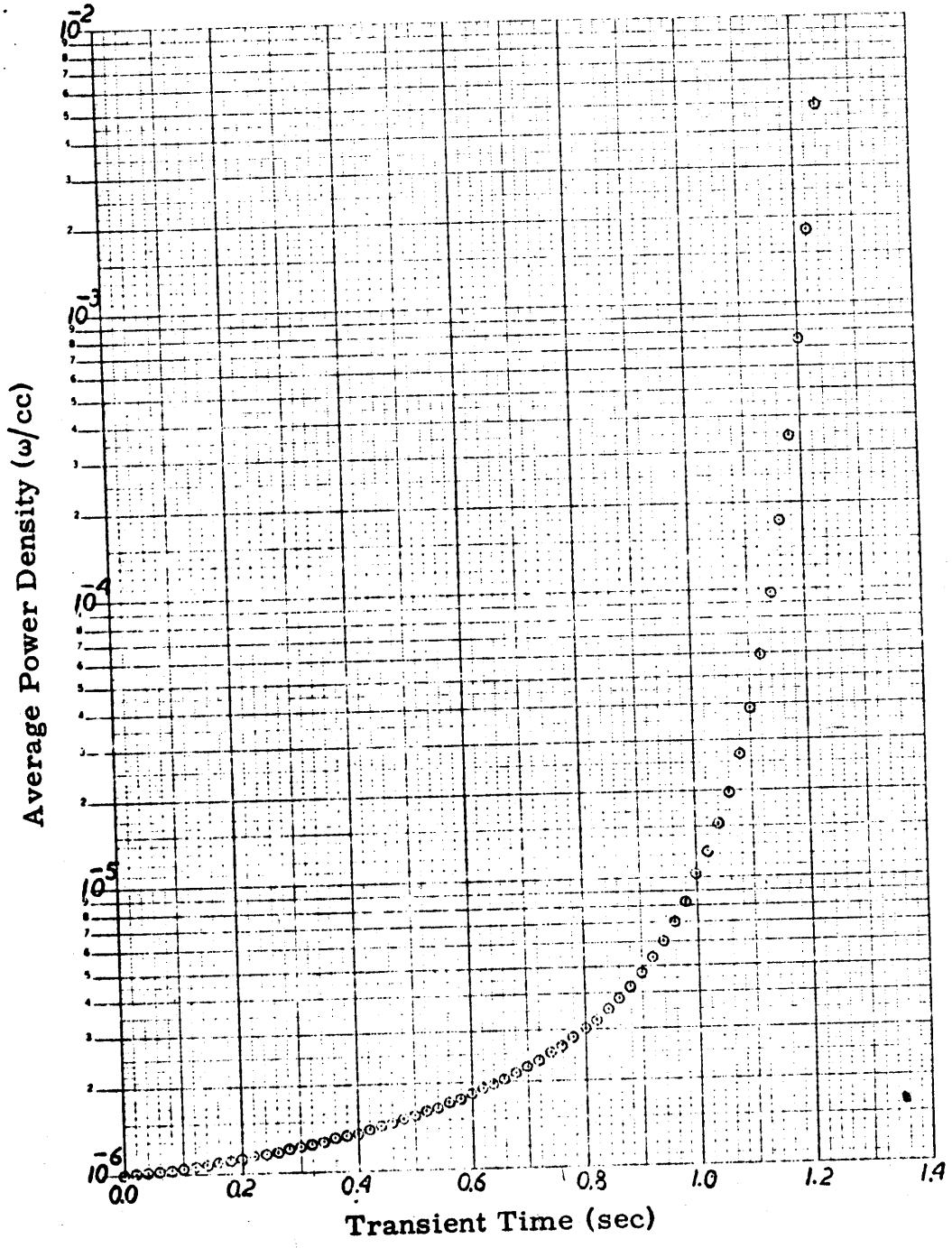

Figure A6.6c Power versus Time for the LRA Two-Dimensional BWR Kinetics Benchmark Problem

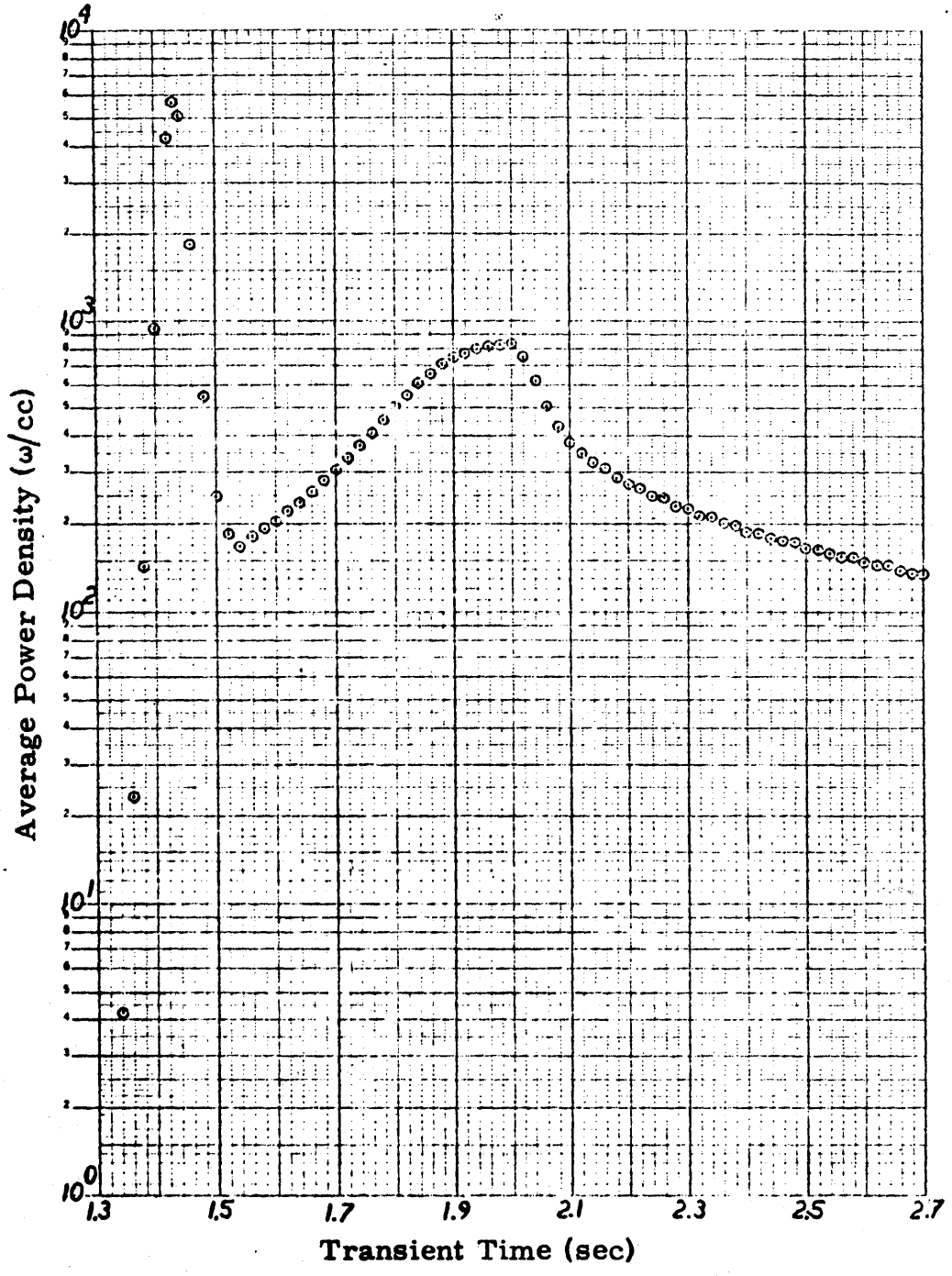

Figure A6.6c, contd.

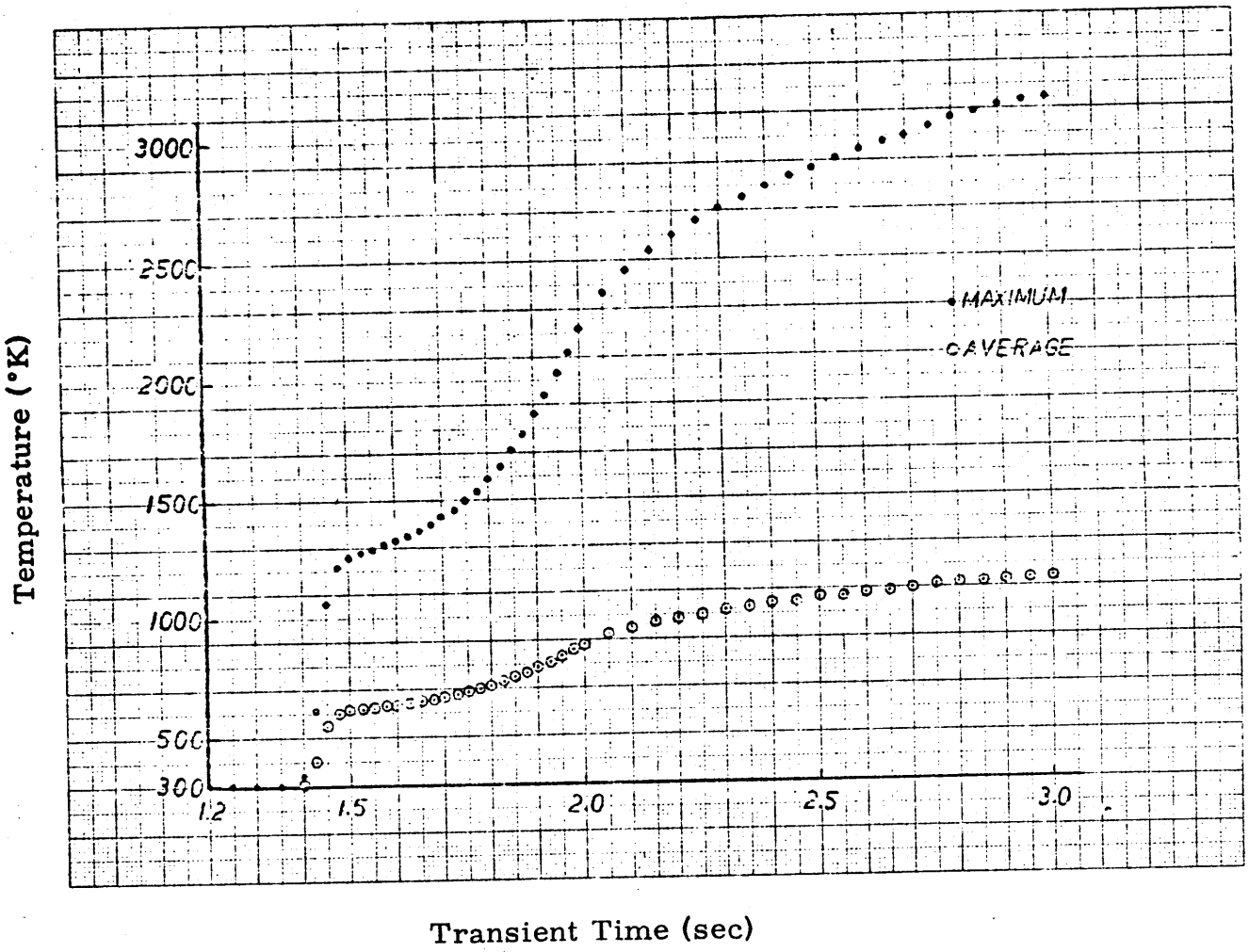

Figure A6.6d Temperature versus Time for the LRA Two-dimensional BWR Kinetics Benchmark Problem

Figure A6.6e Power and Temperature Distributions for the LRA BWR Kinetics Benchmark Problem at Time = 0.0 sec

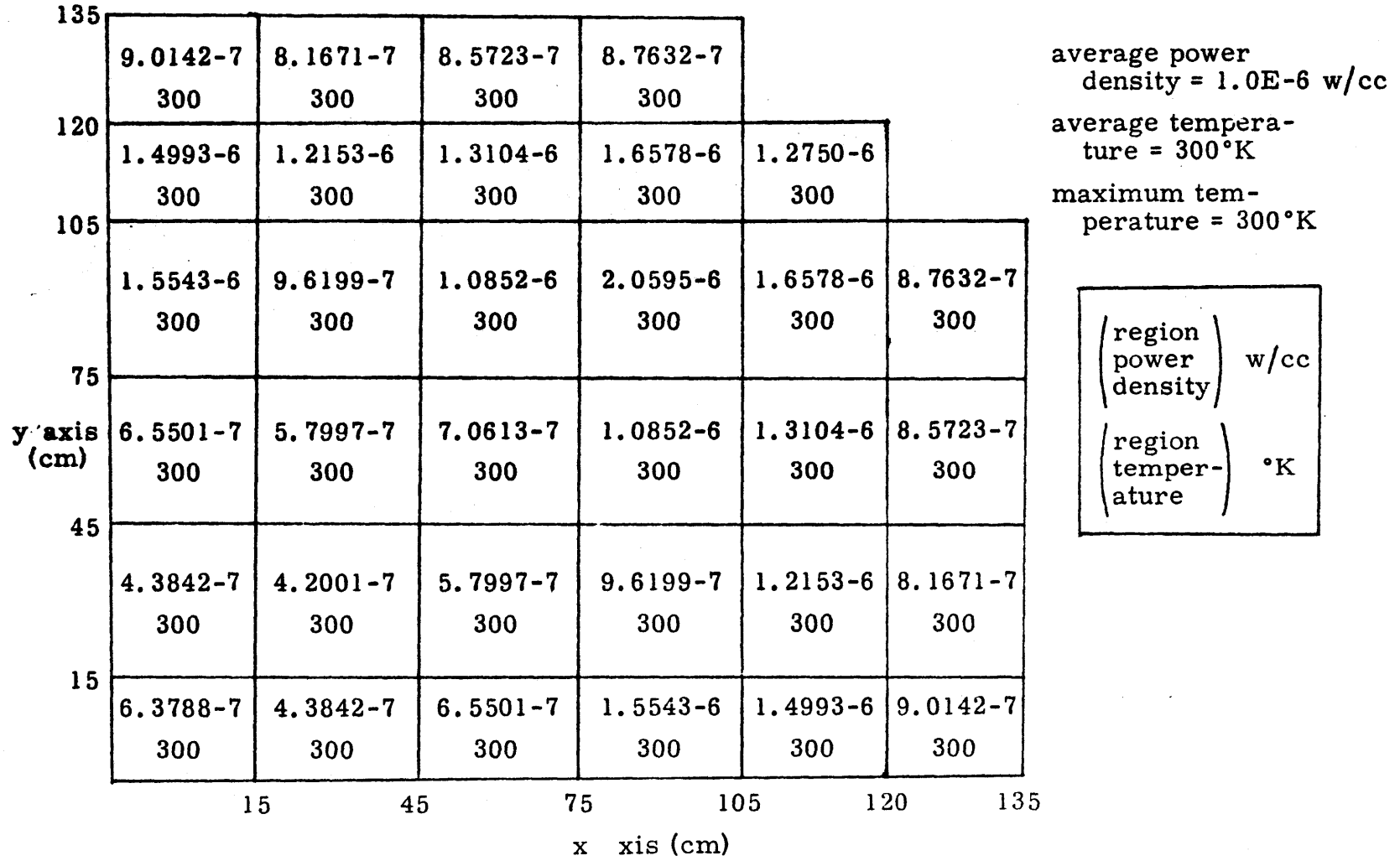

Figure A6.6f Power and Temperature Distributions for the LRA BWR Kinetics Benchmark Problem at Time = 1.40 sec

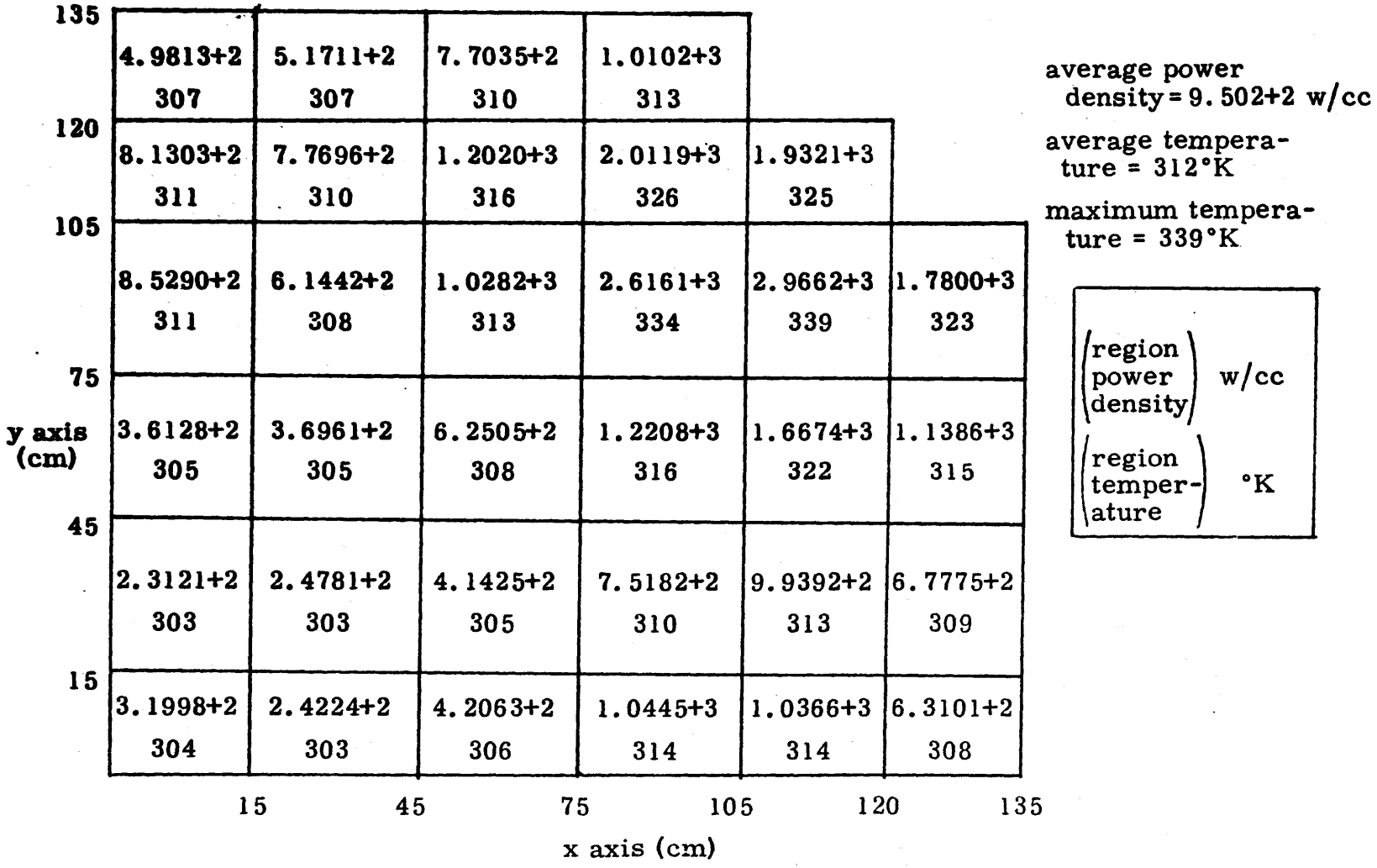

Figure A6.6g Power and Temperature Distributions for the LRA BWR Kinetics Benchmark Problem at Time = 2.00 sec

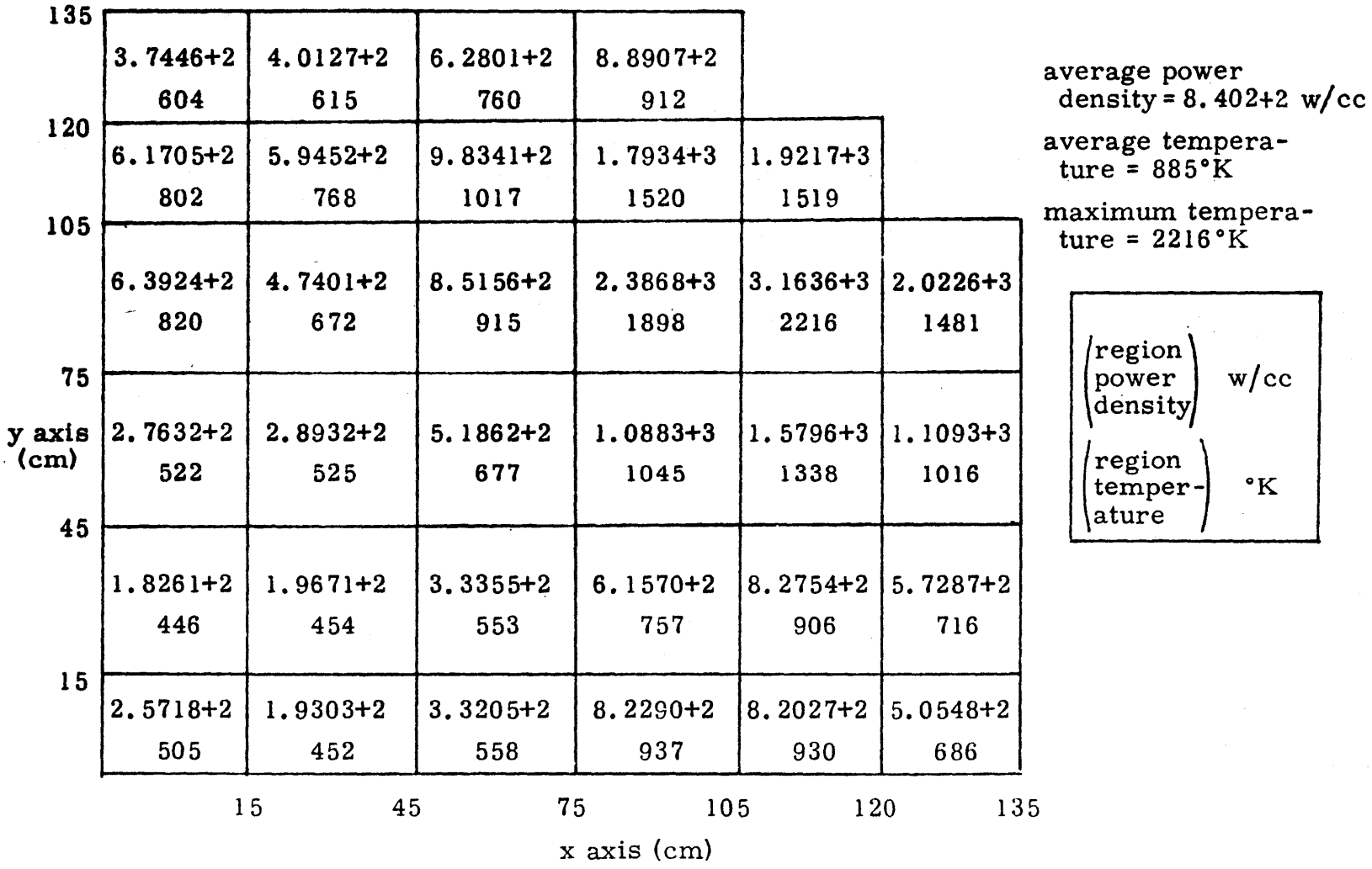

Figure A6.6h Power and Temperature Distributions for the LRA BWR Kinetics Benchmark Problem at Time = 3.00 sec

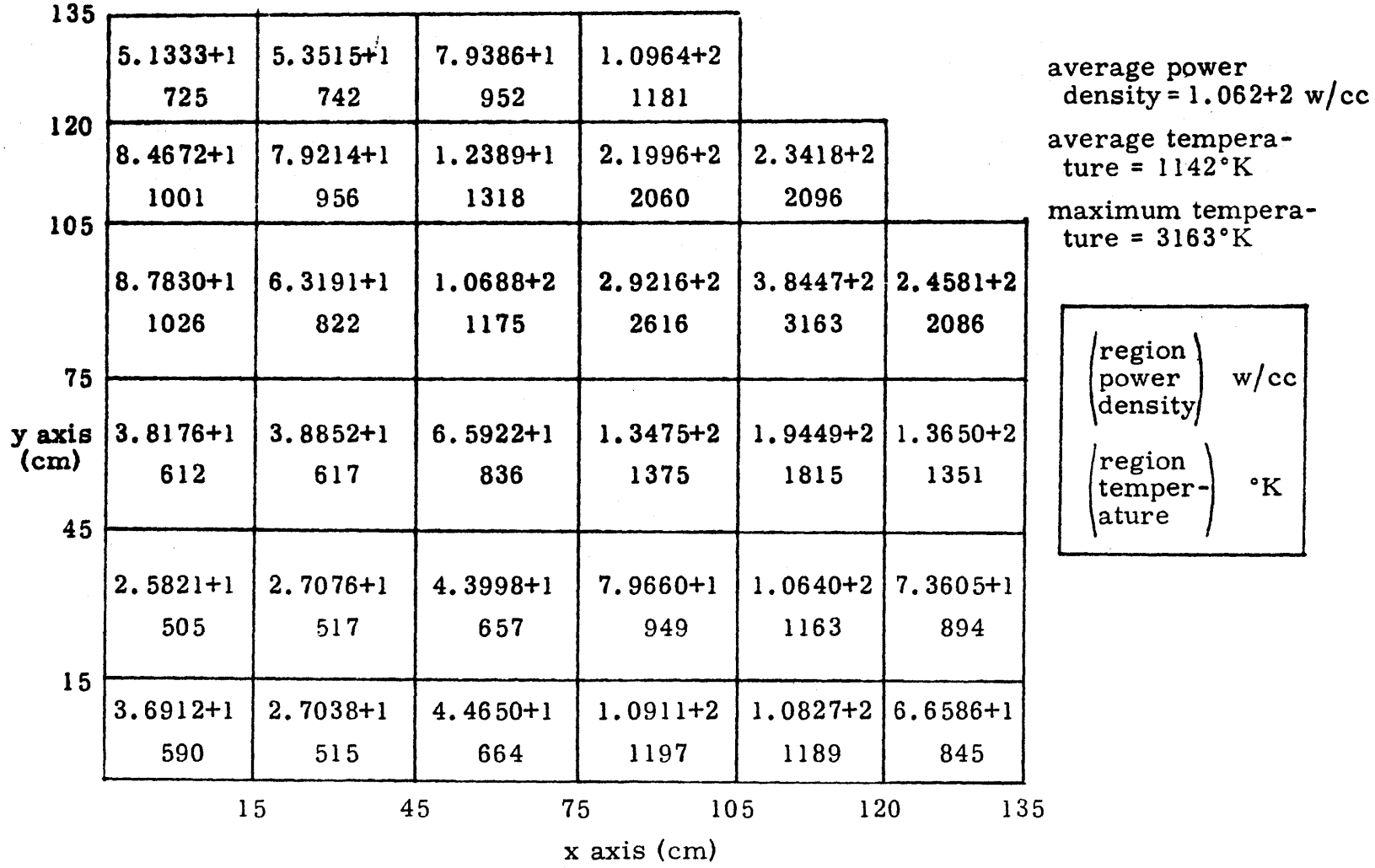

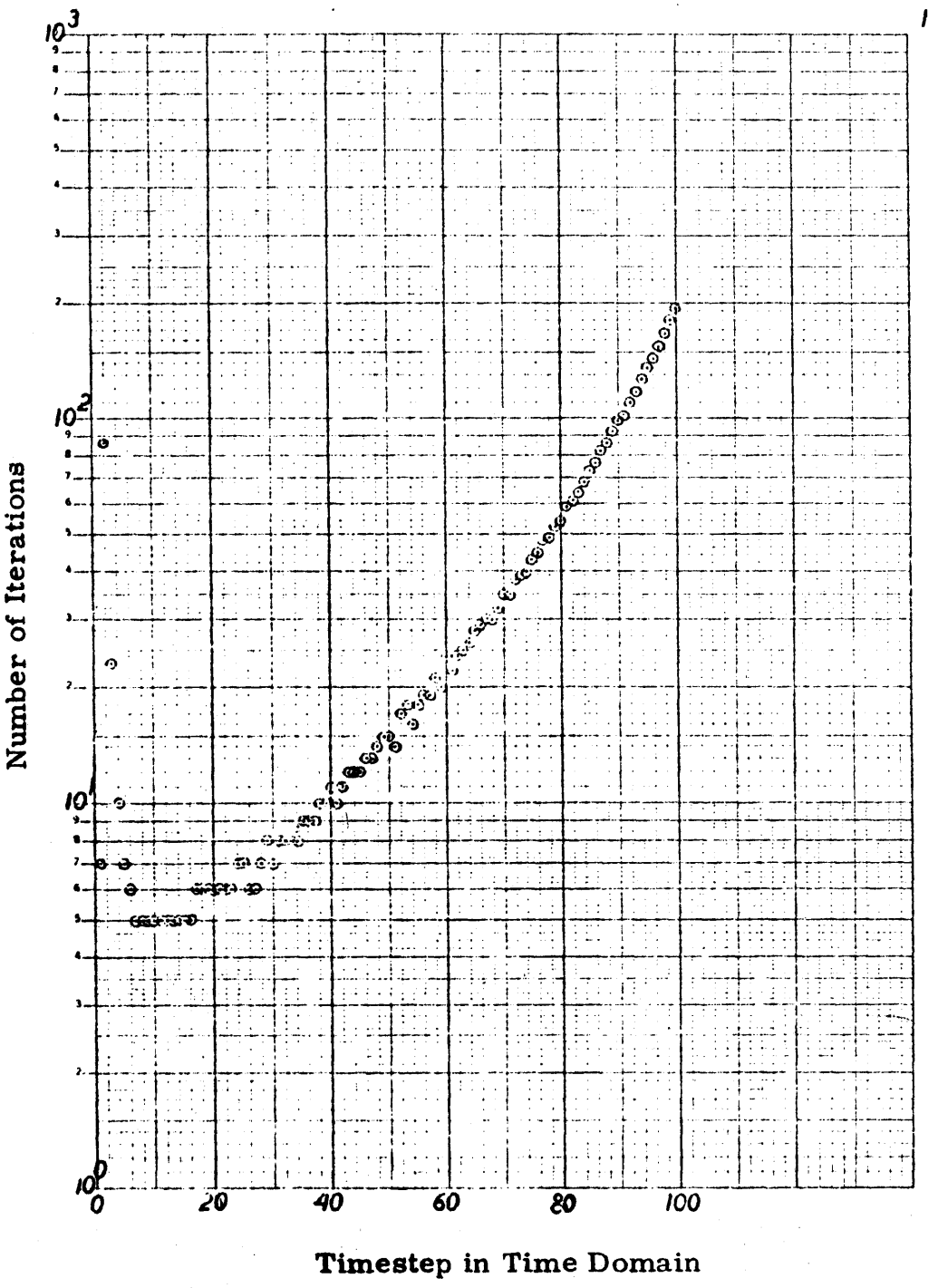

Figure A6.6i Iterations versus Timestep for the LRA Two-dimensional BWR Kinetics Benchmark Problem: First Time Domain

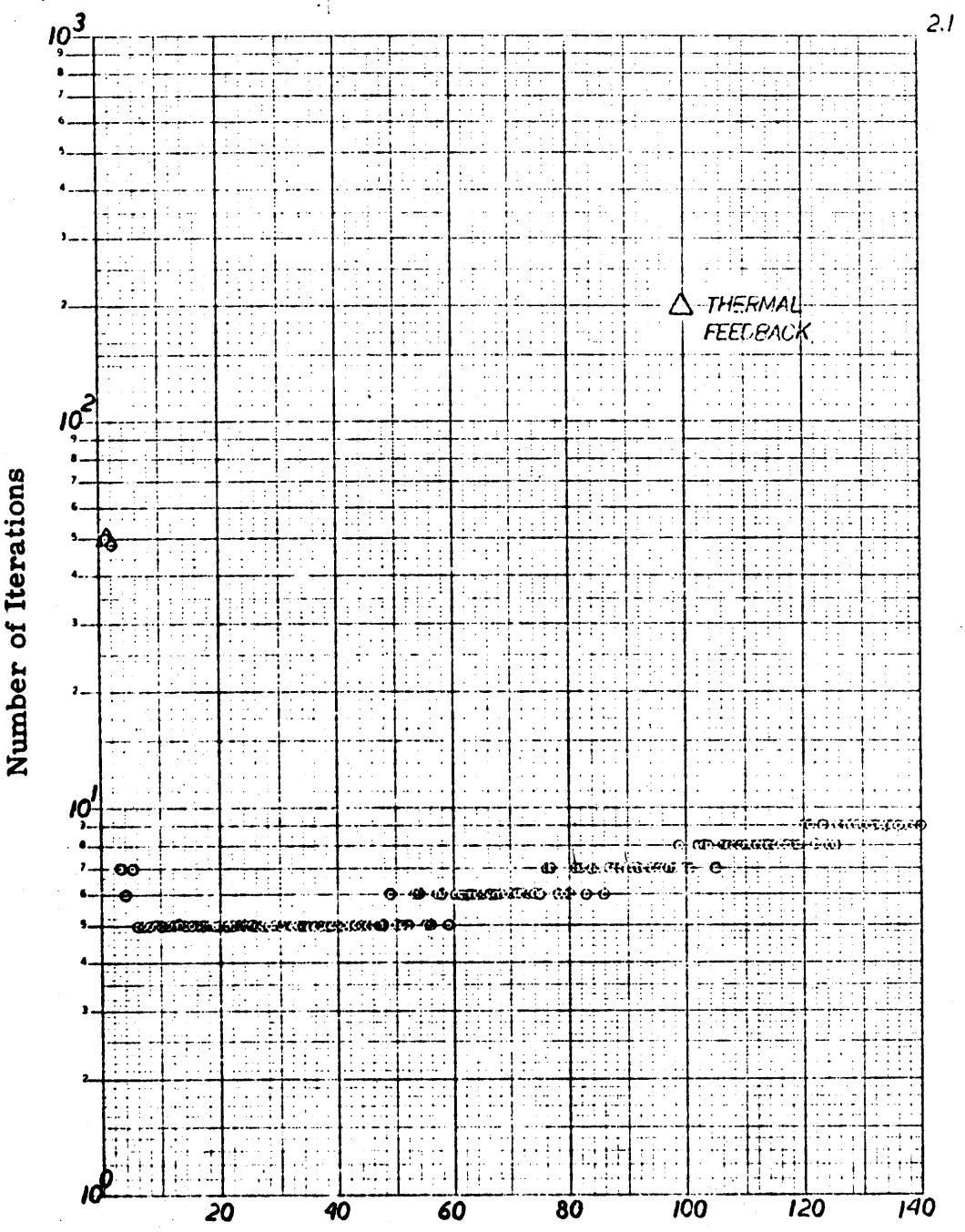

Figure A6.6j Iterations versus Timestep for the LRA Two-dimensional BWR Kinetics Benchmark Problem: Second Time Domain

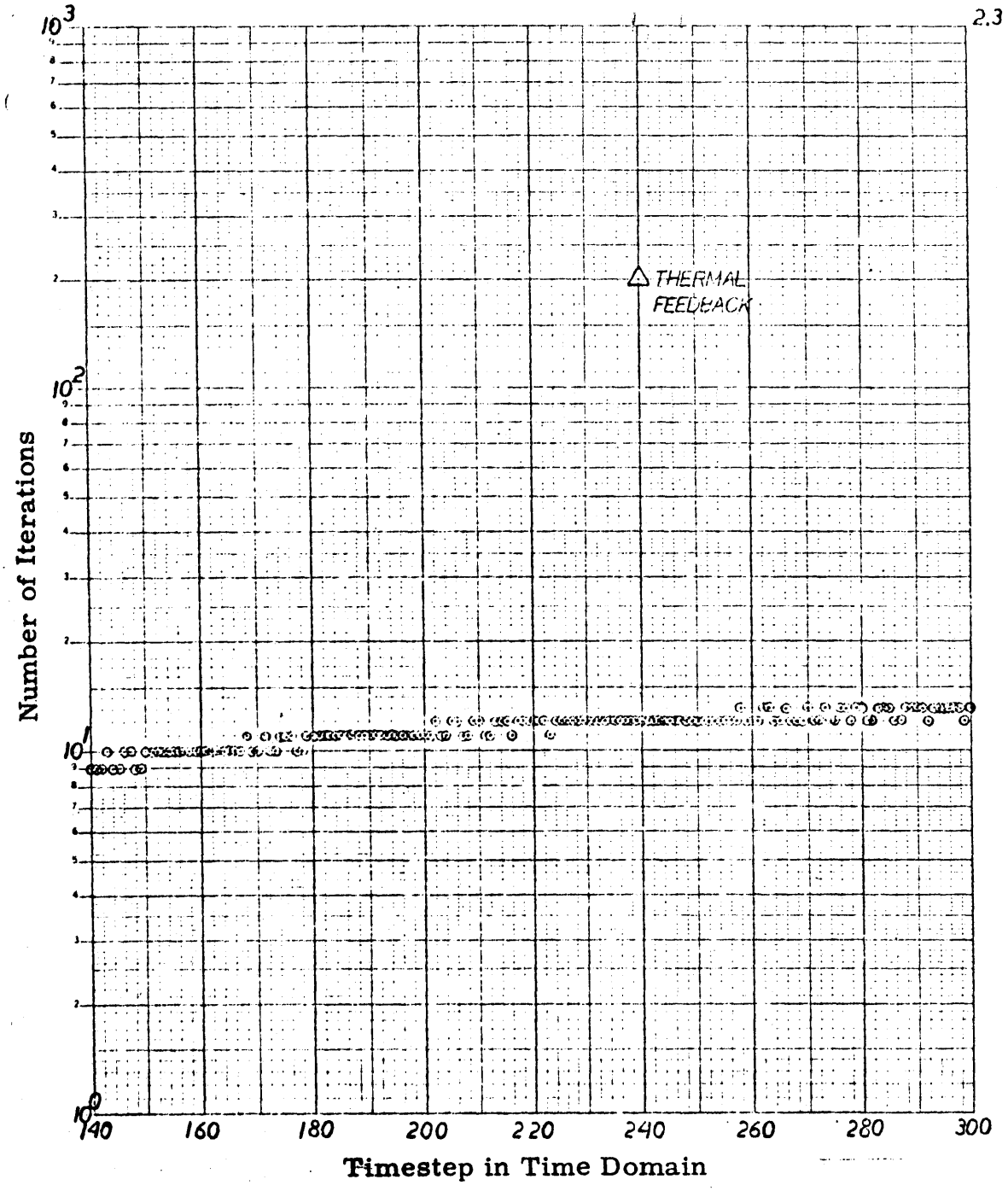

Figure A6.6j, contd.

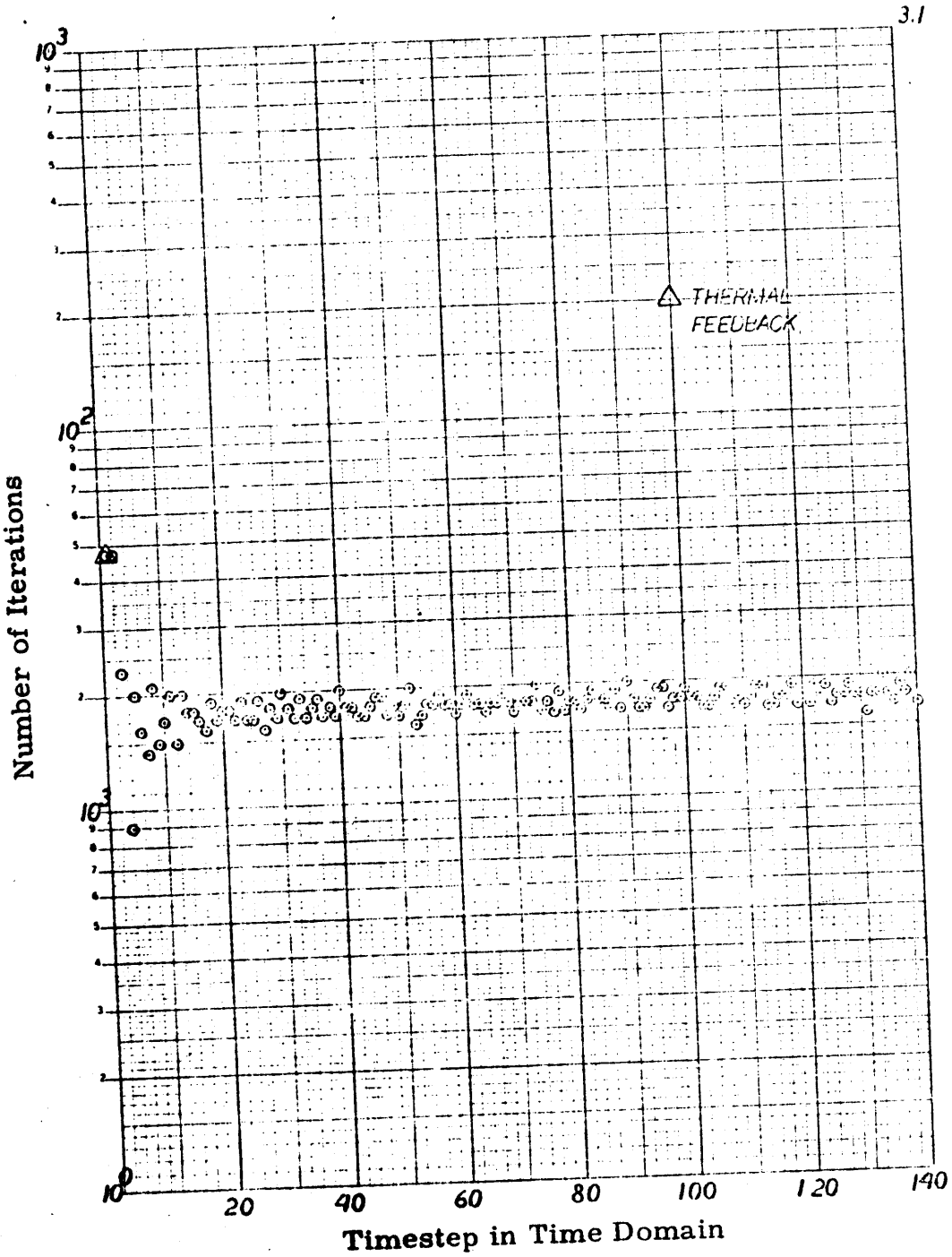

Figure A6.6k Iterations versus Timestep for the LRA Two-dimensional BWR Kinetics Benchmark Problem: Third Time Domain

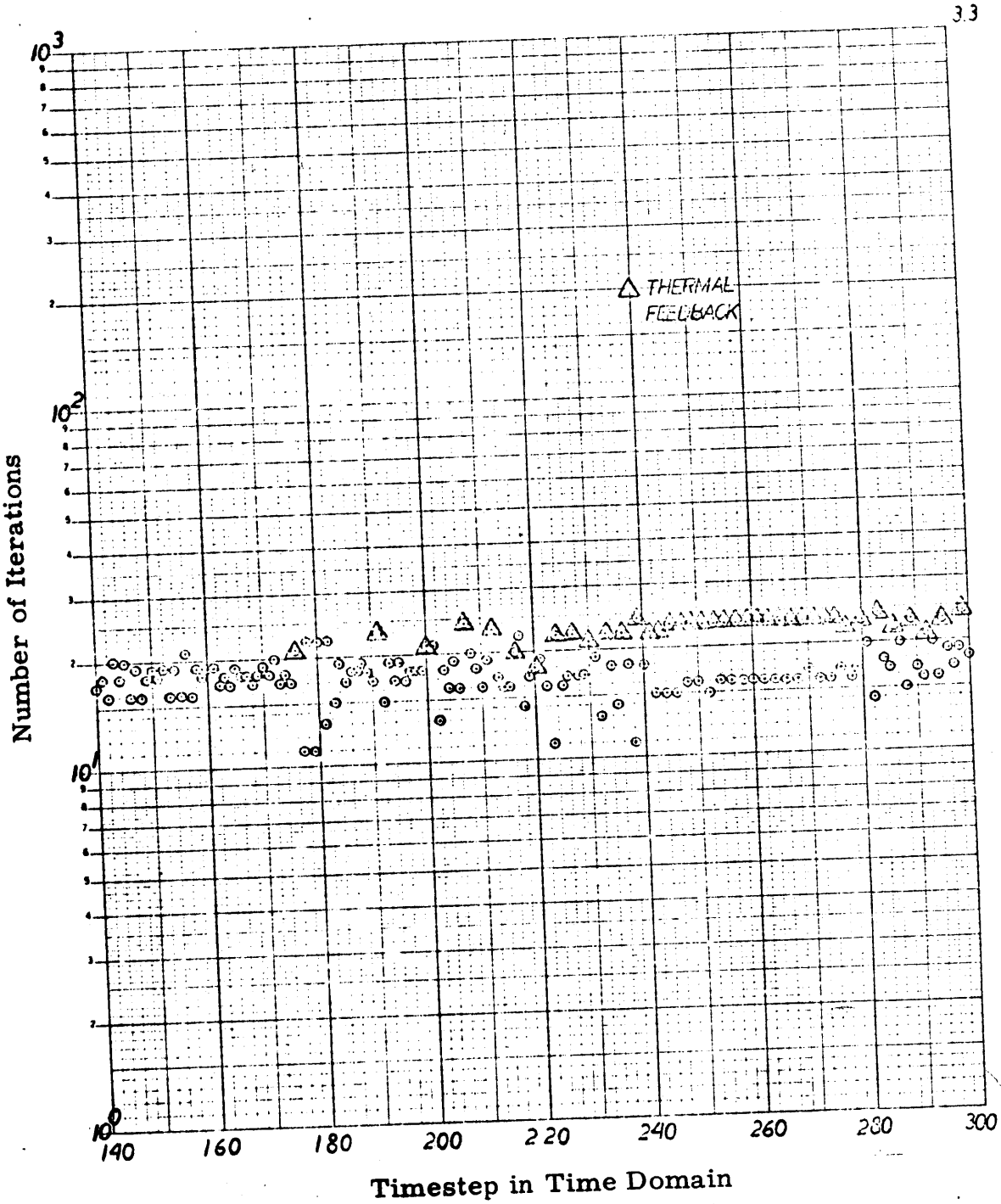

Figure A6.6k, contd.

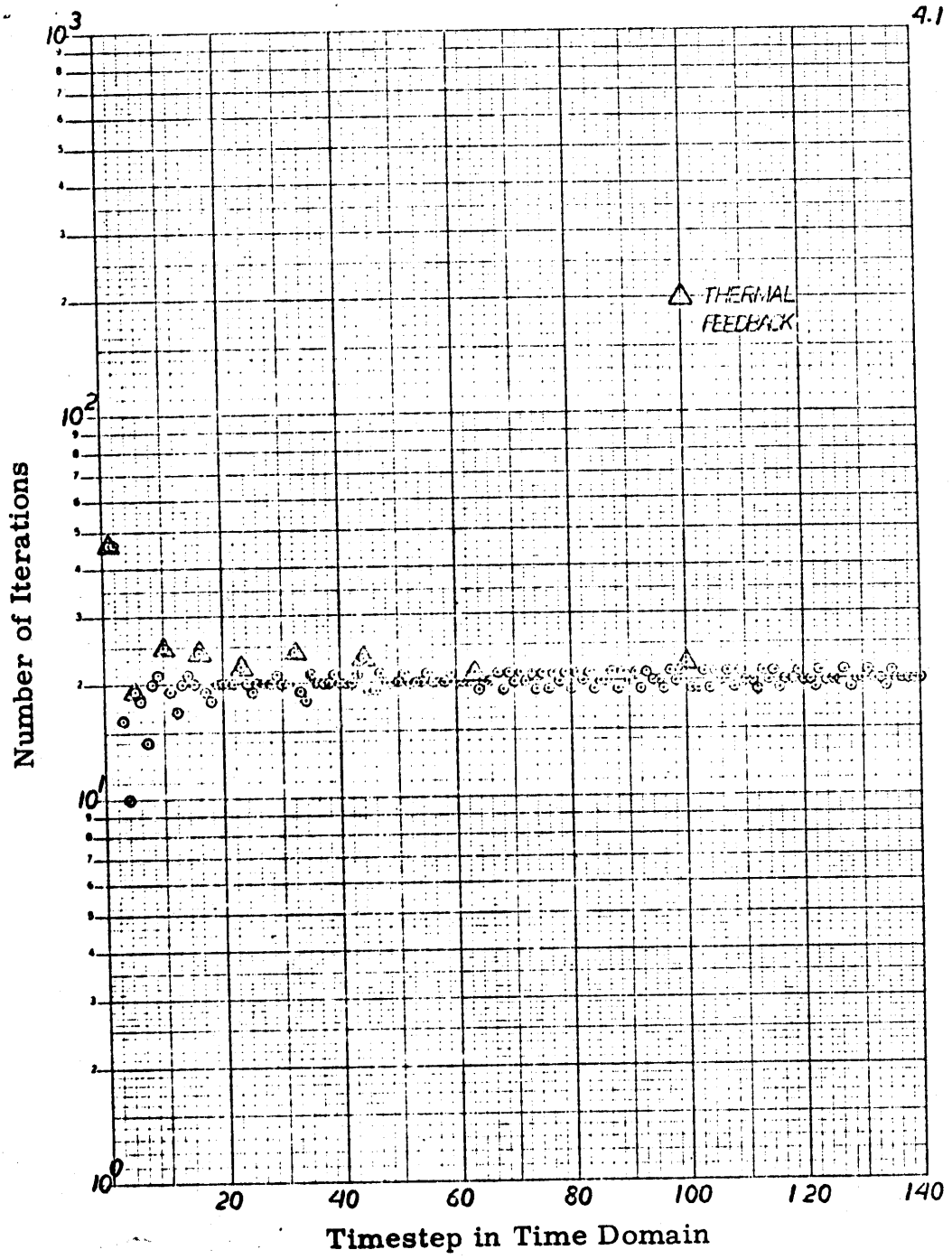

Figure A6.61 Iterations versus Timestep for the LRA Two-dimensional BWR Kinetics Benchmark Problem: Fourth Time Domain

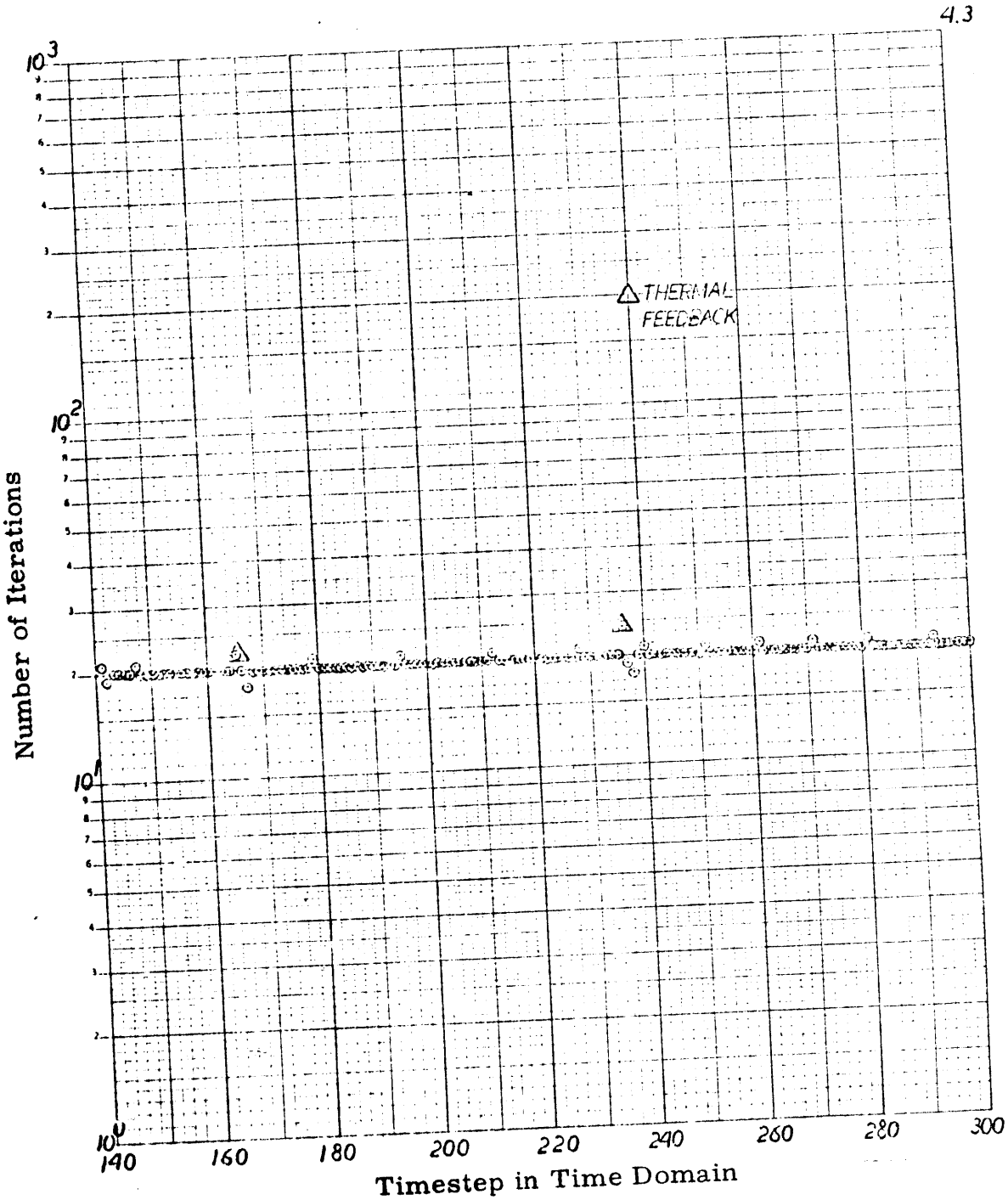

Figure A6.61, contd.

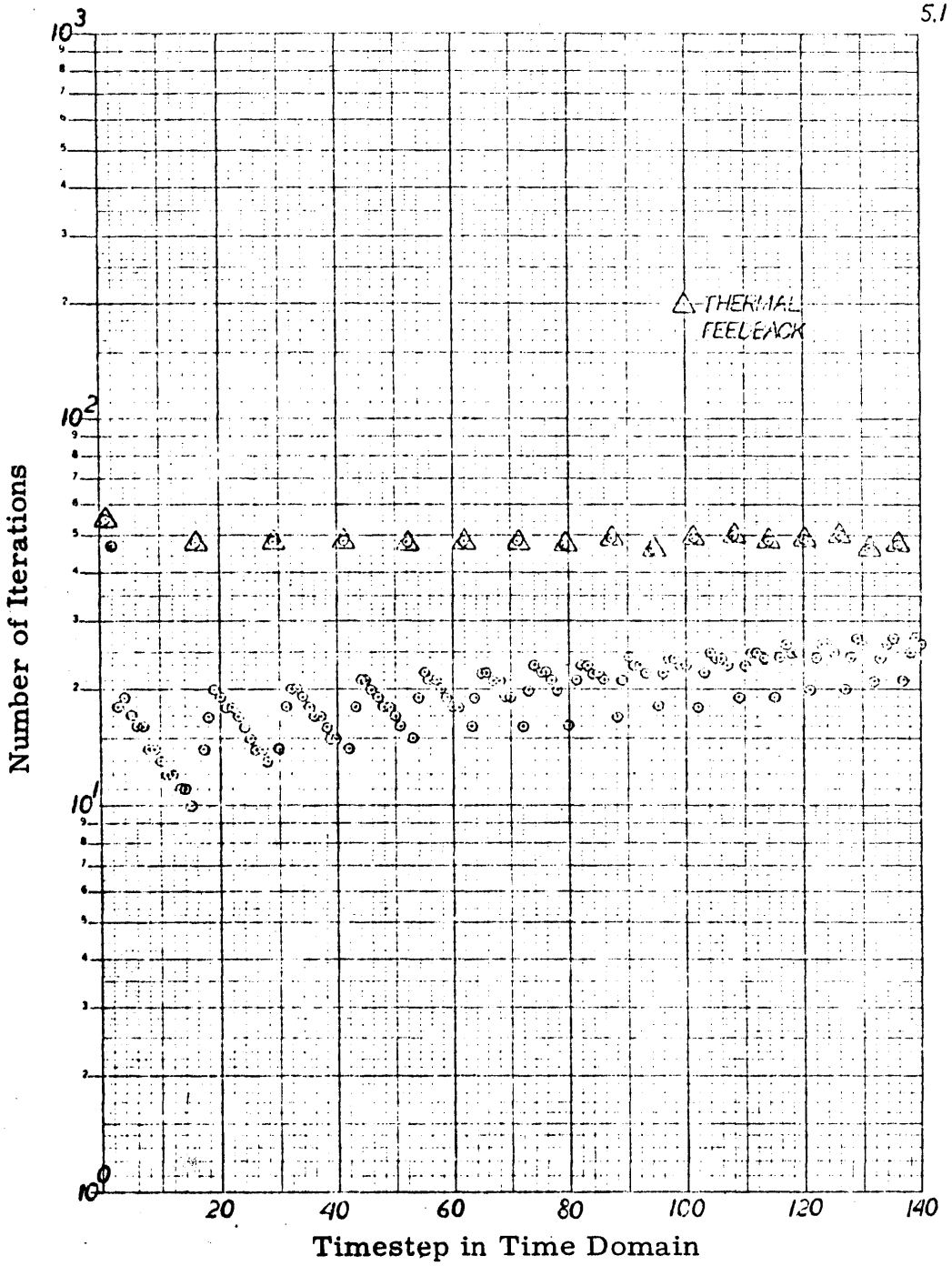

Figure A6.6m Iterations versus Timestep for the LRA Two-dimensional BWR Kinetics Benchmark Problem: Fifth Time Domain

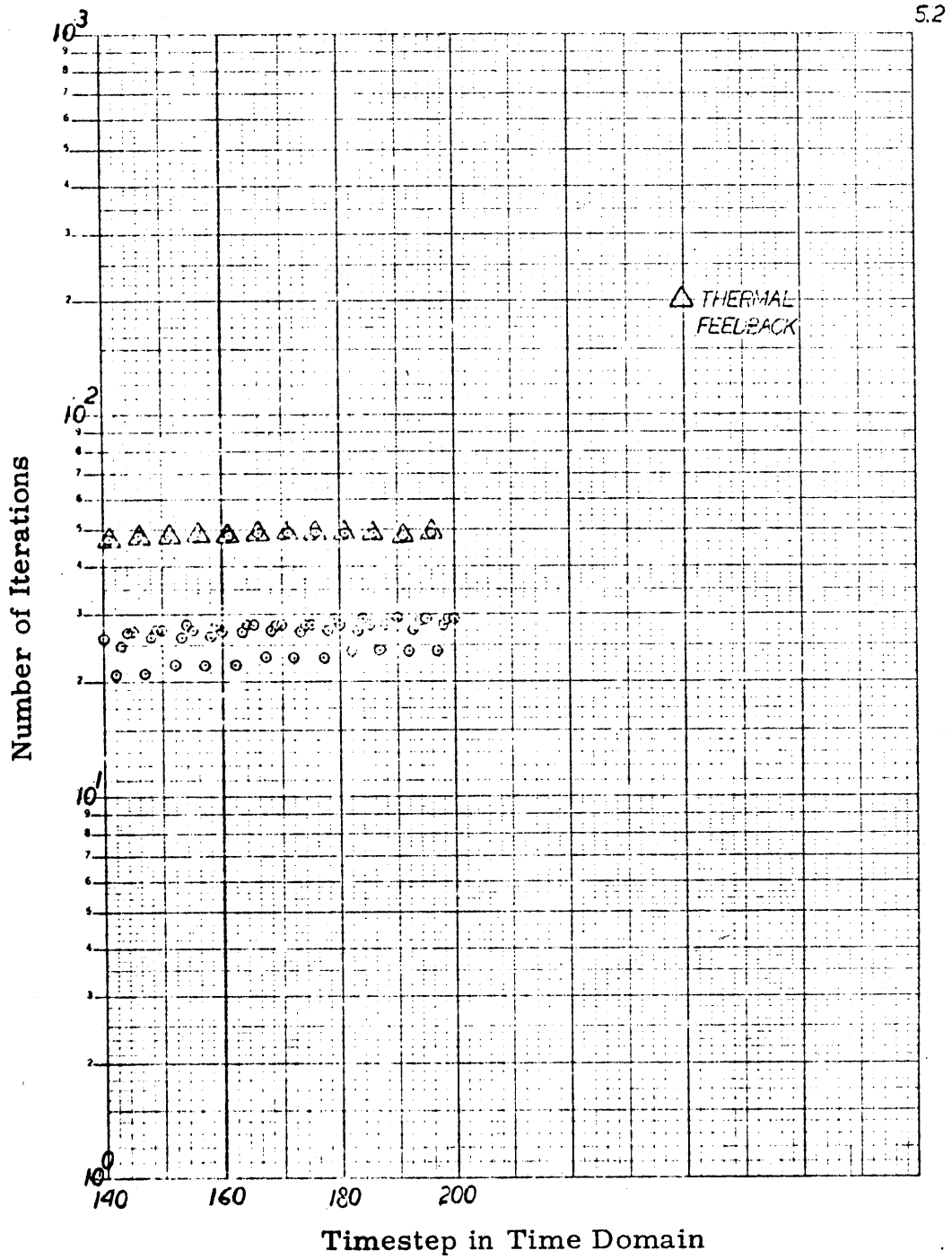

Figure A6.6m, contd.

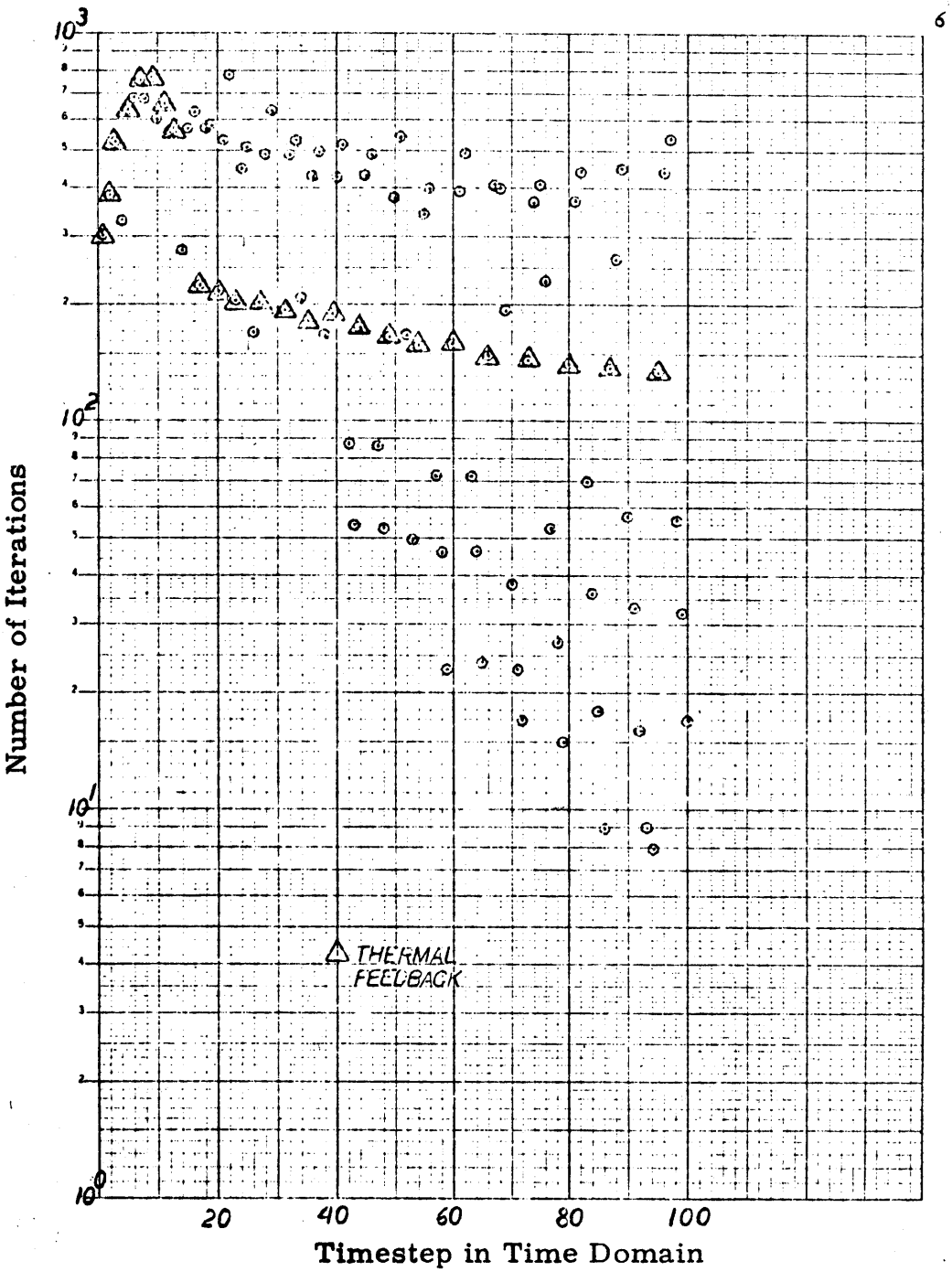

Figure A6.6n Iterations versus Timestep for the LRA Two-dimensional BWR Kinetics Benchmark Problem: Sixth Time Domain